MODELING BUBBLE-PARTICLE INTERACTIONS IN FLOTATION USING HYDROPHOBIC SOLID SURFACES

by

Darrin Heinz Flinn

Dissertation submitted to the Faculty of the
Virginia Polytechnic Institute and State University
in partial fulfillment of the requirements for the degree of

DOCTOR OF PHILOSOPHY
in
Mining and Minerals Engineering

APPROVED:

Dr. Roe-Hoan Yoon
(Chairman)

Dr. Yakov I. Rabinovich

Dr. James P. Wightman

Dr. Gerald H. Luttrell

Richey M. Davis
Dr. Richey M. Davis

May 1996
Blacksburg, Virginia

c. 2

LD
5655
V856
1996
F556
c.2

MODELING BUBBLE-PARTICLE INTERACTIONS IN FLOTATION USING HYDROPHOBIC SOLID SURFACES

by

Darrin Heinz Flinn

Dr. Roe-Hoan Yoon, Chairman
Mining and Minerals Engineering

(ABSTRACT)

An atomic force microscope (AFM) was used to measure surface forces between a glass sphere and a flat fused silica plate under a number of conditions. Hydrophobic surfaces exhibiting contact angles ranging from 0 to 109° were prepared by reacting silica with octadecyltrichlorosilane (OTS). Contact angles, AFM images, and infrared transmission spectra showed that OTS forms clusters on the silica surface. The presence of water in the reaction was shown to greatly influence the formation of these clusters. Forces were measured between surfaces coated with identical (symmetric) and different (asymmetric) amounts of OTS to determine contributions from hydrophobic forces. The results showed that the hydrophobic force parameters of the asymmetric interactions, K_{132}, can be predicted from those of the symmetric interactions, K_{131} and K_{232}, using a geometric mean combining rule. Asymmetric force measurements were conducted between a hydrophobized glass sphere and a bare silica plate in dodecylamine hydrochloride (DAHCl) solutions as a function of pH in an effort to simulate the forces involved in bubble-particle interactions for the quartz-amine flotation system. The appearance of the hydrophobic force in these measurements correlates well with the pH range of maximum flotation recoveries for quartz-amine flotation system.

ACKNOWLEDGMENTS

The author would like to thank his advisor, Dr. Roe-Hoan Yoon, for the guidance, suggestions, criticism, and financial support received throughout the course of this investigation. He also wishes to express his gratitude to Drs. David Guzonas and Yakov I. Rabinovich for their guidance and suggestions that helped make this study possible. Special consideration is also given to Drs. Ravishankar S. A., Cesar Basilio, and Zhenghe Xu, for their assistance. He would also like to thank Alisa Alls, Roy Hill, and Keith Kutz for their help and answers to his sometimes inane questions. Appreciation is extended to Wayne Slusser, Jerry Rose, and Jim Overfelt for their technical assistance. For their useful suggestions and comments, he would like to thank the other members of the surface forces group, Subramanian Vivek and B. Suha Aksoy, as well as the rest of his fellow graduate students at Holden Hall and Plantation road for their friendship.

The author would also like to express his sincere appreciation to his father, Frank, for forty-odd years of hard work to send three children to college; his mother, Elruth, for her understanding; his brother, Brian, and his sister, Heidi, for their patience and affection. Finally, the author gives special consideration to his fiancée, Janet, without whose support, both emotional and financial, this work would not have been possible.

TABLE OF CONTENTS

TITLE PAGE i

ABSTRACT ii

ACKNOWLEDGMENTS iii

TABLE OF CONTENTS iv

LIST OF FIGURES ix

LIST OF TABLES xvi

CHAPTER 1 INTRODUCTION ..... 1 - 43

1.1 General 1

1.2 Scope of Research 6

1.3 Review of Literature 7

1.3.1 Thermodynamics of Particle-Bubble Interactions 7

1.3.2 Modification of Silica Surfaces 11

1.3.2.1 Silica Silanation 13

1.3.2.2 Amine Adsorption and Flotation 15

1.3.3 Surface Forces 19
1.3.3.1 Derjaguin Approximation 19
1.3.3.2 Direct Force Measurement Techniques 21
1.3.3.3 Hydrophobic Force 24
1.3.3.4 Current Theories of Hydrophobic Attraction 26
1.3.3.5 Asymmetric Force Measurements 29
1.3.3.6 Force Measurements in DAHCl Solutions 30
1.4 References 34

CHAPTER 2 CHARACTERIZATION OF SILICA SURFACES HYDROPHOBIZED BY OCTADECYLTRICHLOROSILANE .... 44 - 87

2.1 Introduction 44
2.2 Materials and Methods 46
2.2.1 Chemicals 46
2.2.2 Cleaning of Silica Plates 48
2.2.3 Atomic Force Microscope Imaging 49
2.2.4 FTIR Transmission Measurements 49
2.2.5 Contact Angle Measurements 49
2.2.6 Silanation Reactions 50
2.3 Results and Discussion 51

2.3.1 Characteristics of OTS Films 51

2.3.2 Kinetics of OTS Film Formation 71

2.4 Conclusions 84

2.5 References 85

CHAPTER 3 HYDROPHOBIC INTERACTIONS BETWEEN DISSIMILAR SURFACES .... 88 - 127

3.1 Introduction 88

3.2 Materials and Methods 93

3.2.1 Materials 93

3.2.2 Apparatus 94

3.2.3 Cantilever Calibration 96

3.2.4 Silanation 98

3.2.5 Contact Angle Measurements 99

3.3 Results and Discussion 99

3.3.1 Force Measurements for Symmetric Interactions 99

3.3.2 Force Measurements for Asymmetric Interactions 108

3.3.3 Combining Rules for Hydrophobic Interactions 111

3.4 Conclusions 120

3.5 References 122

CHAPTER 4 DIRECT FORCE MEASUREMENTS FOR THE AMINE-QUARTZ FLOTATION SYSTEM....... 128 - 175

4.1 Introduction.. 128

4.2 Materials and Methods... 132

  4.2.1 Materials.. 132

  4.2.2 Contact Angle Measurements.. 133

  4.2.3 Surface Force Measurements... 133

4.3 Results and Discussion... 134

  4.3.1 Contact Angles.. 134

  4.3.2 Surface Forces 139

    4.3.2.1 Measurements between Two Bare Silica Surfaces.............. 139

    4.3.2.2 Measurements between Two OTS-coated Surfaces............ 146

    4.3.2.3 Measurements between One Bare Silica and One OTS-coated Surface.. 150

  4.3.3 Relevance to Flotation.. 161

4.4 Conclusions.. 168

4.5 References.. 170

CHAPTER 5 CONCLUSIONS.. 176 - 181

CHAPTER 6 RECOMMENDATIONS FOR FUTURE RESEARCH.. 182 - 186

VITA 187

LIST OF FIGURES

Figure 1.1 Interaction energy between two identical macroscopic bodies as described by the classical DLVO theory (Eq. [1.5]). 4

Figure 1.2 The energy balance around the point of three-phase contact for a) a liquid droplet on a solid and b) an air bubble attached to a solid surface in a liquid medium. 8

Figure 1.3 Initial and final states of bubble-particle attachment in flotation. 9

Figure 1.4 The effect of temperature on the surface of hydrated silica 12

Figure 1.5 The correlation between flotation recovery, contact angle, surface coverage, zeta-potential for quartz in $4x10^{-5}$ M dodecylamine solution as a function of pH [from Fuerstenau (44)]. Also shown if the pH dependence of surface tension at the liquid-vapor interface [from Castro *et al.* (117)] 16

Figure 1.6 A distribution diagram of collector species in $4x10^{-5}$ M DAHCl solution as a function of pH. Curves were determined from the thermodynamic data of Ananthpadmanabhan *et al.* (45). Also included are the critical micelle concentration data of Watson and Manser (118). 18

Figure 1.7 The relationship of interaction energies and surface forces based on the Derjaguin approximation for a number of well-known geometries (56, 57). 20

Figure 1.8 Schematic representations of the surface forces apparatus (SFA) and atomic force microscope (AFM) techniques of direct force measurements between solid surfaces. 22

Figure 2.1	Polymerized OTS is believed to form covalent bonds to the silica surface.	47
Figure 2.2	Atomic force microscope image of a clean fused silica plate.	52
Figure 2.3	Typical FTIR transmission spectra showing OTS adsorption at different stages of monolayer growth on an SiO_2 substrate.	53
Figure 2.4a	Wavenumber positions of CH_2 asymmetric and symmetric stretching mode bands as a function of fractional OTS surface coverage.	55
Figure 2.4b	Full peak width at half maximum (FWHM) of CH_2 asymmetric and symmetric stretching mode data for various OTS surface coverages.	56
Figure 2.5a	Advancing contact angle data for silica plates immersed in molar OTS solution concentrations of (□) $5.05x10^{-3}$, (O) $2.54x10^{-3}$, (Δ) $1.01x10^{-3}$, and (◊) $5.05x10^{-4}$ at various time intervals.	58
Figure 2.5b	Hysteresis plot of advancing and receding contact angle data for all silanated silica plates in relation to surface coverage of OTS.	59
Figure 2.6	Cosine of advancing contact angle data showing initially a linear relationship to OTS surface coverage according to Cassie's Law, but changing slope at a fractional coverage of about 0.25-0.3	61
Figure 2.7a	Atomic force microscope image of a silanated surface in air exhibiting an advancing water contact angle of 27°.	63
Figure 2.7b	Atomic force microscope image of a silanated surface in air exhibiting an advancing water contact angle of 45°.	64
Figure 2.7c	Atomic force microscope image of a silanated surface in air exhibiting an advancing water contact angle of 84°.	65

Figure 2.7d Atomic force microscope image of a silanated surface in air exhibiting an advancing water contact angle of 101°. 66

Figure 2.7e Atomic force microscope image of a silanated surface in air exhibiting an advancing water contact angle of 107°. 67

Figure 2.8a Fractional surface coverage (Γ) data for silica plates immersed in molar OTS solution concentrations of (□) 5.05×10^{-3}, (○) 2.54×10^{-3}, (Δ) 1.01×10^{-3}, and (◊) 5.05×10^{-4} at various time intervals. Solid lines represent Langmuir-like isotherms as determined by a least squares fit. 73

Figure 2.8b Exponential constants (k) determined for the isotherms of Figure 2.8a for the given OTS solution concentrations. A linear relationship is found at solution concentrations lower than 3×10^{-3} M. 74

Figure 2.8c Calculated equilibrium fractional surface coverage (Γ_{eq}) values attained by the isotherms shown in Figure 2.8a for the various OTS solution concentrations. 75

Figure 2.9a Contact angle data for silanation reactions carried out in 1.01×10^{-3} M OTS water-saturated cyclohexane (○) and dried cyclohexane (□) solutions. 76

Figure 2.9b Hysteresis plot of advancing and receding contact angle data for silanated samples shown in Figure 2.9a. 77

Figure 2.9c Fractional surface coverage (Γ) values for the plates in Figure 2.9a plotted against immersion time. 78

Figure 2.10 Atomic force microscope image in air of a silanated surface exhibiting an advancing water contact angle of 65° and hysteresis of 10°. 80

Figure 2.11 A proposed model for the OTS on SiO_2 adsorption process, in which (a) OTS molecules are attracted to the hydrated silica surface and (b) hydrolyze to form clusters. These hydrolyzed molecules or clusters (c) are weakly attracted to the physisorbed water on the silica surface and may eventually form patches on the silica surface. In time, (d) more patches form up to a point when (e) single OTS molecules adsorb (f), increasing the surface density to monolayer coverage. 82

Figure 3.1 Schematic representation of the atomic force microscope (AFM) as used for measuring forces in a liquid between a flat silica plate and a glass sphere. 95

Figure 3.2 Schematic representation of the AFM cantilevers used for force measurements: a) a standard triangular Si_3N_4 cantilever for weak interactions, b) a force etched silicon probe (FESP) for moderate forces, and c) a tapping etched silicon probe (TESP) for strongly hydrophobic forces. A range of spring constants, as determined by the inversion technique, are given for each cantilever. 97

Figure 3.3 Results of the AFM force measurements conducted with glass spheres and silica plates. The force (F) was normalized by the radius (R) of the glass sphere and plotted versus the closest separation distance (H). Each force curve was obtained using a sphere and a plate, silanated with octadecyltrichlorosilane (OTS) under identical conditions so that both were of the same contact angle: ●) 0°, □) 81°, ▲) 92°, ○) 100°, and ◆) 109°. The dashed line represents a DLVO fit of the data with $A_{131} = 8\text{x}10^{-21}$ J, $\psi_1 = -60$ mV, $\kappa^{-1} = 42$ nm, while the solid lines represent the extended DLVO theory which includes a power law (Eq [3.5]) to account for the contributions from the hydrophobic force. Hydrophobic force parameters are given in Table 3.1. The arrows show the jump distances. 100

Figure 3.4 F/R vs. H curve obtained with a clean glass sphere and a bare silica plate in water. The dashed line represents a DLVO fit with $A_{131} = 8\text{x}10^{-21}$ J, $\psi_1 = -60$ mV, $\kappa^{-1} = 42$ nm, while the solid line represents the extended DLVO theory which includes the hydration force. The dotted line represents the hydration force (Eq. [3.4]) with C_1 = 12 mN/m, D_1 = 0.4 nm, C_2 = 1.1 mN/m, and D_2 = 3.0 nm. 107

Figure 3.5 F/R vs. H curves obtained between silanated glass sphere with contact angle of 109° and silanated silica plates with the following contact angles: (◊) 0°, (■) 75°, (Δ) 83°, (●) 92°, (◆) 97°, (□) 100°, (▲) 105°, and (O) 109°. The dashed line represents the classical DLVO theory (Eq. [3.1]) with $A_{131} = 8\text{x}10^{-21}$ J, ψ_1 = -60 mV, κ^{-1} = 42 nm. The solid lines represent the extended DLVO theory incorporating a power law (Eq [3.5]) to account for the contributions from the hydrophobic force. The arrows show the jump distances. Hydrophobic force parameters are given in Table 3.2. 109

Figure 3.6 Log K vs. cos θ plots for K_{131} (□), K_{232} (O), and K_{132} (■). The solid lines represents the best fit of log K_{131} values. Dashed lines represent the K_{132} values predicted from the values of K_{131} and K_{232} using arithmetic, geometric, and harmonic means. 117

Figure 3.7 Log K vs. $(\cos\theta)_{avg}$ plots for the K_{131}, K_{232}, and K_{132} values determined using AFM for silanated glass sphere and silica plates. 119

Figure 4.1. Changes in contact angle with time for bare silica and OTS-coated silica in $4\text{x}10^{-5}$ M DAHCl solutions at different pH. 135

Figure 4.2. Results of contact angle measurements conducted as a function of pH using the captive bubble technique in $4\text{x}10^{-5}$ M DAHCl solutions for a) bare silica surfaces and b) OTS-coated silica surfaces. Open circles represent initial contact angles measured within 15 seconds after introducing the air bubble into the cell, while filled circles are the data obtained after the bubble had aged 30 minutes. Solid lines are surface tension data at the liquid-vapor interface from Refs. 18 and 48. 137

Figure 4.3. Results of AFM force measurements conducted between a clean glass sphere and a bare silica plate in $4x10^{-5}$ M DAHCl solution at different pH values. The measured force (F) is normalized by the radius (R) of the glass sphere and plotted versus the closest separation distance (H). Force data obtained in pure water are shown in the inset. The dashed line represents the London-van der Waals force (F_d) as calculated using Eq. [4.5] with A_{131} = $8x10^{-21}$ J. The solid lines represent DLVO and extended DLVO fits of the measured forces. Values of the fitting parameters are provided in Table 4.1. The arrows indicate the distances (H_j) at which the surfaces jumped into contact. 140

Figure 4.4. F/R vs. H curves obtained from AFM force measurements conducted between an OTS-coated glass sphere and an OTS-coated silica plate in $4x10^{-5}$ M DAHCl solutions at several pH values. The force data obtained in pure water are also included. The dashed line represents F_d as calculated using Eq. [4.5] with A_{232} = $8x10^{-21}$ J. The solid lines are fits of the force data using the extended DLVO model, Eq. [4.2], in which Eq. [4.4] is used to account for the contributions from the hydrophobic force. Values of the fitting parameters are provided in Table 4.2. The arrows indicate jump distances (H_j). 147

Figure 4.5. F/R vs. H curves obtained from AFM force measurements conducted between an OTS-coated glass sphere and a bare silica plate in $4x10^{-5}$ M DAHCl solutions at different pH values. The force data obtained from measurements conducted in pure water are shown in the inset. The dashed line represents F_d as calculated using Eq. [4.5] with A_{132} = $8x10^{-21}$ J. The solid lines are fits of the force data using the classical DLVO theory (Eq. [4.1]) or the extended DLVO model (Eq. [4.2]) using Eq. [4.4] to account for the hydrophobic force. Values of the fitting parameters are provided in Table 4.3. The arrows indicate jump distances (H_j). 152

Figure 4.6. Values of the Hamaker constant (A) plus the hydrophobic force parameter (K) plotted on a logarithmic scale versus pH. The values of K were obtained from AFM force measurements between i) bare silica surfaces, ii) OTS-coated surfaces, and iii) a bare silica surface and an OTS-coated surface in 4x10^{-5} M DAHCl solutions at different pH. The dashed line represents A = 8x10^{-21} J for silica in water.......... 157

Figure 4.7. Log K values obtained in the present study are plotted versus cos θ_{eff} (= ½(cos θ_1 + cos θ_2)). Squares represent K values plotted versus cos θ_{eff} determined from initial contact angles, cos $\theta_{eff,i}$; whereas, diamonds are K values plotted against cos θ_{eff} determined from final contact angles, cos $\theta_{eff,f}$. The dashed line represents the value of the Hamaker constant for silica surfaces in water, 8x10^{-21} J. 160

Figure 4.8. The pH dependence of activation energy (E_a) per unit area determined from AFM force measurements conducted in 4x10^{-5} M DAHCl solutions between i) a clean glass sphere and a bare silica plate and ii) an OTS-coated sphere and a bare silica plate.......... 164

LIST OF TABLES

Table 2.1 Fractional surface coverage values estimated from atomic force microscopy and Fourier transform infrared transmission spectra. 69

Table 3.1 Force Parameters Obtained for Symmetric Interactions........ 103

Table 3.2 Force Parameters Obtained for Asymmetric Interactions........ 112

Table 4.1 Force Parameters for Measurements between Bare Silica Surfaces in $4x10^{-5}$ M DAHCl Solution at Various pH. 142

Table 4.2 Force Parameters for Measurements between Hydrophobized Silica Surfaces in $4x10^{-5}$ M DAHCl Solution at Various pH........ 148

Table 4.3 Force Parameters for Measurements between a Bare Silica Surface and a Hydrophobized Silica Surface in $4x10^{-5}$ M DAHCl Solution at Various pH........ 153

Table 4.4 Calculated Activation Energy Values for a Bare Silica Surface Interacting with a Fresh Air Bubble and an Aged, Surfactant-Coated Air Bubble in DAHCl Solutions at Varying pH. 166

CHAPTER 1 INTRODUCTION

1.1 *General*

Gaudin (1) describes froth flotation as a separation process in which some particulate matter, suspended in aqueous solution, adhere to gas bubbles either generated or introduced in the suspension, while other solids adhere to the aqueous medium. Adhesion to gas bubbles enables those particles to be recovered in a froth having a different composition than the suspension. The first reported process recognizing gas bubbles as a means of mineral separation was patented by the Bessel brothers in Germany in 1886 (2, 3). Early research focused on the use of flotation to recover fine particles that eluded separation by commonly used methods of gravity concentration (4). Since its commercial inception in 1905 (2), froth flotation has quickly grown to become one of the most commonly used mineral processing techniques. Today, it is responsible for recovering nearly 100 types of metallic and non-metallic minerals and has applications in deinking, recycling, oil recovery, waste water treatment, etc. (5, 6). However, even today relatively little is known about this complex process involving colloid and surface chemistry, physics, and crystallography

(4) and present research focuses on determining the physical and chemical mechanisms responsible for flotation.

The rate of flotation (k) is related to the probability of flotation (P) according to the following relationship (7):

$$k = \frac{1}{4} P S_{\mathrm{b}}, \tag{1.1}$$

where S_{b} is the surface area rate of bubbles rising through the pulp. Sutherland (8) has proposed that the probability of flotation can be represented by three components as follows:

$$P = P_{\mathrm{c}} \cdot P_{\mathrm{a}} \cdot (1 - P_{\mathrm{d}}), \tag{1.2}$$

where P_{c} is the probability of bubble-particle collision, P_{a} is the probability of bubble-particle adhesion, and P_{d} is the probability of detachment. For intermediate flow conditions, P_{c} can be expressed by (9)

$$P_{\mathrm{c}} = \left[\frac{3}{2} + \frac{4Re^{0.72}}{15}\right]\left(\frac{D_{\mathrm{p}}}{D_{\mathrm{b}}}\right)^2, \tag{1.3}$$

where Re is the Reynolds number, D_{p} is the particle diameter, and D_{b} is the bubble diameter. Hydrodynamics govern the magnitude of P_{c}; whereas P_{a} and P_{d} are affected by both hydrodynamics and surface forces. It is the balance between the adhesion of a bubble to a particle and the hydrodynamics of the system that determine P_{d}. Coarse particles are expected to detach more easily (10); whereas, for very fine particles, P_d may be neglected (11).

On the other hand, P_a depends on hydrodynamics to provide kinetic energy to the particle in order to overcome the energy barrier, or activation energy (E_a), required for bubble-particle adhesion and can be described by the following relationship (12, 13):

$$P_a = \exp\left(-\frac{E_a}{E_k}\right), \qquad [1.4]$$

where E_k is the kinetic energy of the particle. Figure 1.1 illustrates the interaction energy (V_t) between two macroscopic bodies as predicted from the classical DLVO theory (14, 15),

$$V_t = V_d + V_e, \qquad [1.5]$$

where V_d represents the dispersion interaction energy, and V_e is ion-electrostatic interaction energy. The London-van der Waals dispersion energy (V_d) between a flat and spherical surface is described by the expression

$$V_d = -\frac{A_{132}R}{6H}, \qquad [1.6]$$

in which A_{132} is the Hamaker constant between surfaces **1** and **2** interacting in medium **3**, R is the radius of the sphere, and H is the shortest separation distance. The

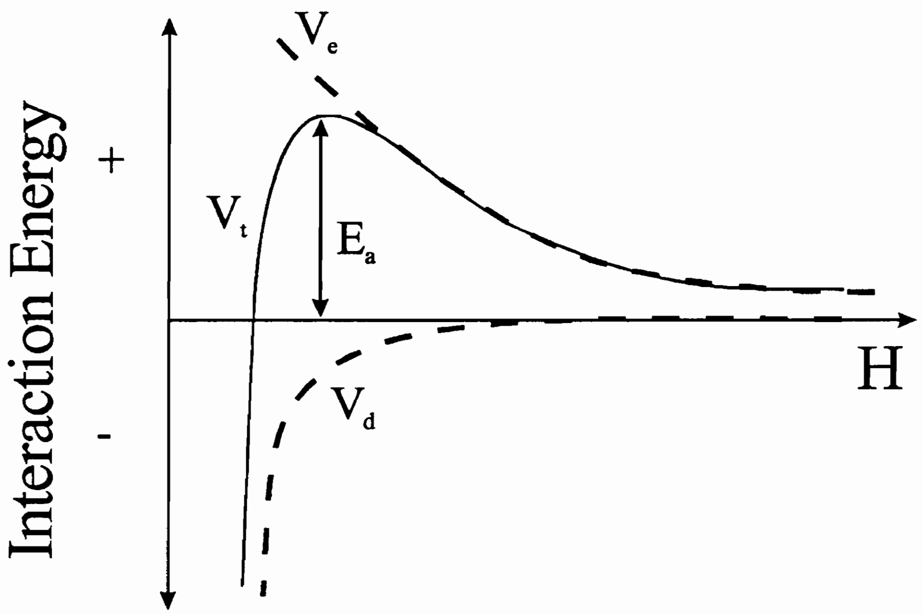

Figure 1.1 Interaction energy between two identical macroscopic bodies as described by the classical DLVO theory (Eq. [1.5]).

interaction energy due to the overlapping of electrical double layers (V_e) is estimated by (16)

$$V_e = \frac{\varepsilon R(\psi_1 + \psi_2)}{4}\left[\frac{2\psi_1\psi_2}{\psi_1^2 + \psi_2^2}\ln\left(\frac{1+e^{-\kappa H}}{1-e^{-\kappa H}}\right) + \ln\left(1 - e^{-2\kappa H}\right)\right], \qquad [1.7]$$

where ψ_1 and ψ_2 are the potentials of surfaces **1** and **2**, ε is the dielectric constant of the medium, and κ is the reciprocal Debye length. However, as Xu and Yoon (17, 18) demonstrated by the spontaneous coagulation of hydrophobized silica particles, Eq. [1.5] does not account for the hydrophobic interaction energy (V_h), and, therefore, the DLVO model must be extended to include a third term,

$$V_t = V_d + V_e + V_h. \qquad [1.8]$$

Ideally, direct force measurements between an air bubble and a hydrophobic solid would provide the data necessary to accurately calculate activation energy and determine P_a. However, attempts to do so (19, 20) failed to quantify the forces involved due to the pliability of the bubble-liquid interface and only reported a long-range attraction attributed to the hydrophobic interaction. Craig *et al* (21, 22) have also provided evidence for the hydrophobic attraction of air bubbles. Water molecules at the air-water interface have been shown to form a similar hydrogen bonding network to that present at a hydrophobic solid-water interface, indicating that air bubbles are indeed hydrophobic (23). Furthermore, Aksoy (24) conducted experiments on the rupture thickness of free films and estimated the hydrophobicity of an air bubble in pure water to be comparable to a solid surface having a contact angle in excess of 90°. For these reasons, it is reasonable to suggest relevant flotation data may be obtained from direct force measurements conducted between solid surfaces in which one surface is sufficiently hydrophobic to simulate an air bubble.

1.2 *Scope of Research*

In the absence of a reliable technique to directly measure the forces acting between a bubble and a mineral surface, it is the objective of this work to explore the possibilities of obtaining useful flotation data from direct force measurements in which a hydrophobized sphere is used in place of an air bubble. In, Chapter 2 a method of preparing a stable well-characterized hydrophobized surface that can be used to model an air bubble is described. Force measurements conducted between surfaces unequally hydrophobized by insoluble surfactant (*i.e.*, asymmetric force measurements) are presented in Chapter 3. A relationship is developed to predict the magnitude of the asymmetric hydrophobic attraction from the results of symmetric measurements. In Chapter 4, the asymmetric force measurements will be applied to a real flotation system by studying the pH effects of an amine collector on measured forces and comparing them to real bubble-particle interactions. Chapters 2, 3, and 4 presented in this study are self-contained in that each consists of an introduction, explanation of experimental methods, details of results, and conclusions.

1.3 *Review of Literature*

1.3.1 Thermodynamics of Particle-Bubble Interactions

From the work of Thomas Young (25) nearly 200 years ago, it is generally accepted that for a liquid drop forming a finite angle on a smooth solid surface, an energy balance can be conducted around the point of three-phase contact. Figure 1.2a depicts this situation in which vectors represent the surface free energy per unit area at the liquid-vapor (γ_{LV}), solid-vapor (γ_{SV}), and solid-liquid (γ_{SL}) interfaces. The angle formed at the three-phase point of contact as measured through the liquid is known as the contact angle (θ). An analogous situation is shown in Figure 1.2b, in which an air bubble is in contact with a solid surface in a liquid medium. An energy balance around the point of three-phase contact yields the Young equation,

$$\gamma_{SL} - \gamma_{LV}\cos\theta = \gamma_{SV}\,. \qquad [1.9]$$

Laskowski (26) has shown that the attachment of a bubble to a mineral particle can similarly be described thermodynamically. Figure 1.3 illustrates the change from the initial state where the particle and bubble exist separately to the final state after

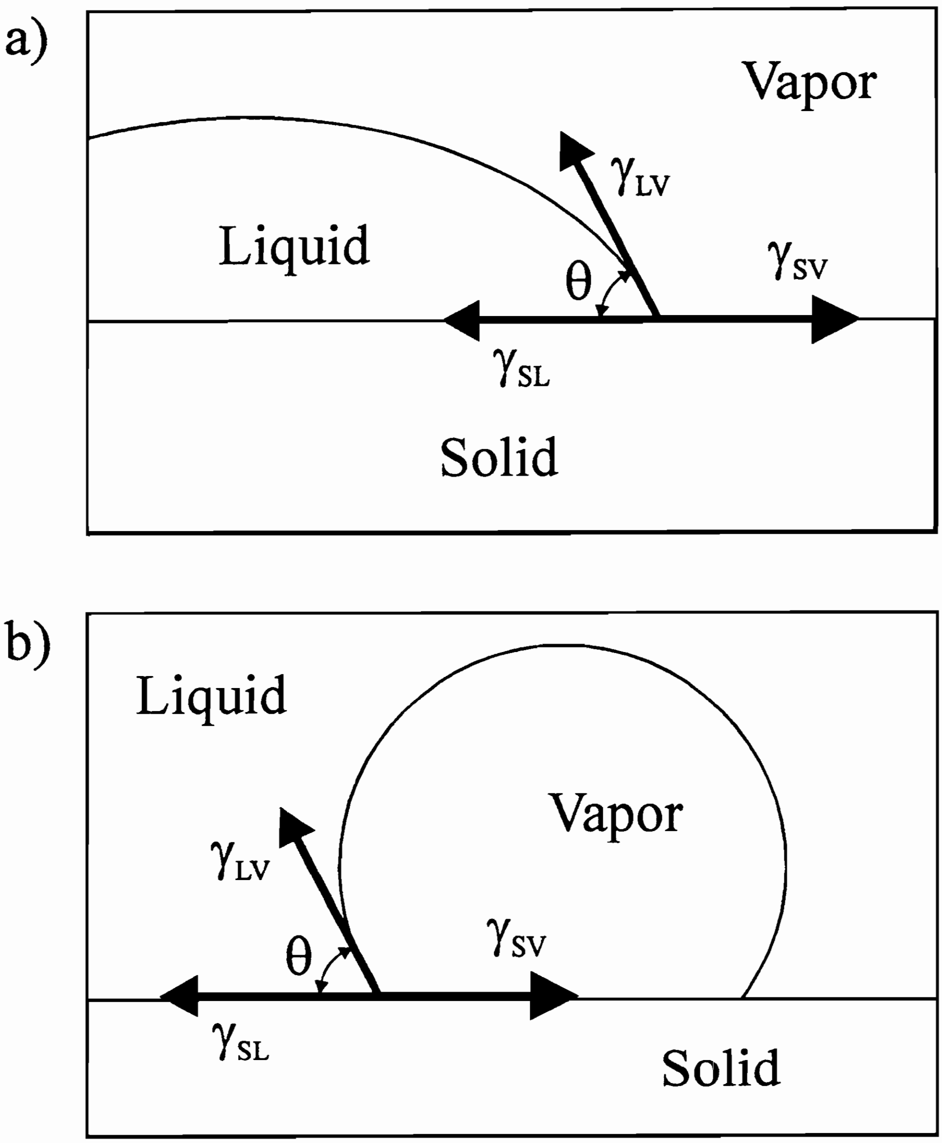
a)
Vapor
Liquid
γ_{LV}
γ_{SV}
θ
γ_{SL}
Solid
b)
Liquid
Vapor
γ_{LV}
θ
γ_{SV}
γ_{SL}
Solid

Figure 1.2 The energy balance around the point of three-phase contact for a) a liquid droplet on a solid surface and b) an air bubble attached to a solid surface in a liquid medium.

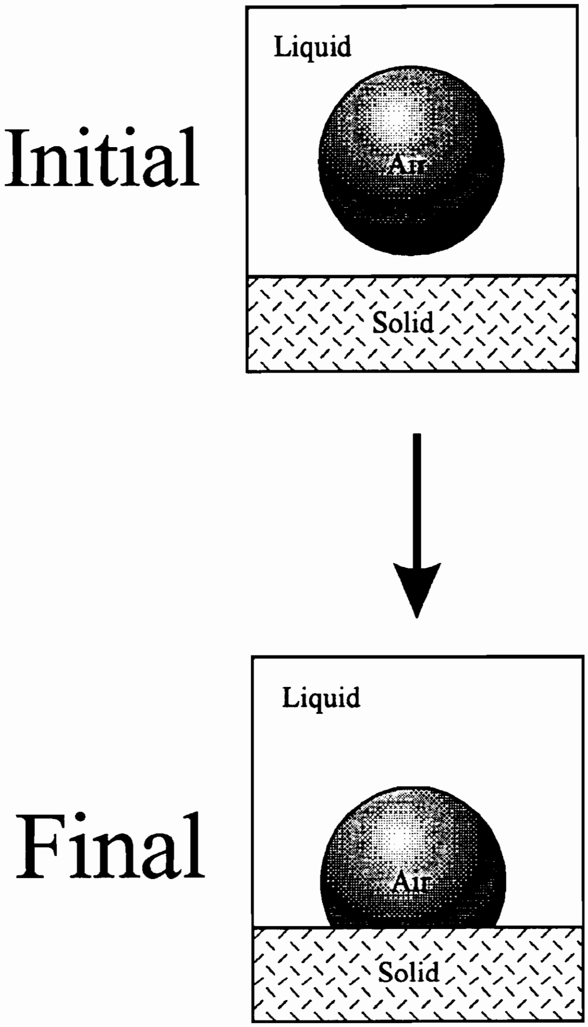
Initial
Liquid
Air
Solid
Final
Liquid
Air
Solid

Figure 1.3 Initial and final states of bubble-particle attachment in flotation.

attachment has taken place. The change in free energy (ΔG) can then be described as

$$\begin{aligned}\Delta G &= G_{\mathrm{f}} - G_{\mathrm{i}} \\ &= \gamma_{\mathrm{SL}} - \gamma_{\mathrm{SV}} - \gamma_{\mathrm{LV}}.\end{aligned} \qquad [1.10]$$

Substituting Young's equation, Eq. [1.9], into Eq. [1.10] produces the following simplified thermodynamic equation describing flotation criteria:

$$\Delta G = \gamma_{\mathrm{LV}}(\cos\theta - 1). \qquad [1.11]$$

Thus, it can be seen that for particle-bubble attachment to be favorable ($\Delta G < 0$), contact angle must have a finite value. Typically, values of contact angles must exceed 50° to successfully float a mineral particle (27).

Since larger contact angles are conducive to particle-bubble attachment, one can rearrange Eq. [1.9] to illustrate a fundamental principle of mineral flotation with

$$\cos\theta = \frac{\gamma_{\mathrm{SV}} - \gamma_{\mathrm{SL}}}{\gamma_{\mathrm{LV}}}. \qquad [1.12]$$

To improve the probability of a particle being floated, *i.e.*, increasing contact angle, one needs to increase the difference between the surface energy of the solid (γ_{SV}) and the surface energy, or surface tension, at the liquid-vapor interface (γ_{LV}). Pure water has a very high surface tension (= 72.8 mN/m), and the addition of surfactants such as collectors and frothers tend to reduce γ_{LV}. On the other hand, values of γ_{SV} for high energy mineral surfaces such as silica ($\gamma_{\mathrm{SV}} \approx 120$ mN/m) (28) can also be reduced by the adsorption of surfactant, which is known as "hydrophobizing" the mineral surface.

1.3.2 Modification of Silica Surfaces

In order to understand how a silica surface can be rendered hydrophobic, it is necessary to under stand the surface chemistry of bare silica surfaces. Crystalline silica consists of silicon atoms tetrahedrally bonded to four oxygen atoms. A freshly exposed surface will no doubt break some of these bonds, and the surface silicon atoms will react with water to form hydroxyl groups (OH^-) on the surface. Infrared studies (29) have shown these hydroxyl groups exist as free hydroxyl groups or vicinal hydroxyl groups. Hair and Hertl (30) reported that these free hydroxyl groups account for most surfactant adsorption. On the other hand, the hydrogen-bonded, vicinal hydroxyl groups have a propensity to physisorb multilayers of water. Typically, there are 4 to 5 hydroxyl groups/nm^2 (30) of which 30% are free hydroxyl groups (31).

The amount and nature of the hydroxyl groups on the silica surface can be manipulated by temperature adjustment, resulting in a simple and somewhat reversible method of controlling the hydrophobicity of the silica surface (29). Figure 1.4 shows that at room temperature, a hydrated silica surface will have both free hydroxyl groups and hydrogen-bonded hydroxyl groups on which water is physisorbed. Heating to 150°C reversibly dehydrates the surface. Between 170 and 400°C, the vicinal hydroxyl groups are replaced by siloxane bridges between surface silicon atoms. The process is

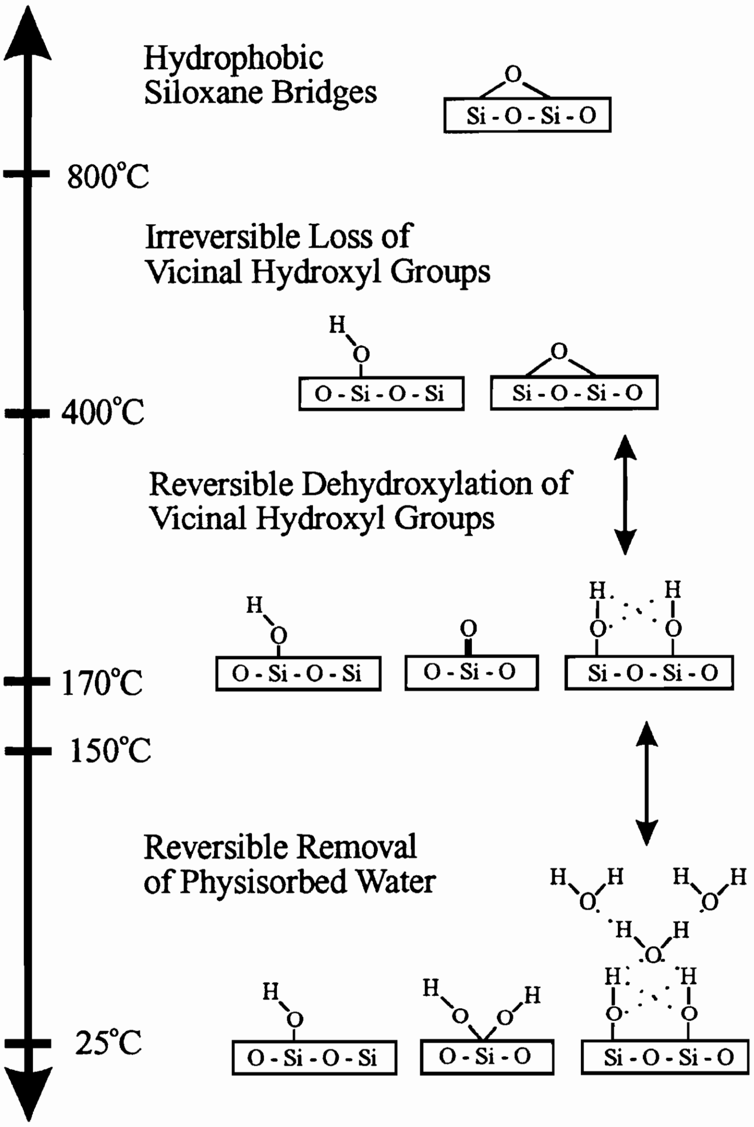
Hydrophobic Siloxane Bridges
800°C
Irreversible Loss of Vicinal Hydroxyl Groups
400°C
Reversible Dehydroxylation of Vicinal Hydroxyl Groups
170°C
150°C
Reversible Removal of Physisorbed Water
25°C
Si - O - Si - O
O - Si - O - Si
O - Si - O
H
O

Figure 1.4 The effect of temperature on the surface of hydrated silica.

reversible and rehydroxylation occurs as temperature is decreased. Above 400°C, however, dehydroxylation of the vicinal groups is irreversible, and only isolated hydroxyl groups exist on the surface. Further heating removes the remaining free hydroxyl groups, and the surface consists of only hydrophobic siloxane bridges exhibiting a contact angle of more than 40° (32).

1.3.2.1 *Silica Silanation*

The presence of free hydroxyl groups on the silica surface allows chemisorption of hydrophobic alkylchlorosilanes. The silanation reaction is believed to proceed in several parts (33), the first of which involves hydrolysis of the alkylchlorosilane to an alkylsilanol as follows:

$$R_3SiCl + H_2O \rightarrow R_3SiOH + HCl\,. \qquad [1.13]$$

As the alkylsilanol approaches the silica surface, hydrogen bonds are formed between the surface hydroxyl groups as a prelude to the formation of strong chemical bonds to the surface silicon atoms (Si_S) as indicated in the following:

$$Si_SOH + R_3SiOH \rightarrow R_3SiOSi_S + H_2O\,. \qquad [1.14]$$

The previous reactions can been carried out on silica surfaces using mono- (R_3SiCl), di- (R_2SiCl_2), and tri- ($RSiCl_3$) functional alkylchlorosilanes (34). Depending on the functionality of the silane head group and the length of the hydrocarbon chains, the surface energy of silica can be lowered to as much as 23 mN/m^2 (35), corresponding to a water contact angle of 112° (36).

Octadecyltrichlorosilane (OTS), $CH_3(CH_2)_{17}SiCl_3$, is a popular silanating agent because of its tendency to form stable hydrophobic monolayer films (37). One of the reasons for this is that tri-functional alkylchlorosilanes form strong covalent bonds with one another. This cross-linking polymerization step,

$$\mathrm{RSi(OH)_3 + RSi(OH)_3 \rightarrow RSi(OH)_2 - O - (OH)_2SiR + H_2O}, \qquad [1.15]$$

is believed to occur prior to chemisorption (33), *i.e.*, between Eq. [1.13] and [1.14]. Some investigators (38-40) have proposed that by performing the reaction in an anhydrous solvent, hydrolysis will occur with physisorbed water at the silica surface prior to chemisorption. The adsorbed alkylsilanol molecules can then cross-polymerize to form a robust, interlocking monolayer. Regardless of the reaction mechanism order, it is quite clear that the presence of water in the system strongly influences the reaction. A recent study (39) proposed that the OTS molecules do not react with the surface silanol groups at all but form cross-linked monolayers on the physisorbed water present on the hydrated silica surface. FTIR measurements of OTS adsorbed on silica reported by Tripp and Hair (41) found no evidence for interaction of the alkylsilane with surface silanol groups.

1.3.2.2 *Amine Adsorption and Flotation*

The hydroxyl ions that adsorb on silica in water impart a negative charge on the surface which can be controlled by adjusting pH. Below pH 3, the silica surface has a positive charge, but as pH is raised, thus increasing the concentration of OH^- ions in solution, the surface reverses charge, reaching its most negative value near pH 10 (28). The negative charge of silica and many silicate minerals in water makes it possible to adsorb cationic surfactants such those formed by the dissolution of alkylammonium salts (42). The most common reagent used for flotation of silicate minerals is a dodecylammonium salt such as dodecylamine hydrochloride (DAHCl) (5). The flotation of silica using DAHCl is a complex chemical process in that the adsorption of collector at the solid liquid and liquid-vapor interfaces has been shown to be dependent on pH, not only because of its effect on the surface potential of silica but also the solution chemistry of the collector (43). Figure 1.5 illustrates the correlation between flotation recovery, contact angle, surfactant surface coverage, and zeta-potential for quartz in $4x10^{-5}$ M dodecylammonium salt solution (44). Numerous studies of the quartz-amine flotation system have shown that maximum recovery is achieved in the pH range of 8 to 10 (43-50). An early study by de Bruyn (51) showed that the adsorption of amine on quartz under acidic conditions is relatively low; at alkaline pH, however, adsorption increases sharply, believed to be caused by the adsorption of both

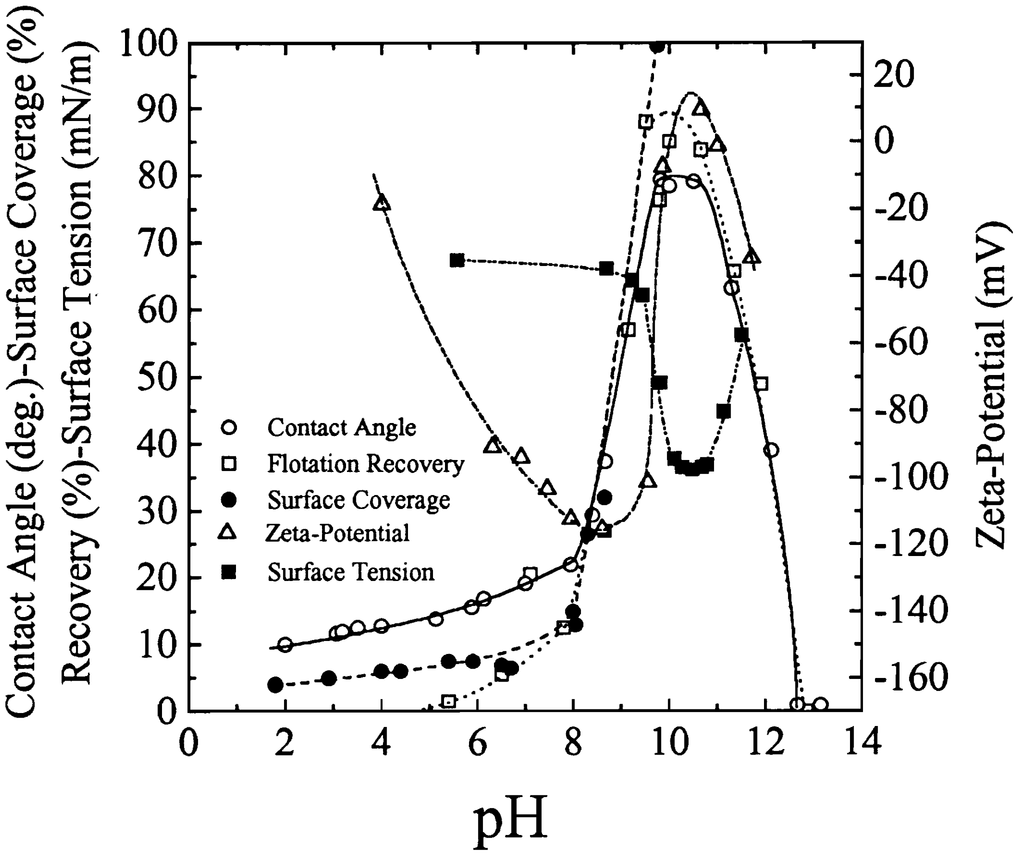

Figure 1.5 The correlation between flotation recovery, contact angle, surface coverage, zeta-potential for quartz in 4x10^{-5} M dodecylamine solution as a function of pH [from Fuerstenau (44)]. Also shown if the pH dependence of surface tension at the liquid-vapor interface [from Castro *et al.* (116)].

cationic and neutral collector species (47, 52). Figure 1.6 depicts the distribution of collector species as a function of pH in 4×10^{-5} M DAHCl solution based on the thermodynamic data of Ananthpadmanabhan *et al.* (45). Gaudin and Fuerstenau (52) proposed that the adsorption of alkylammonium ions on a silica surface is enhanced by the adsorption of neutral amine molecules also present in solution at alkaline pH. Their hypothesis considered that the repulsive electrostatic force between the ionic head groups of the surfactant would be reduced by neutral amine molecules adsorbing in between alkylammonium ions. Furthermore, at concentrations two orders of magnitude less than that of bulk micelle formation (indicated by the dotted line in Figure 1.6), it was suggested that RNH_3^+ ions and RNH_2 molecules form hemimicelles at the solid-liquid interface forming hydrophobic patches of collector on the silica surface. Novich and Ring (48) have used the pH values at which the concentration of RNH_3^+ ions exceeds 0.01 CMC as the upper and lower limits of their flotation model.

Somasundaran (47) has proposed that amine adsorption and, consequently, flotation recovery increase due to the presence of an ionomolecular species, $(RNH_2\text{-}RNH_3)^+$, in solution similar to that described by Kung and Goddard (53). Such a complex is expected to be highly surface active due to its large molecular size and might assume a configuration in which the hydrocarbon chains are intertwined with one another to minimize the surface area exposed to the aqueous solution, and the polar

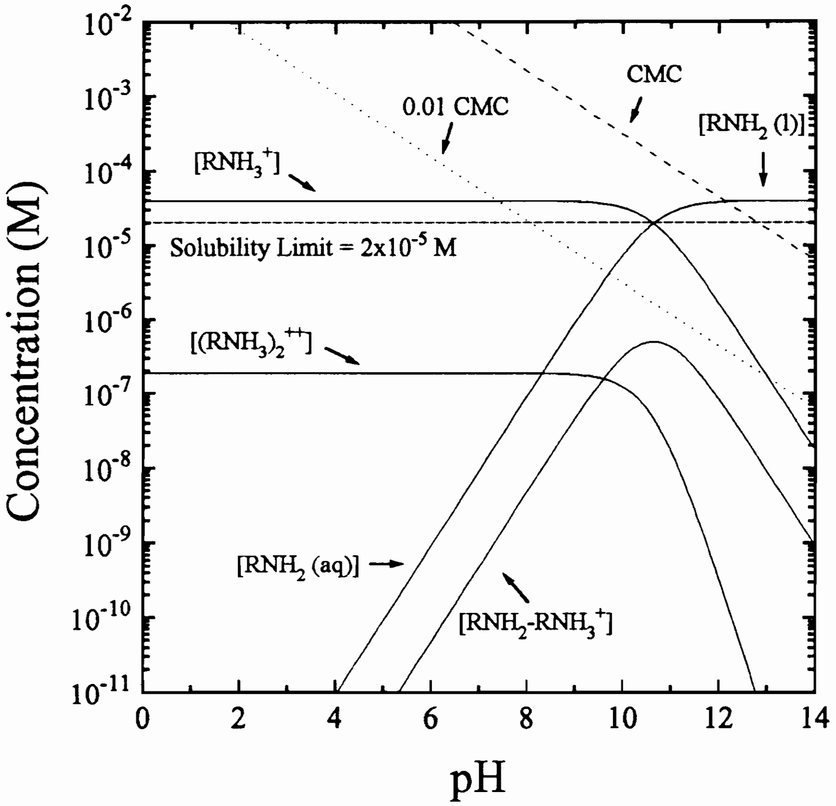

Figure 1.6 A distribution diagram of collector species in $4x10^{-5}$ M DAHCl solution as a function of pH. Curves were determined from the thermodynamic data of Ananthpadmanabhan *et al.* (45). Also included are the critical micelle concentration data of Watson and Manser (118).

head groups are situated side by side (54). Based on thermodynamic data of fatty acids (55), the maximum concentration of this ionomolecular complex was estimated to coincide the pH range of maximum flotation recovery of quartz in DAHCl (45).

1.3.3 Surface Forces

1.3.3.1 *Derjaguin Approximation*

It is possible to compare the results of theoretical interaction energy calculations made between macroscopic spherical surfaces to direct force measurements through the use of the Derjaguin Approximation (56). Derjaguin proposed that the total forces ($F_{sp\text{-}sp}$) acting between two spheres as a function of separation distance (H) is related to the interaction energy between two flat plates ($E_{fl\text{-}fl}$) as follows:

$$F_{sp-sp}(H) = 2\pi\left(\frac{R_1 R_2}{R_1 + R_2}\right)E_{fl-fl}(H), \qquad [1.16]$$

where R_1 and R_2 are the radii of the spheres. The implication of Eq. [1.16] is that it allows the conversion of interaction energies and forces for a number of known geometries, thus enabling direct force measurement techniques to be developed utilizing these geometries, as shown in Figure 1.7 (57).

$F_{x\text{-}x} = -\dfrac{dE_{x\text{-}x}}{dH}$	Sphere-Sphere 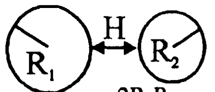 $R_{sp} = \dfrac{2R_1R_2}{R_1+R_2}$	Cylinder-Cylinder 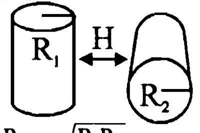 $R_{cyl} = \sqrt{R_1R_2}$	Sphere-Flat 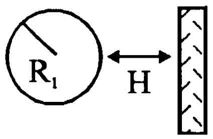
Flat-Flat 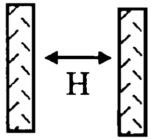	$E_{fl\text{-}fl} = \dfrac{1}{\pi R_{sp}} F_{sp\text{-}sp}$ $F_{fl\text{-}fl} = \dfrac{-1}{\pi R_{sp}} \dfrac{dF_{sp\text{-}sp}}{dH}$	$E_{fl\text{-}fl} = \dfrac{1}{2\pi R_{cyl}} F_{cyl\text{-}cyl}$ $F_{fl\text{-}fl} = \dfrac{-1}{2\pi R_{cyl}} \dfrac{dF_{cyl\text{-}cyl}}{dH}$	$E_{fl\text{-}fl} = \dfrac{1}{2\pi R} F_{sp\text{-}fl}$ $F_{fl\text{-}fl} = \dfrac{-1}{2\pi R} \dfrac{F_{sp\text{-}fl}}{dH}$
Sphere-Flat	$E_{sp\text{-}fl} = \dfrac{2R}{R_{sp}} E_{sp\text{-}sp}$ $F_{sp\text{-}fl} = \dfrac{2R}{R_{sp}} F_{sp\text{-}sp}$	$E_{sp\text{-}fl} = \dfrac{R}{R_{cyl}} E_{cyl\text{-}cyl}$ $F_{sp\text{-}fl} = \dfrac{R}{R_{cyl}} F_{cyl\text{-}cyl}$	
Cylinder-Cylinder	$E_{cyl\text{-}cyl} = \dfrac{2R_{cyl}}{R_{sp}} E_{sp\text{-}sp}$ $F_{cyl\text{-}cyl} = \dfrac{2R_{cyl}}{R_{sp}} F_{sp\text{-}sp}$		

Figure 1.7 The relationship of interaction energies and surface forces based on the Derjaguin approximation for a number of well-known geometries (56, 57).

1.3.3.2 Direct Force Measurement Techniques

The most common method used to directly measure forces between solid surfaces in a liquid is that of the surface force apparatus (SFA) as developed by Israelachvili and Adams (58) from the work of Tabor and Winterton (59). A schematic of the apparatus is provided in Figure 1.8. The measurement is conducted between two curved surfaces (usually mica) offset by 90°, *i.e.*, crossed-cylinder geometry, where one is mounted on a piezo-electric crystal and the other on a weak adjustable spring. White light is directed through the surfaces, and fringes are produced which are used to monitor the separation distance between the surfaces with an accuracy of 0.1 nm. The observed forces are calculated from the deflection of the spring as the surfaces approach one another. Large forces can be measured by increasing the stiffness of the spring. Though the SFA has been used to measure forces between mica and, recently, silica (60) surfaces, it is limited to solid substrates that are optically transparent and can be easily mounted on the curved discs used in the apparatus.

The development of the atomic force microscope (AFM) in 1985 (61) provided a simpler technique to directly measure surface forces. Ducker *et al.* (62) were the first to measure forces between macroscopic bodies using the AFM, when they adhered a glass microsphere to the cantilever and measured forces between the sphere and a flat silica surface in water. The technique is shown schematically in Figure 1.8. The

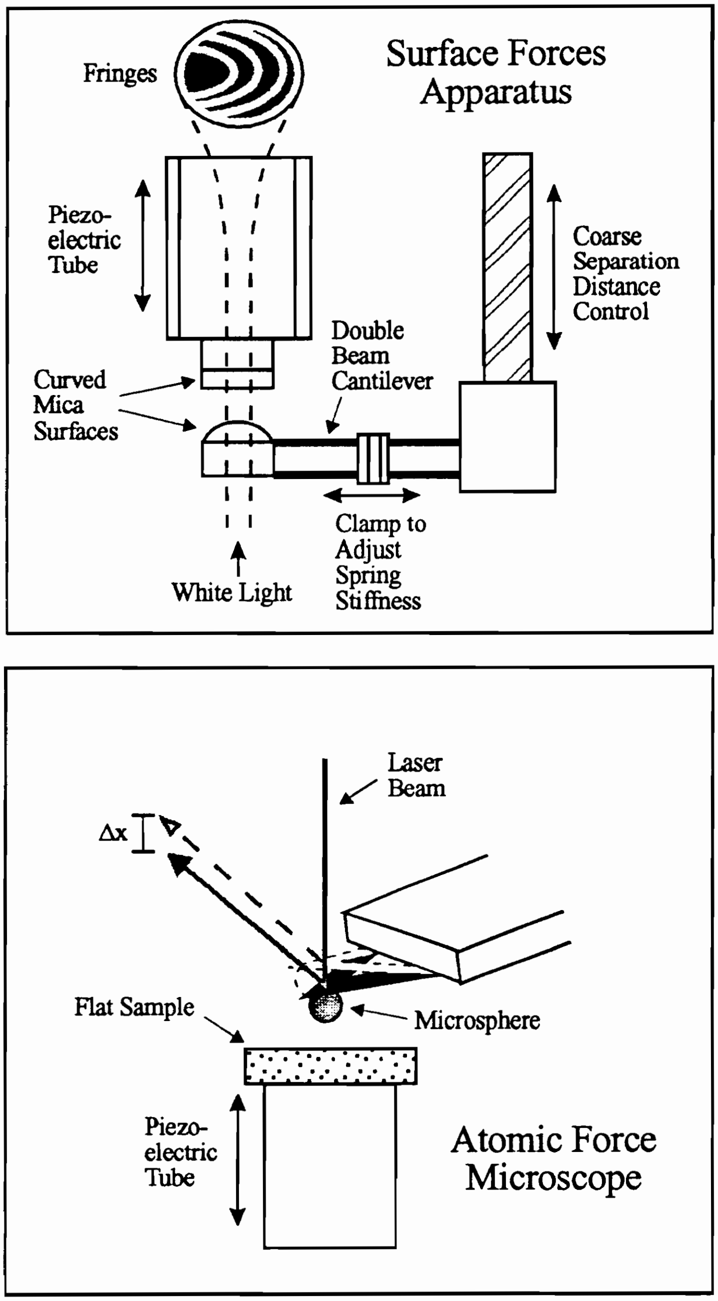
Fringes
Surface Forces Apparatus
Piezo-electric Tube
Coarse Separation Distance Control
Double Beam Cantilever
Curved Mica Surfaces
Clamp to Adjust Spring Stiffness
White Light
Laser Beam
Δx
Flat Sample
Microsphere
Piezo-electric Tube
Atomic Force Microscope

Figure 1.8 Schematic representations of the surface forces apparatus (SFA) and atomic force microscope (AFM) techniques of direct force measurements between solid surfaces.

microsphere is attached to the tip of a cantilever which is mounted directly above the flat sample. Light emitted from a laser diode is reflected off the back of the cantilever into a split photo diode detector. A piezo-electric crystal moves the sample towards the sphere, and any ensuing deflection of the cantilever due to surface forces is monitored by the detector. One of the great advantages of this technique over the SFA is that the solid samples need not be optically transparent which allows direct force measurement between a great number of materials, the only criteria being that the samples must be smooth and available in spherical form. Recent investigations have successfully measured forces between polypropylene (63), gold (62, 64), zirconia (65), titanium oxide (66), and zinc sulfide (67) surfaces. One of the biggest drawbacks of the AFM technique is that the stiffness of the spring cannot be adjusted *in situ* such as with the SFA. Instead, different cantilevers must be used to attain various levels of sensitivity; furthermore, these cantilevers must be calibrated separately from the force measurements. Methods used for calibration include estimation from elasticity modulus (63, 68-71), resonant frequency (19, 20, 64, 68, 71-73), and deflection due to an applied load (20, 65, 66, 69, 70, 74).

Another novel technique, developed by Parker *et al.* (75, 76), is a modification of the SFA in which the spring is replaced by a cantilever composed of two pieces of piezo-electric material called a bimorph. Calibration of the bimorph allows determination of force as well as surface separation. Other techniques, such as the interaction between crossed silica fibers by Rabinovich *et al.* (77, 78) and the force balance of Peschel *et al.* (79), have also been employed to directly measure forces between surfaces.

1.3.3.3 *Hydrophobic Force*

In 1982, Israelachvili and Pashley (80, 81) showed that direct force measurements between mica surfaces in cetyltrimethylammonium bromide (CTAB) solution could not be explained by the classical DLVO theory (14, 15) which accounts for the London-van der Waals dispersion forces and the ion-electrostatic force resulting from the overlap of electrical double layers. The authors observed an additional attractive force which they attributed to the hydrophobic interaction between the surfactant-coated surfaces and reported that this hydrophobic force (F_h) could be described with an exponential relationship (80, 81),

$$\frac{F_h}{R} = -C_o \exp\left(\frac{-H}{D_o}\right), \qquad [1.17]$$

where R is the effective radius of the curved mica surfaces, H is the separation distance, C_o is a constant (= -140 mN/m) , and D_o is the decay length (= 1.0 ± 0.1 nm). Subsequent measurements of mica surfaces in surfactant solutions have produced comparable decay length values ranging from 1.0 to 2.5 nm (82-85). Force measurements conducted between surfaces on which surfactant has been adsorbed by Langmuir-Blodgett (LB) deposition (86-92) or silanation (69, 78, 93, 94) have resulted in hydrophobic forces that are up to 4 orders of magnitude stronger than those previously measured. To account for this long-range hydrophobic force, a double exponential expression is often used,

$$\frac{F_{\mathrm{h}}}{R} = -C_1 \exp\left(\frac{-H}{D_1}\right) - C_2 \exp\left(\frac{-H}{D_2}\right), \qquad [1.18]$$

in which the first exponential term is used to describe a short-range hydrophobic force, and the second exponential term is included when considering a long-range hydrophobic force. Though no long-range hydrophobic forces have been detected between surfaces on which ionic surfactant has self-assembled, a recent study (84, 95) has reported long-range hydrophobic force for self-assembled layers of ionic surfactant in the presence of neutral surfactant, indicating that the length and packing density of the hydrocarbon chains adsorbed on the surfaces greatly influences the range of the force. (92, 96). The hydrophobic force can also be described by a power law (88, 97),

$$\frac{F_{\mathrm{h}}}{R} = -\frac{K}{H^2}, \qquad [1.19]$$

where K is the hydrophobic force parameter. The use of Eq. [1.19] is sometimes preferred because it has only one unknown parameter which can be directly compared to the Hamaker constant (A) for the London-van der Waals dispersion forces.

1.3.3.4 *Current Theories of Hydrophobic Attraction*

The fact that Eqs. [1.17] - [1.19] are purely empirical relationships to describe the hydrophobic force has led many investigators to explore the origin of the hydrophobic force. In fact, over the past decade since the presence of the force was first detected, numerous studies have focused on how the hydrophobic force responds to changes in conditions in order to disprove current theories; however, the results have been somewhat inconsistent and even contradictory. An increase of electrolyte concentration seems to have a deleterious effect on the long-range hydrophobic force in several studies (89-91, 98, 99), but the absence of this effect between polypropylene surfaces (63) and fluorosilanated surfaces (100) as well as concern for the degradation of LB monolayers in the presence of electrolyte (89-91) provide some uncertainty. Craig *et al.* (21, 22) have shown that hydrophobic attraction is decreased by some electrolytes while unaffected by others. A study on the effect of temperature (92) found that an increase from 25° to 50°C also reduced the attractive strength of the hydrophobic force between LB deposited surfactant films on mica; whereas, a study of silanated surfaces shows an increase in attraction at elevated temperature (100). Measurements conducted in de-aerated water (63, 93) had little if any effect on the hydrophobic attraction; however, a study conducted with argon-saturated water resulted in an increase in the hydrophobic force (93). Parker and Claesson (101) studied the effect of water-ethylene glycol mixtures on the hydrophobic force and found that water must constitute less than 50% of the medium between the surfaces to significantly decrease the hydrophobic attraction.

Several theories have evolved over the past decade to provide explanations of the origin of the hydrophobic force and tend to fall into three groups: a solvent structure effect, a solvent density effect, and an electrostatic correlation effect (99). One theory proposes that the hydrophobic attraction is caused by a change in entropy brought about by the ordering of water molecules between two hydrophobic surfaces (102). Though, water molecules have been shown to orient in a more crystalline-like configuration near a hydrophobic surface (23), the ordering is thought to propagate, at most, only 0.7 to 1.0 nm into the bulk medium (103). Thus, the rearrangement of water molecules can only explain short-range hydrophobic forces and, in fact, has provided theoretical basis for Eq. [1.17] (50, 104).

It has also been proposed that instabilities of thin water films between hydrophobic surfaces cause the spontaneous formation of a vapor bridge. Though, large vapor cavities have been observed between surfaces in contact (87, 105), no studies have reported the formation macroscopic vapor cavities between surfaces initially approaching one another. However, Parker *et al.* (100) have reported small steps in a hydrophobic force curve which they attribute to the bridging of submicroscopic vapor cavities present on the hydrophobic surfaces. Ruckenstein and Churaev (106) suggested that a thin vacuum gap exists between a hydrophobic surface and water at the solid-liquid interface and that fluctuations of this layer correlate with those on the opposing hydrophobic surface to produce a long-range attraction. Yushchenko *et al.* (107) determined cavitation to be thermodynamically favorable only when the receding contact angle of the hydrophobic surfaces exceeds 90°; however, Yaminsky and Ninham (108) proposed that voids created between water molecules near hydrophobic surfaces due to lateral thermal fluctuation may align themselves to form a vapor bridge between surfaces whose contact angle is less than 90°. It is generally agreed that cavity formation would be enhanced at higher temperatures due to a decrease in the solubility of gases in solution and result in a greater attractive force; however, experimental evidence has shown the contrary (92). Also, the effect of solvent on cavitation is expected to be more significant than that reported by Parker and Claesson (101).

Several theories have been developed suggesting that the hydrophobic force is electrostatic in nature. Attard (109) proposed that unusual polarization of the water molecules near hydrophobic surfaces possibly due to density fluctuations can correlate to produce a long-range attraction. Podgornik (110) suggested that the hydrophobic force is due to a fluctuating electric field produced by laterally mobile ions specifically adsorbed at the solid-liquid interface. It was also suggested that ordered domains present in adsorbed surfactant films form in-plane dipole moments producing electric fields that penetrate through the thin aqueous film at a distance governed by domain size and spacing (93, 96, 99). However, each of these electrostatic theories predict that the hydrophobic force should decay at half the Debye screening length of the electrolyte present in solution, which has been contradicted experimentally (63, 91, 100).

Yoon and Ravishankar (95) have pointed out that the decay length of the hydrophobic force increases sharply when the contact angle of the surfaces involved is greater than 90°, indicating that short-range and long-range hydrophobic forces may be caused by separate mechanisms. These authors suggest that long-range forces occurring when $\theta > 90°$ may be caused by cavitation or the large dipoles caused by increased hydrocarbon chain packing of surfactant domains on the solid surfaces.

1.3.3.5 *Asymmetric Force Measurements*

To date, the vast majority of direct force measurements have been conducted between identical surfaces. However, many interactions occurring in nature, including flotation, involve dissimilar surfaces, and there has been some interest in conducting measurements between asymmetric surfaces (20, 93, 94, 99, 100, 111). Claesson *et al.* (111) measured forces in water between a bare mica surface and a mica surface having a LB film of dimethyldioctylammonium (DDOA$^+$) ions and reported an attraction stronger than that observed between two DDOA$^+$-coated mica surfaces. The authors suggested that the force was due to electrostatic attraction between the negatively charged mica surface and the positively charged DDOA$^+$-coated surface. Tsao *et al.* (99), however, stated that the ion-electrostatic double layer force between these surfaces is repulsive, citing negative surface potentials for both bare mica and DDOA$^+$-coated mica as evidence. Thus, these authors proposed that the large attraction is a non-DLVO force caused by dipoles formed by surfactant domains correlating with induced dipoles on the bare mica surface. Subsequent measurements (93, 94, 100) conducted between a hydrophobic silanated surface and a hydrophilic surface have reported only slight short-range deviations from the classical DLVO theory. Ducker *et al.* (20), on the other hand, observed a large unstable attraction between silanated glass and a clean silica surface at separations up to 75 nm.

1.3.3.6 *Force Measurements in DAHCl Solutions*

Several force direct measurements have been conducted between mica surfaces (80, 82-85, 95, 112-115) and glass surfaces (116) in alkylammonium salt solutions, and a few involve DAHCl (83, 84, 95, 113-115). Studies investigating the effect of DAHCl concentration on the forces measured between mica surfaces at neutral pH (83, 84, 95) have shown that sparsely-packed monolayers form on mica in dilute DAHCl solutions near 10^{-5} M, which become more densely-packed with increasing concentration. However, RNH_3^+ ions also adsorb on the surfactant layer with their polar head groups oriented toward the bulk solution. A stable bilayer is believed to be complete near $3x10^{-3}$ M DAHCl (83). The presence of short-range hydrophobic forces ($D_1 < 1.4$ nm) have been reported for measurements conducted between mica surfaces in 10^{-6} to 10^{-3} M DAHCl solutions (83, 84, 95).

The pH dependence of surface forces has been investigated by Rutland *et al.* (113) and Yoon and Ravishankar (115). These authors observed that at low pH, where only minimal amounts of RNH_3^+ ions adsorb on the surface, the forces are repulsive at long-range and show at most only a short-range hydrophobic attraction. Under slightly alkaline conditions near pH 9.5, a long-range hydrophobic force is detected, presumably due to the coadsorption of dodecylammonium ions and neutral dodecylamine molecules (115). A further increase in pH leads to the formation of bulk amine precipitate (117) and results in a steric repulsion as the precipitate deposits on the mica surfaces (115).

Herder (114) conducted force measurements between two hydrophobic DDOA$^+$-coated mica surfaces in DAHCl solutions. The long-range hydrophobic force present between these surfactant-coated surfaces in pure water was significantly decreased in the presence of DAHCl. The effect was more pronounced at higher surfactant concentrations, indicating that the dodecylamine adsorbs in reverse orientation on the DDOA film and diminishes the hydrophobicity of the surface (114). Elton (119) reported that hydrophobic surfaces in dodecyltrimethylammonium bromide (DTAB) become more hydrophilic due to the adsorption of surfactant molecules in an inverse orientation in which the polar head groups are directed towards the bulk solution. Rupprecht (120) found similar results and noted that the hydrophilic bilayer becomes more closely-packed, and therefore more hydrophilic, in the presence of electrolyte due to a reduction in the electrostatic repulsion between polar head groups. Likewise, Yoon and Ravishankar (84) suggested that the reduction of lateral repulsion between ionic head groups can also be achieved by adding nonionic surfactant. As a result, inverted molecules in an interdigitated flip-flop layer may form a close-packed hydrophilic bilayer (84, 121, 122).

In general, while the presence of dodecylammonium salts imparts hydrophobicity on high surface energy substrates such as silica and mica, it has a deleterious effect on the hydrophobic force between two non-wetting surfaces (114). One may suggest that this situation is analogous to the flotation process in that quartz becomes hydrophobic in surfactant solutions under the correct conditions; whereas, an air bubble may be considered more hydrophilic due to the adsorption of amphiphilic molecules at the liquid-vapor interface.

1.4 REFERENCES

1. Gaudin, A. M., “Flotation”, MacGraw-Hill, New York, 1932.
2. Crabtree, E. H., and Vincent, J. D., *in* “Froth Flotation, 50th Anniversary Volume” (D. W. Fuerstenau, Ed.) Chapter 3. AIME, New York, 1962.
3. Schulze, H. J., “Physico-chemical Elementary Processes in Flotation”, Elsevier, New York, 1984.
4. Hines, P. R., *in* “Froth Flotation, 50th Anniversary Volume” (D. W. Fuerstenau, Ed.) Chapter 1. AIME, New York, 1962.
5. Leja, J. “Surface Chemistry of Froth Flotation”, Plenum Press, New York, 1982.
6. Yoon, R.-H., Proceedings, 2nd Int. Sym. on East Asian Resources Recycling Tech. Seoul, Korea, 14-16 October 1993.
7. Luttrell, G. H., and Yoon, R.-H. *in* “Beneficiation of Phosphate: Theory and Practice”, Proceedings of the Engineering Foundation Conference, Palm Coast, Florida, 1993. Chapter 37.
8. Sutherland, K. L., *J. Phys. Chem.* **52**, 394 (1948).
9. Yoon, R.-H., and Luttrell, G. H., *Miner. Proc. Extract. Metall. Rev.* **5**, 101 (1989).

10. Yoon, R.-H., and Mao, L., *J. Colloid Interface Sci.* Accepted.

11. Dobby, G. S., and Finch, J. A., *J. Colloid Interface Sci.* **109**, 493 (1986).

12. Luttrell, G. H., and Yoon, R.-H. *J. Colloid Interface Sci.* **154**, 129 (1992).

13. Yoon, R.-H., *Aufbereitungs-Technik* **32**, 474 (1991).

14. Derjaguin, B. V., and Landau, L., *Acta. Physiochim. URSS* **14**, 633 (1941).

15. Verwey, E. J. W., and Overbeek, J. Th. G., "Theory of Stability of Lyophobic Colloids", Elsevier, Amsterdam, 1948.

16. Hogg, R., Healy, T. W., and Fuerstenau, D. W., *Trans. Faraday Soc.* **62**, 1638 (1966).

17. Xu, Z., and Yoon, R.-H., *J. Colloid Interface Sci.* **132**, 532 (1989).

18. Xu, Z., and Yoon, R.-H., *J. Colloid Interface Sci.* **134**, 427 (1990).

19. Butt, H.-J., *J. Colloid Interface Sci.* **166**, 109 (1994).

20. Ducker, W. A., Xu, Z., Israelachvili, J. N., *Langmuir* **10**, 3279 (1994).

21. Craig, V. S. J., Ninham, B. W., and Pashley, R. M., *J. Phys. Chem.* **97**, 10192 (1993).

22. Craig, V. S. J., Ninham, B. W., and Pashley, R. M., *Science* **364**, 317 (1993).

23. Du, Q., Freysz, E., and Shen, Y. R., Science 264, 826 (1994).

24. Aksoy, B. S., Ph.D. Dissertation, Mining and Minerals Engineering, Virginia Polytechnic Institute and State University, Blacksburg, Virginia, 1996.

25. Young, T., *Phil. Trans. Roy. Soc. London* **95**, 65 (1805).

26. Laskowski, J. *in* "Advances in Mineral Processing" (P. Somasundaran, Ed.) Chapter 11. AIME, Littleton, CO, 1986.

27. Shaw, D. J. "Introduction to Surface and Colloid Chemistry, 3rd Ed.", Butterworths, Boston, 1989.

28. Iler, R. K. "The Chemistry of Silica", Wiley-Interscience, New York, 1979.

29. Hair, M. L. "Infrared Spectroscopy in Surface Chemistry", Marcel Dekker, New York, 1967.

30. Hair, M. L., and Hertl, W., *J. Phys. Chem.* **73**, 4269 (1969).

31. Armistead, C. G., Tyler, A. J., Hambleton, F. H., Mitchell, S. A., and Hockey, J. A., *J. Phys. Chem.* **73**, 3947 (1969).

32. Lamb, R. N., and Furlong, D. N., *Trans. Faraday. Soc. Trans. I* **78**, 61 (1982).

33. Morrall, S. W., and Leyden, D. E., in "Silanes, Surfaces, and Interfaces" (D. E. Leyden, Ed.) p.501. Gordon and Breach, New York, 1985.

34. Hair, M. L., and Hertl, W. *J. Phys. Chem.* **73**, 2372 (1969).

35. Lindner, E., and Arias, E., *Langmuir* **8**, 1195 (1992).

36. Maoz, R., and Sagiv, J., *J. Colloid Interface Sci.* **100**, 465 (1984).

37. DePalma, V., and Tillman, N., *Langmuir*, **5**, 868 (1989).

38. Sagiv, J., *J. Am. Chem. Soc.* **102**, 92 (1980).

39. Silberzan, P., Léger, L., Ausserré, D., and Benattar, J. J., *Langmuir*, **7**, 1647 (1991).

40. Zettlemoyer, A. C., and Hsing, H. H., *in* "Colloid and Interface Science, Vol 1" (M. Kerker, A. C. Zettlemoyer, and R. L. Rowell, Eds.) p. 279. Academic Press, New York, 1977.

41. Tripp, C. P., and Hair, M. L., *Langmuir* **7**, 923 (1991).

42. Adamson, A. W. "Physical Chemistry of Surfaces, 5th Ed.", Wiley-Interscience, New York, 1990.

43. Somasundaran, P., in "Solution Chemistry of Surfactants, Vol. 2" (K. L. Mittal, Ed.) p. 777. Plenum Press, New York, 1979.

44. Fuerstenau, D. W. *Trans. AIME* **208**, 1365 (1957).

45. Ananthpadmanabhan, K., Somasundaran, P., and Healy, T. W. *Trans. Amer. Inst. Min. Metall. Pet. Eng* **266**, 2003 (1979).

46. Smith, R. W., and Lai, R. W. M. *Trans. AIME* **235**, 413 (1966).

47. Somasundaran, P. *Int. J. of Miner. Process.* **3**, 35 (1976).

48. Novich, B. E., and Ring, T. A. *Langmuir* **1**, 701 (1985).

49. Yoon, R.-H., and Yordan, J. L. J. *Colloid and Interface Sci.* **141**, 374 (1991).

50. Liu, S.-T., *Kolloidnyi Zhurnal* **52**, 858 (1990).

51. de Bruyn, P., *Trans. AIME* **202**, 291 (1955).

52. Gaudin, A. M., and Fuerstenau, D. W., Trans. AIME 202, 958 (1955).

53. Kung, H. C., and Goddard, E. D. *Kolloid Z. und Z. Polymere*, **232**, 812 (1969).

54. Mukerjee, P., Mysels, K. J., and Dulin, C. I., *J. Phys. Chem.* **62**, 1390 (1958).

55. Mukerjee, P., *J. Phys. Chem.* **69**, 2821 (1965).

56. Derjaguin, B., *Kolloid-Zeitchrift* **69**, 155 (1934).

57. Israelachvilli, J. N., "Intermolecular and Surface Forces, 2nd Ed.", Academic Press, New York, 1992.

58. Israelachvili, J. N., and Adams, G. E., *J. Chem. Soc. Faraday Trans I* **74**, 975 (1978).

59. Tabor, D., and Winterton, R. H. S., *Proc. Roy. Soc. A* **312**, 435 (1969).

60. Horn, R. G., Smith, D. T., and Haller, W., *Chem. Phys. Letters* **162**, 404 (1989).

61. Binnig, G., Quate, C. F., and Gerber, Ch., *Phys. Rev. Letters* **56**, 930 (1986).

62. Ducker, W. A., Senden, T. J., and Pashley, R. M., *Nature* **353**, 239 (1991); *Langmuir* **8**, 1831 (1992).

63. Meagher, L., and Craig, V. S. J., *Langmuir* **10**, 2736 (1994).

64. Biggs, S., Mulvaney, P., Zukoski, C. F., and Grieser, F. *J. Am. Chem. Soc.* **116**, 9150 (1994).

65. Biggs, S., *Langmuir* **11**, 156 (1995).

66. Larson, I., Drummond, C. J., Chan, D. Y. C., and Grieser, F., *J. Am. Chem. Soc.* **115**, 11885 (1993).

67. Atkins, D. T., and Pashley, R. M., *Langmuir* **9**, 2232 (1993).

68. Albrecht, T. R., Akamine, S., Carver, T. E., and Quate, C. F., *J. Vac. Sci. Technol. A* **8**, 3386 (1990).

69. Rabinovich, Ya. I., and Yoon, R.-H., *Langmuir*, **10**, 1903 (1994).

70. Senden, T. J., and Ducker, W. A., *Langmuir* **10**, 1003 (1994).

71. Cleveland, J. P., Manne, S., Bocek, D., and Hansma, P. K., *Rev. Sci. Instrum.* **64**, 403 (1993).

72. Butt, H.-J., Siedle, P., Seifert, K., Fendler, K., Seeger, T., Bamberg, E., Wesienhorn, A. L., Goldie, K., and Engel, A., *J. Microscopy* **169**, 75 (1993).

73. Hutter, J. L., and Bechhoefer, J., *Rev. Sci. Instrum.* **64**, 1868 (1993).

74. Li, Y. Q., Tao, N. J., Pan, J., Garcia, A. A., and Lindsay, S. M., *Langmuir* **9**, 637 (1993).

75. Parker, J. L., Christenson, H. K., and Ninham, B. W., *Rev. Sci. Instrum.* **60** 3135 (1989).

76. Parker, J. L., *Langmuir* **8**, 551 (1992).

77. Rabinovich, Ya. I., Derjaguin, B. V., and Churaev, N. V., *Adv. Colloid Interface Sci.* **16**, 63 (1982).

78. Rabinovich, Ya. I., and Derjaguin, B. V., *Colloids Surf.* 30, 243 (1988).

79. Peschel, G., Belouschek, P., Müller, M. M., Müller, R. M., and König, R., *Colloid Polymer Sci.* **260**, 444 (1982).

80. Israelachvili, J. N., and Pashley, R. M., *Nature* **300**, 341 (1982).

81. Israelachvili, J. N., and Pashley, R. M., *J. Colloid Interface Sci.* **98**, 500 (1984).

82. Kékicheff, P., Christenson, H. K., and Ninham, B. W., *Colloids Surf.* **40**, 31 (1989).

83. Herder, P. C., *J. Colloid Interface Sci.* **134**, 346 (1990).

84. Yoon, R.-H., and Ravishankar, S. A., *J. Colloid Interface Sci.* **166**, 215 (1994).

85. Pashley, R. M., McGuiggan, P. M., Ninham, B. W., and Evans, D. F., *Science* **229**, 1088 (1985).

86. Claesson, P. M., Blom, C. E., Herder, P. C., and Ninham, B. W., J. *Colloid Interface Sci.* **114**, 234 (1986).

87. Christenson, H. K., and Claesson, P. M., *Science* **239**, 390 (1988).

88. Claesson, P. M., and Christenson, H. K., *J. Phys. Chem.* **92**, 1650 (1988).

89. Christenson, H. K., Claesson, P. M., Berg, J., and Herder, P. C., *J. Phys. Chem.* **93**, 1472 (1989).

90. Kurihara, K., Kato, S., and Kunitake, T., *Chem. Letters* 1555 (1990)

91. Christenson, H. K., Fang, J., Ninham, B. W., and Parker, J. L., *J. Phys. Chem.* **94**, 8004 (1990).

92. Tsao, Y., Yang, S. X., Evans, D. F., and Wennerström, H., *Langmuir* **7**, 3154 (1991).

93. Rabinovich, Ya. I., and Yoon, R.-H., *Colloids Surf.* **93**, 263 (1994).

94. Parker, J. L., and Claesson, P. M., *Langmuir* **10**, 635 (1994).

95. Yoon, R.-H., and Ravishankar, S. A., *J. Colloid Interface Sci.* **179**. In Press.

96. Rabinovich, Ya. I., Guzonas, D. A., and Yoon, R.-H., *Langmuir* **9**, 1168 (1993).

97. Rabinovich, Ya. I., and Derjaguin, B. V. *in* "Proceedings of the 5th Hungarian Conference on Colloid Chemistry", Loránd Eötvös University, Balatonfured, Hungary, 1988.

98. Christenson, H. K., Claesson, P. M., and Parker, J. L., *J. Phys. Chem.* **96**, 6725 (1992).

99. Tsao, Y., Evans, D. F., and Wennerström, H., *Langmuir* **9**, 779 (1993).

100. Parker, J. L., Claesson, P. M., and Attard, P., *J. Phys. Chem.* **98**, 8468 (1994).

101. Parker, J. L., and Claesson, P. M., *Langmuir* **8**, 757 (1992).

102. Eriksson, J. C., Ljunggren, S., and Claesson, P. M., *J. Chem. Soc., Farday Trans. 2* **85**, 163 (1989).

103. Lee, C. Y., McCammon, J. A., and Rossky, P. J., *J. Chem. Phys.* **80**, 4448 (1984).

104. van Oss, C. J., Chaudhury, M. K., and Good, R. J., *Adv. Colloid Interface Sci.* **28**, 35 (1987).

105. Yaminsky, V. V., Yushchenko, V. S., Amelina, E. A., and Shchukin, E. D., *J. Colloid Interface Sci.*, **96**, 301 (1983).

106. Ruckenstein, E., and Churaev, N., *J. Colloid Interface Sci.* **147**, 535 (1991).

107. Yushchenko, V. S., Yaminsky, V. V., and Shchukin, E. D., *J. Colloid Interface Sci.*, **96**, 307 (1983).

108. Yaminsky, V. V., and Ninham, B. W., *Langmuir* **9**, 3618 (1993).

109. Attard, P., *J. Phys. Chem.* **93**, 6441 (1989).

110. Podgornik, R., *J. Chem. Phys.* **91**, 5840 (1989).

111. Claesson, P. M., Herder, P. C., Blom, C. E., and Ninham, B. W., *J. Colloid and Interface Sci.* **118**, 68 (1987).

112. Christenson, H. K., Claesson, P. M., and Pashley, R. M., *Proc. Indian Acad. Sci.* **98**, 379 (1987).

113. Rutland, M., Waltermo, A., and Claesson, P, *Langmuir* **8**, 176 (1992).

114. Herder, P. C., *J. Colloid Interface Sci.* **134**, 336 (1990).

115. Yoon, R.-H., and Ravishankar, S. A., *J. Colloid Interface Sci.* **179**. In Press.

116. Parker, J. L., Yaminsky, V. V., and Claesson, P. M., *J. Phys. Chem.* **97**, 7706 (1993).

117. Castro, S. H., Vurdela, R. M., and Laskowski, J. S., *Colloids Surf.* **21**, 87 (1986).

118. Watson, D., and Manser, R. M., *Trans. Inst. Min. Metall. Sec. C* **77**, C57 (1968).

119. Elton, G. A. H. *in* "Proceedings of the 2nd International Congress of Surface Activity, Vol. 3", p.161. Academic Press, New York, 1957.

120. Rupprecht, H., *Kolloid Z. u. Z. Polymere* **249**, 1127 (1971).

121. Swalen, J. D., Allara, D. L., Andrade, J. D., Chandross, E. A., Garoff, S., Israelachvili, J., McCarthy, R., Murray, R., Pease, R. F., Rabolt, J. F., Wynne, K. J., and Yu, H., *Langmuir* **3**, 932 (1987).

122. Chen, Y. L., Chen, S., Frank, C., and Israelachvili, J., *J. Colloid Interface Sci.* **153**, 244 (1992).

CHAPTER 2 CHARACTERIZATION OF SILICA SURFACES HYDROPHOBIZED BY OCTADECYLTRICHLOROSILANE

2.1 INTRODUCTION

The study of thin aqueous films on hydrophobic surfaces is important in many areas, including mineral flotation, where it is vital to understand the interaction mechanism between an air bubble and a solid particle. Silica is often used as a model mineral substrate because of its optical properties, and its surface can be made to exhibit various degrees of hydrophobicity by the adsorption of surfactants or by reaction with alkylchlorosilanes. The latter method is believed to produce surfaces which are more robust because of suspected covalent linkage of the alkylsilane to the surface.

Although the silanation process has been well studied (1-3), the exact mechanism of the reaction remains somewhat uncertain, especially the role of water. Most previous infrared studies of surfaces modified by reactions with alkylchlorosilanes have either been transmission studies of high surface area fumed silicas (2, 4, 5) or have used attenuated total reflection (ATR) infrared spectroscopy to examine silanes reacting with native oxide layers on silicon ATR crystals (6-9). Some work has been done using transmission FTIR to study OTS adsorption on thin mica sheets (10, 11). In the present study, transmission FTIR has been used to characterize OTS adsorption on silica plates.

Two types of hydroxyl groups are believed to exist on silica surfaces (12), i.e., hydrogen-bonded hydroxyl groups on which weakly-bound multilayers of water can physisorb and free hydroxyl groups which show no affinity for water. Heating the silica to 150°C removes all physisorbed water, while further heating to 400°C reversibly reduces hydrogen-bonded hydroxyl groups. Heating between 400°C and 800°C irreversibly eliminates adjacent hydroxyl groups. Above 800°C, it is believed that few free hydroxyl groups remain amongst hydrophobic siloxane bridges (6, 13). The result is a progression of hydrophobicity and a change in surface reactivity which have been used with trimethylchlorosilane to produce silica samples of varied contact angles (14).

Octadecyltrichlorosilane (OTS) has been found to produce extremely durable monolayer films with water contact angles greater than 100° (15). The silanation reaction has been described by Morrall and Leyden (16) as follows. First, the OTS molecule hydrolyzes to form:

$$\text{R-Si-Cl}_3 + 3\ \text{H}_2\text{O} \rightarrow \text{R-Si-(OH)}_3 + 3\ \text{HCl}$$

which may polymerize in solution as follows:

$$2\ \text{R-Si-(OH)}_3 \rightarrow \text{R-Si(OH)}_2\text{-O-Si(OH)}_2\text{-R} + \text{H}_2\text{O}$$

The polymer subsequently adsorbs on silica through hydrogen bonding before forming covalent siloxane linkages with the silica surface as depicted in Figure 2.1. It is possible, however, that the hydrolyzed OTS molecules may adsorb on silica individually prior to cross-linking (1, 3, 17).

More recent work has found no direct evidence that OTS molecules chemically bond with the surface hydroxyl groups. They do not even react with the first layers of adsorbed water, but rather with outer water layers (2). Recently, Trau *et al.* (18) measured the thickness of alkylsilane films on silica and reported thick, heterogeneous layers when OTS or trichloromethylsilane were used.

Although the exact mechanism is not known, it appears certain that methylation of silica requires water. It is, therefore, the purpose of the present work to study the effect of water on the adsorption of OTS on silica. The result of the present investigation will be useful for producing well-characterized OTS films on silica, which is essential for direct force measurements between an air bubble and hydrophobic solids.

2.2 MATERIALS AND METHODS

2.2.1 *Chemicals*

Octadecyltrichlorosilane (OTS) was obtained from Aldrich Chemical Co. at 95% purity. HPLC grade cyclohexane (Aldrich) was dried overnight over 8-12 mesh Davison 3

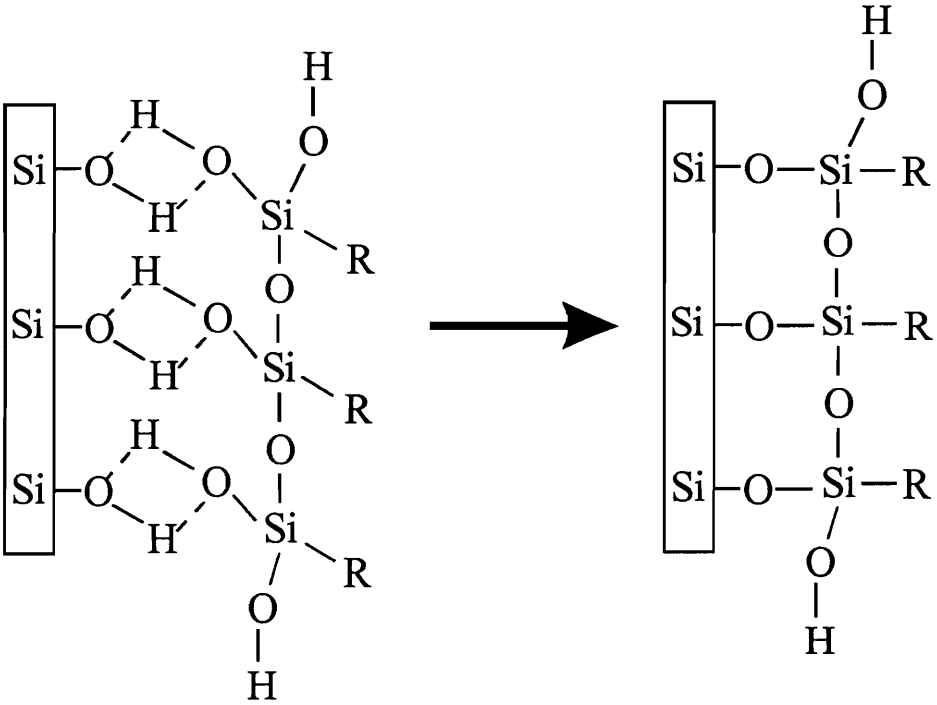

Figure 2.1 Polymerized OTS is believed to form covalent bonds to the silica surface.

Å molecular sieves, activated at 250°C, prior to each experiment. Reagent grade ammonium hydroxide, certified 30% hydrogen peroxide, and reagent grade concentrated nitric acid were obtained from Fisher Scientific Co. Reagent grade chloroform from JT Baker Inc. and ethanol (200 proof) from Aaper Alcohol and Chemical Co. were also used as received. Conductivity water produced using a Barnstead Nanopure water purification system was used in all experiments.

2.2.2 *Cleaning of Silica Plates*

Optically smooth Herasil 3 fused silica plates were obtained ground and polished from Herasil Amersil Inc. and measured 1 x 1 x 1/16 in. Prior to each experiment, the plates were cleaned in vigorously boiling (110°C) concentrated nitric acid for 5 hours, then rinsed with Nanopure water. The plates were then immersed in a 5 H_2O: 1 H_2O_2: 1 NH_4OH mixture (RCA Standard Clean 1) (19) for 20 minutes at 70 to 80°C. This combination of cleaning methods was able to remove OTS layers from the silica plates, and the resulting clean plates had water contact angles (in air) of 4°±3°. No infrared bands due to organic contamination could be detected on these plates. The cleaned plates were stored under Nanopure water until further use. Well-defined fringes were observed when drying the silica plates with a nitrogen jet prior to the FTIR measurements.

2.2.3 *Atomic Force Microscope Imaging*

A Nanoscope III atomic force microscope (AFM) from Digital Instruments, Inc. was used to produce images of the silanated silica surfaces. Images were obtained in air with a standard triangular silicon nitride cantilever (spring constant = 0.06 N/m) provided by Digital Instruments, Inc.

2.2.4 *FTIR Transmission Measurements*

Infrared transmission spectra were measured using a Digilab FTS-60A Fourier transform infrared spectrometer equipped with a mercury-cadmium-telluride (MCT) detector. A total of 1024 interferograms were co-added at 4 cm^{-1} resolution. The silica plates were held in a Teflon holder with an aperture of sufficient diameter to ensure no vignetting of the beam. A background spectrum of each plate was collected immediately after cleaning. After the silanation was complete, an infrared spectrum was recorded, and the background spectrum subtracted. The difference spectrum was then baseline-corrected prior to analysis.

2.2.5 *Contact Angle Measurements*

Water contact angles were measured with a Ramé-Hart Model 100 goniometer. A Hamilton microliter syringe was used to place a 5 μL drop of Nanopure water onto the silica plate. Advancing angles were measured on one side of the drop immediately after contacting the substrate to minimize contamination. Receding angles were obtained by reinserting the syringe and reducing the volume of the drop by one half. This process was repeated three times for each plate with an inherent error of ±3° in the angle.

2.2.6 *Silanation Reactions*

All operations involving OTS were carried out in a nitrogen-filled glove bag to minimize exposure of the OTS solutions to atmospheric water vapor. The silanation reactions were performed in PTFE beakers in an ultrasonic bath in the glove bag; PTFE beakers were used to avoid reaction of the OTS with the beaker walls.

The clean silica plates were removed from storage in Nanopure water, dried with a high pressure dry nitrogen jet, and placed in an air tight vessel containing a beaker of Nanopure water. The plates were left in this vessel for 1 hour to allow for water adsorption on the silica surface to equilibrate. This step ensures that a small amount of water is present on the silica surfaces at the beginning of the silanation process. Upon removal from the air-tight vessel, the plates were stored under water-saturated cyclohexane and transferred into the glove bag.

OTS solutions were prepared in 200 ml of dried cyclohexane and placed in the ultrasonic bath in the glovebag. The silica samples, held in a PTFE holder, were placed in the freshly prepared OTS solution. After the appropriate reaction time, each plate was removed from the OTS solution and rinsed thoroughly with chloroform to remove excess OTS, then stored in a chloroform bath. After removal from the glove bag, each plate was further rinsed with ethanol and dried with nitrogen before measurement of the infrared spectrum and contact angles.

It should be noted that the reaction temperature in the OTS solution increased steadily from 21.5 to 29.5°C due to the ultrasonic bath. Brzoska *et al.* (20) have recently discussed temperature effects on the formation of alkylchlorosilane monolayers; however, the temperatures used in the present work are below the threshold temperatures they reported and should not, therefore, have a significant effect on the adsorption mechanism.

2.3 RESULTS AND DISCUSSION

2.3.1 *Characteristics of OTS Films*

An atomic force microscope image of a clean silica plate is shown in Figure 2.2. The surface consists of grains with an average area of 4 μm^2 and a surface roughness of less than 5 Å. The intergranular boundaries have a measured depth of ca. 10 nm and contributed to an average surface roughness of less than 3 nm for the entire silica plate.

Figure 2.3 shows a series of infrared spectra of the CH_2 stretching region obtained after exposing clean silica plates to several concentrations of OTS solution for various

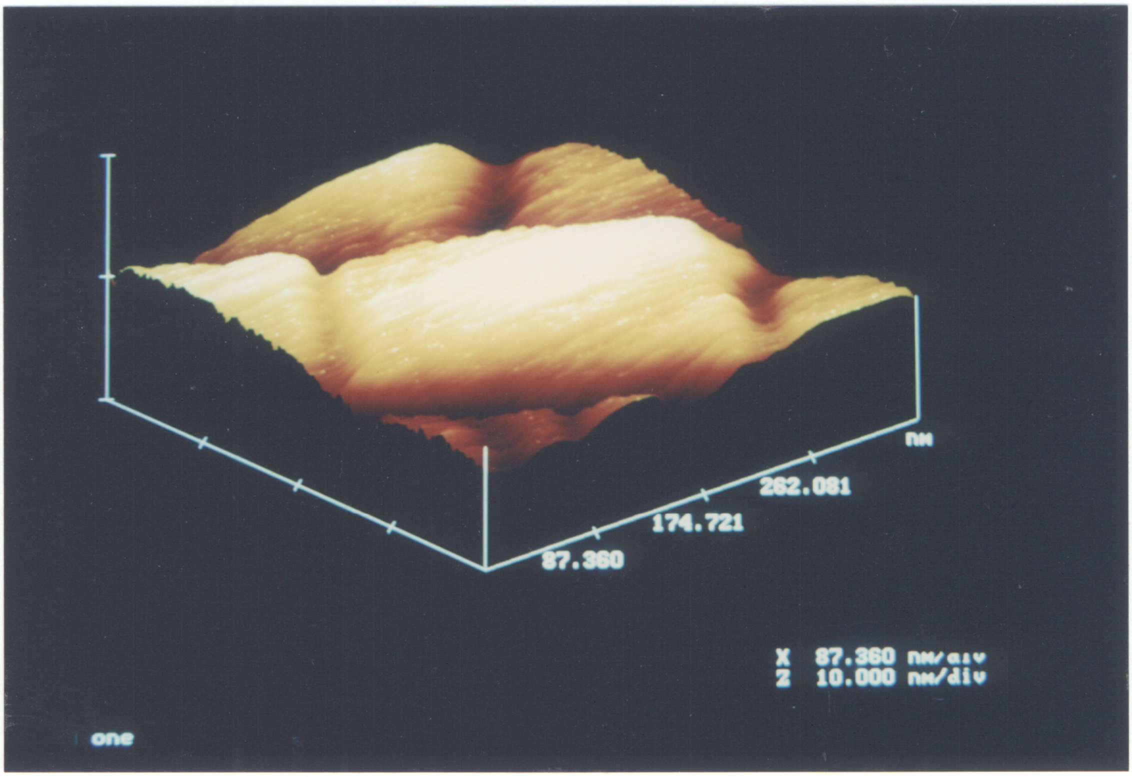
nm
262.081
174.721
87.360
X 87.360 nm/div
Z 10.000 nm/div
one

Figure 2.2 Atomic force microscope image of a clean fused silica plate.

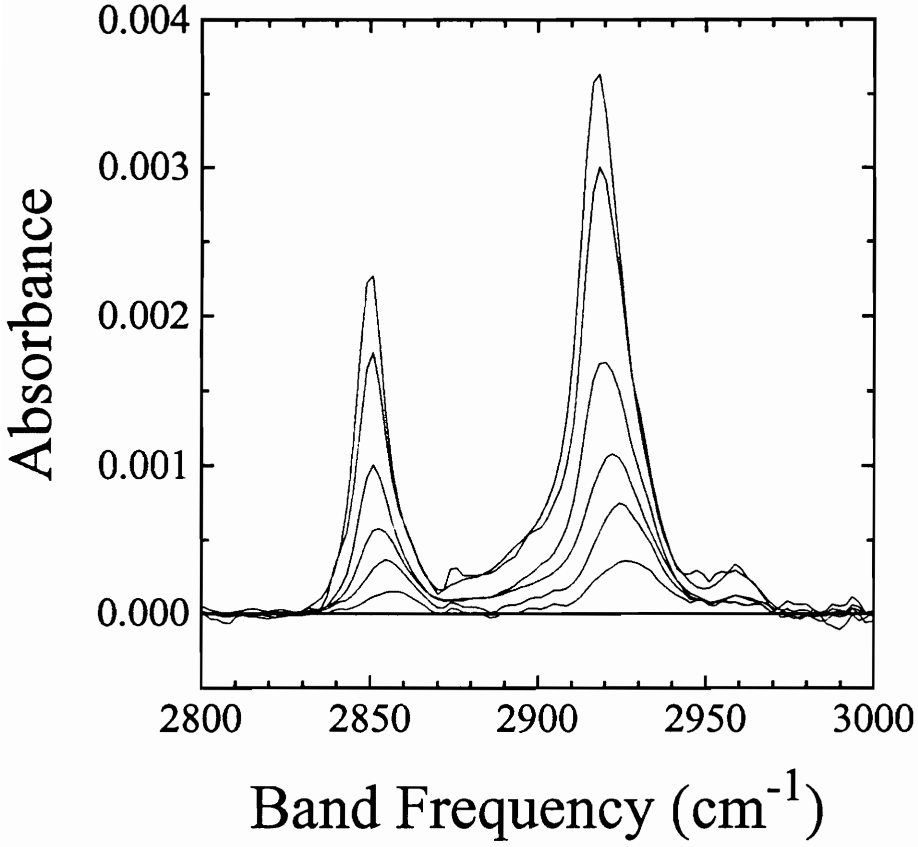

Figure 2.3 Typical FTIR transmission spectra showing OTS adsorption at different stages of monolayer growth on an SiO_2 substrate.

lengths of time. The CH_2 asymmetric stretching mode at ca. 2920 cm^{-1} can be used to quantify the surface concentration of OTS, if the absorbance per CH_2 group is known. To convert absorbances to surface concentrations, the equation obtained by Chen and Frank (21) for long-chained fatty acids on glass,

$$\textit{Surf. Conc.} = (0.00425 \ / \ \textit{Abs.}) \times 17, \qquad [2.1]$$

was used. The validity of Eq. [2.1] was checked against a monolayer film of dioctadecyldimethylammonium bromide of known surface density deposited on a mica sheet using a Langmuir trough. When plotting absorbance vs. immersion time for the 2920 cm^{-1} band at a number of OTS solution concentrations, a plateau of 3.65×10^{-3} absorbance units was reached for the highest OTS solution concentrations. Using Eq. [2.1], this corresponds to a surface concentration of 5.1 molecules/nm^2, equivalent to an area of 0.2 nm^2 per molecule. This agrees quite well with the values previously reported for closely-packed hydrocarbon chains (9, 11). At lower OTS concentrations, the plateau value is less than that at monolayer coverage. Similar conclusions are obtained from absorbance for the CH_2 symmetric stretch at 2850 cm^{-1}.

Using the absorbance at monolayer coverage, the absorbances at other reaction conditions can be converted to fractional surface coverages. Figure 2.4 illustrates the dependence of band frequencies (Figure 2.4a) and full widths at half maximum (FWHM) (Figure 2.4b) of the CH_2 symmetric and asymmetric stretches on the fractional surface

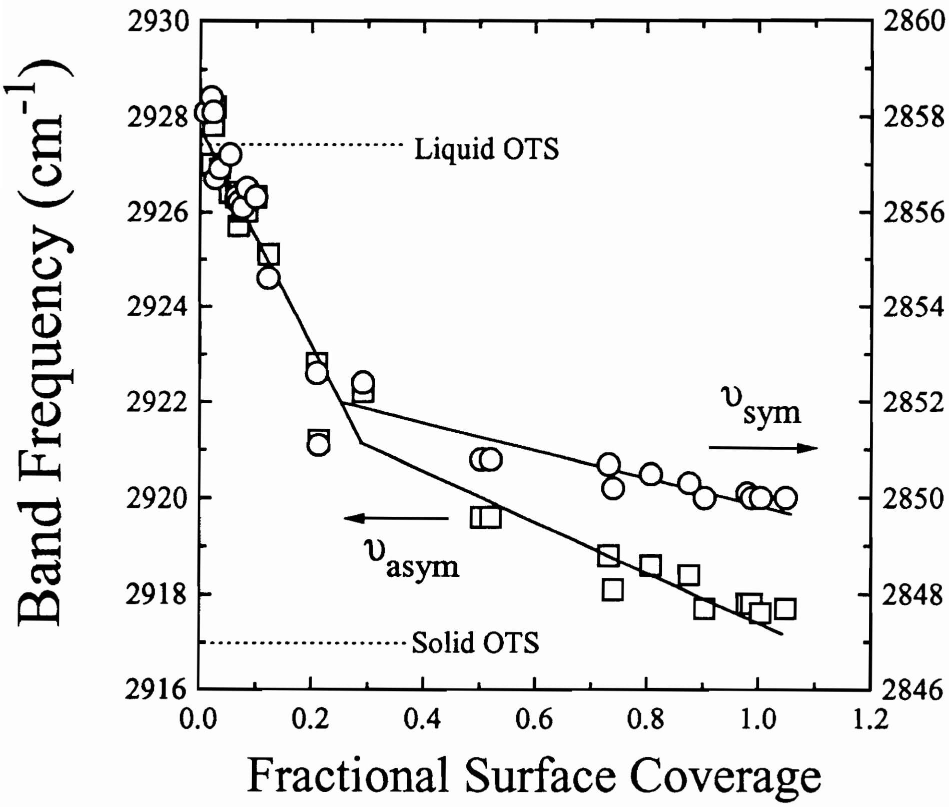

Figure 2.4a Wavenumber positions of CH_2 asymmetric and symmetric stretching mode bands as a function of fractional OTS surface coverage.

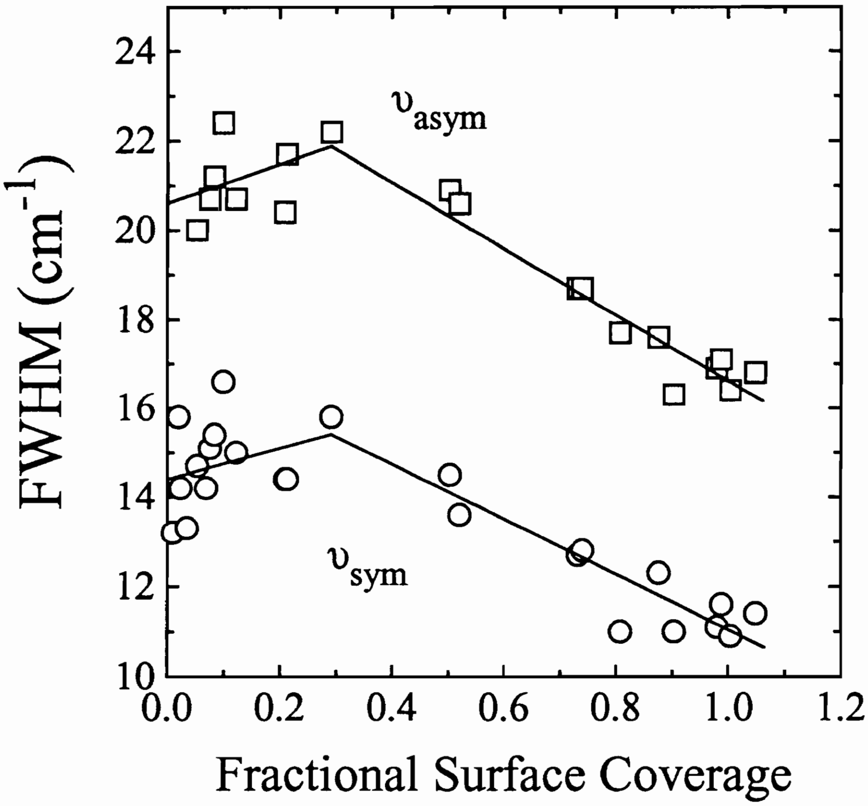

Figure 2.4b Full peak width at half maximum (FWHM) of CH_2 asymmetric and symmetric stretching mode data for various OTS surface coverages.

coverage. Band frequencies for polymerized OTS solid and for OTS in CCl_4 solution are also shown for comparison. The frequencies, relative intensities, and band widths of the CH_2 stretching modes in both the IR and Raman spectra have been used as diagnostics for the ordering of hydrocarbon chains (22). It has been found that the CH_2 bands at 2850 and 2920 cm^{-1} shift to lower frequencies and become narrower as the hydrocarbon chains interact with one another at higher surface OTS concentrations; thus, the band frequencies and FWHM indicate a change from a liquid-like, disordered state to a highly-ordered, quasi-crystalline state as the surface density increases. Similar observations have been reported by Tillman *et al.* (8) and Ulman (23) for long chain hydrocarbons. Figure 2.4b shows a monolayer peak width of approximately 16 cm^{-1} which is in good agreement with Tillman's findings for OTS adsorbed on silicon. The band frequencies in Figure 2.4a decrease linearly with a change in slope at a fractional coverage of 0.25-0.3. Although the FWHM values are more scattered at low coverages, a slight increase is noted below a fractional coverage of 0.3, followed by a linear decrease.

A plot of advancing water contact angle as a function of the reaction time at various concentrations is shown in Figure 2.5a. A maximum advancing water contact angle of 109° was found for reaction times corresponding to monolayer coverage. Oleophobicity was only achieved at monolayer coverage, a property noted by Sagiv (1) for fatty acid monolayers. Figure 2.5b graphically represents the hysteresis for these films in relation to

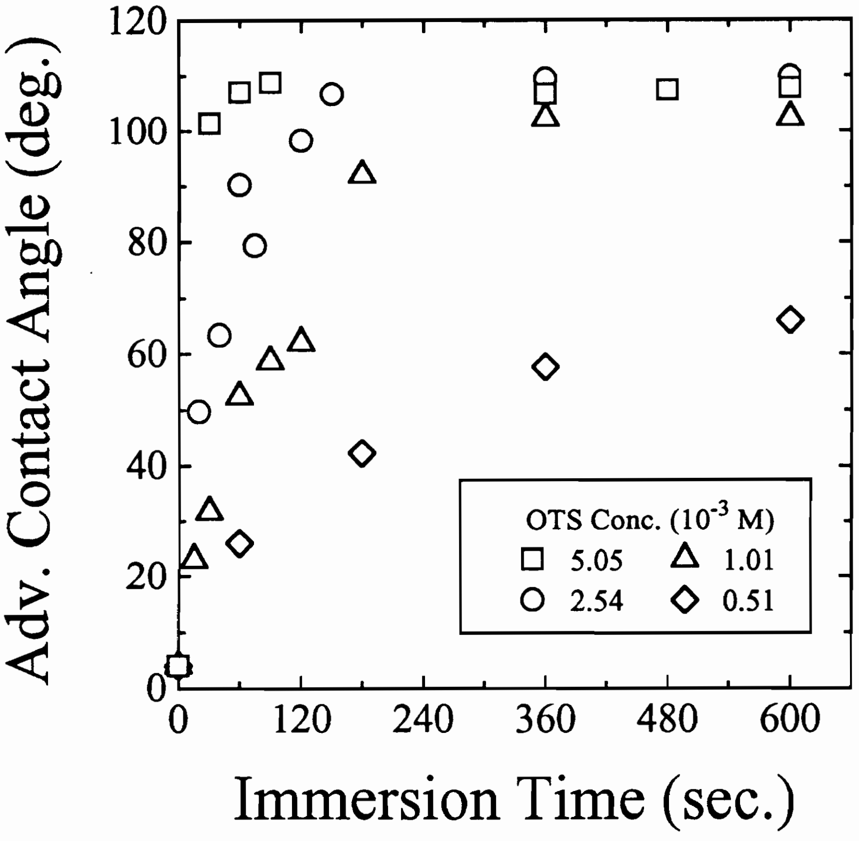

Figure 2.5a Advancing contact angle data for silica plates immersed in molar OTS solution concentrations of (□) $5.05\text{x}10^{-3}$, (○) $2.54\text{x}10^{-3}$, (△) $1.01\text{x}10^{-3}$, and (◇) $5.05\text{x}10^{-4}$ at various time intervals.

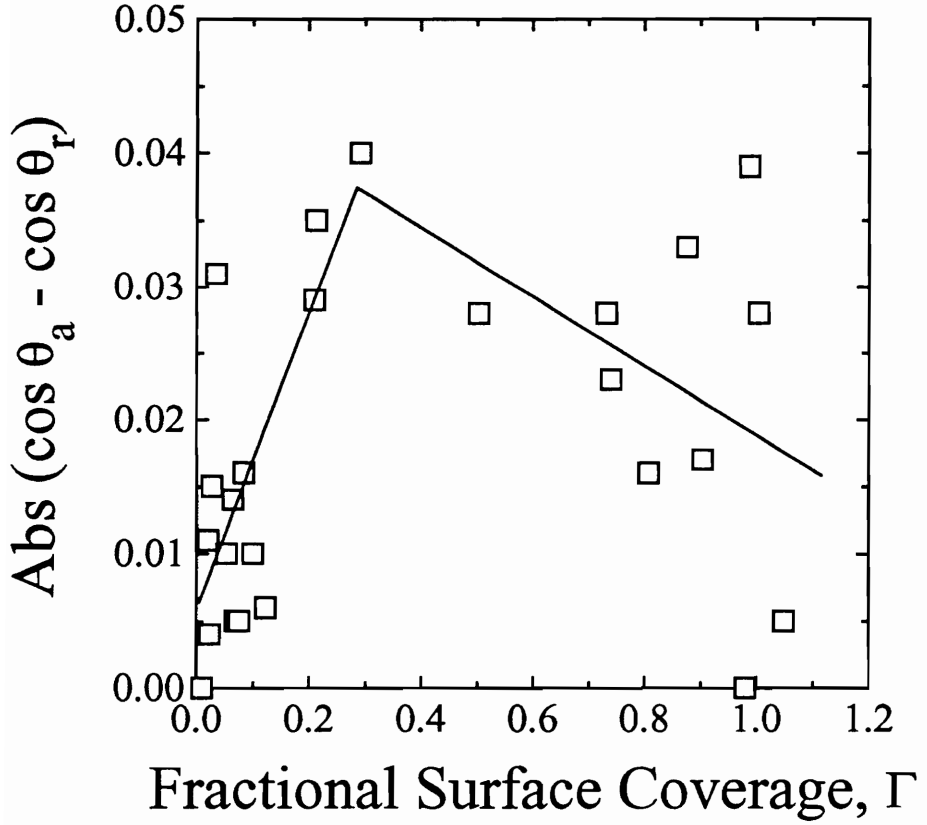

Figure 2.5b Hysteresis plot of advancing and receding contact angle data for all silanated silica plates in relation to surface coverage of OTS.

fractional surface coverage. Although the hysteresis is virtually negligible, a trend is detected with the same point of inflection near 0.3 fractional surface coverage as shown in Figures 4a and 4b.

Plotting the cosine of the advancing angle vs. the surface concentration obtained from the FTIR measurements yields Figure 2.6. Cos θ_a shows a linear behavior similar to that seen for the band frequencies, exhibiting a change in slope at a fractional coverage (f_{OTS}) of about 0.3. Assuming the surface is composed of a mixture of microscopic domains of OTS and bare silica, a linear relationship is expected on the basis of Cassie's equation (24)

$$\cos\theta = f_1\cos\,\theta_1 + f_2\cos\theta_2\ . \qquad [2.2]$$

Israelachvilli and Gee (25) have suggested a replacement for Cassie's equation for chemical heterogeneity of molecular dimensions

$$\cos\theta = \left[f_1(1+\cos\,\theta_2)^2 + f_2(1+\cos\,\theta_2)^2\right]^{.5} - 1\ . \qquad [2.3]$$

The present data are better fit by Cassie's equation, suggesting that the heterogeneity of the surfaces is in the form of microscopic domains rather than on a molecular scale.

This conclusion was verified using atomic force microscopy to image the silanated surfaces. Figure 2.7 shows five AFM images of silanated silica surfaces exhibiting water contact angles of 27°, 45°, 84°, 101°, and 107°. It is apparent from the AFM images at 27°, 45°, and 84° that below monolayer coverage, OTS is adsorbed in patches rather than a

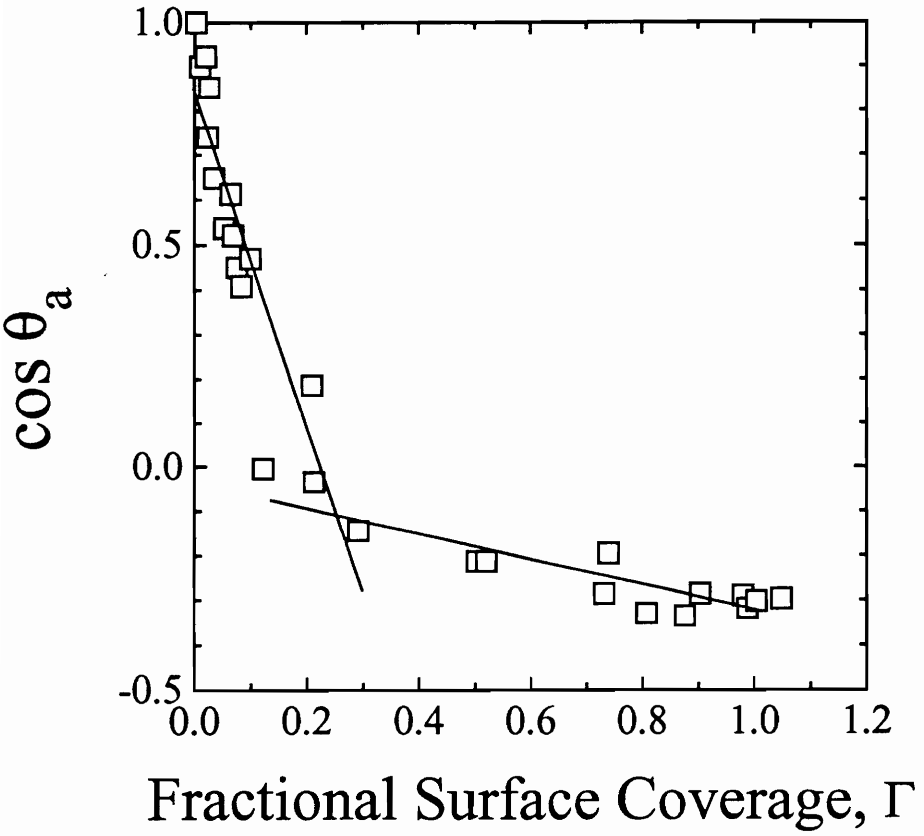

Figure 2.6 Cosine of advancing contact angle data showing initially a linear relationship to OTS surface coverage according to Cassie's Law, but changing slope at a fractional coverage of about 0.25-0.3.

homogeneous layer. The patches are ellipsoidal with average dimensions of 20 x 40 nm. Initially, the OTS patches are found predominantly in the regions between the silica grains (Figure 2.7a), possibly because the concentration of adsorbed water may be greater in this region due to the edge effect. An alternative explanation is that the patches are weakly bound to the surface and may be displaced by the AFM tip during measurement which would explain the unusually large amount of noise encountered during initial scans. The patches observed in the recesses between the grains may then be trapped by the edges of the grains. The ability of the AFM tip to move adsorbed molecules has been previously noted (26). The weak bond of OTS to the silica surface indicated by this observation supports the conclusions of Tripp and Hair (2) that OTS does not chemically react with surface hydroxyl groups on silica. As the surface coverage increases (Figure 2.7b and 2.7c), the patches do not increase in size but rather become more numerous and cover the silica surface, i.e., the patches are not nucleation sites for further growth. Finally, at a contact angle of 101° (Figure 2.7d) and to a further extent at 107° (Figure 2.7e), the surface is covered with a nearly uniform layer of OTS molecules.

The fraction of surface covered by the patches has been estimated from the AFM images and are presented in Table 1 along with the fractional surface coverage values obtained from the infrared measurements. Also shown in Table 1 are the data obtained at monolayer coverage for comparison. It is evident from Table 1 that the surface coverages

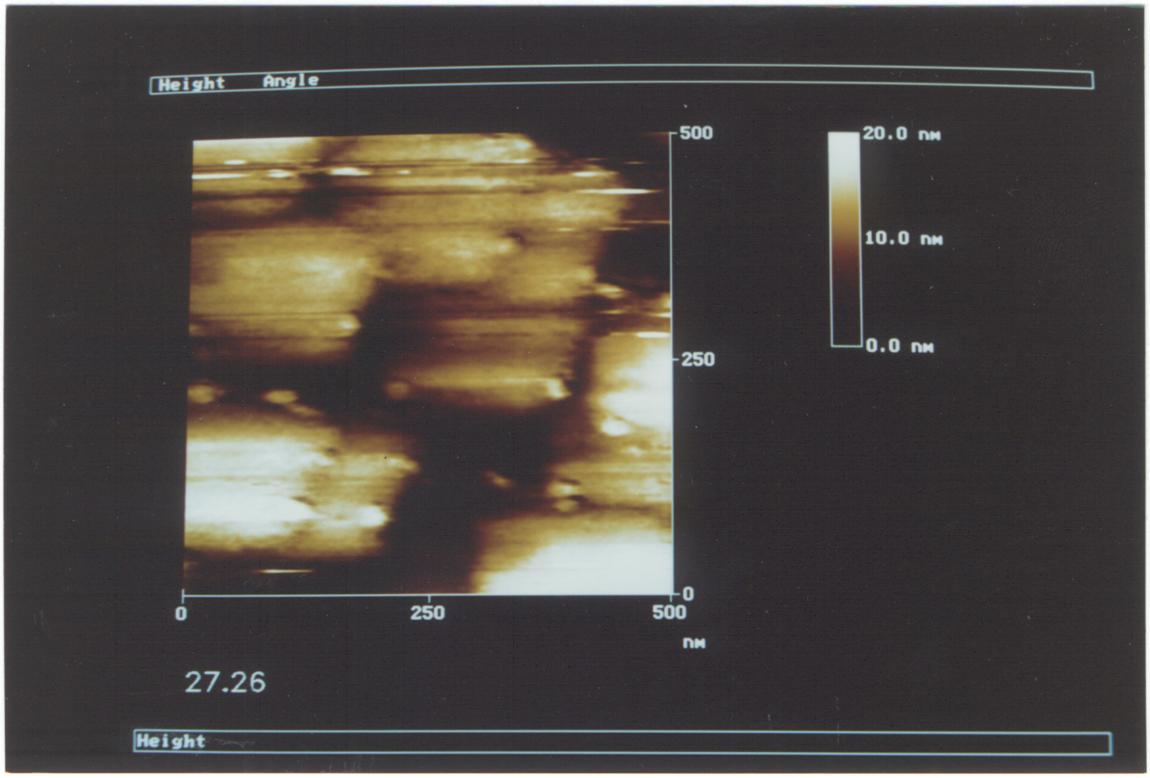
Height
Angle
500
250
0
20.0 nm
10.0 nm
0.0 nm
0
250
500
nm
27.26
Height

Figure 2.7a Atomic force microscope image of silanated surface in air exhibiting an advancing water contact angle of 27°.

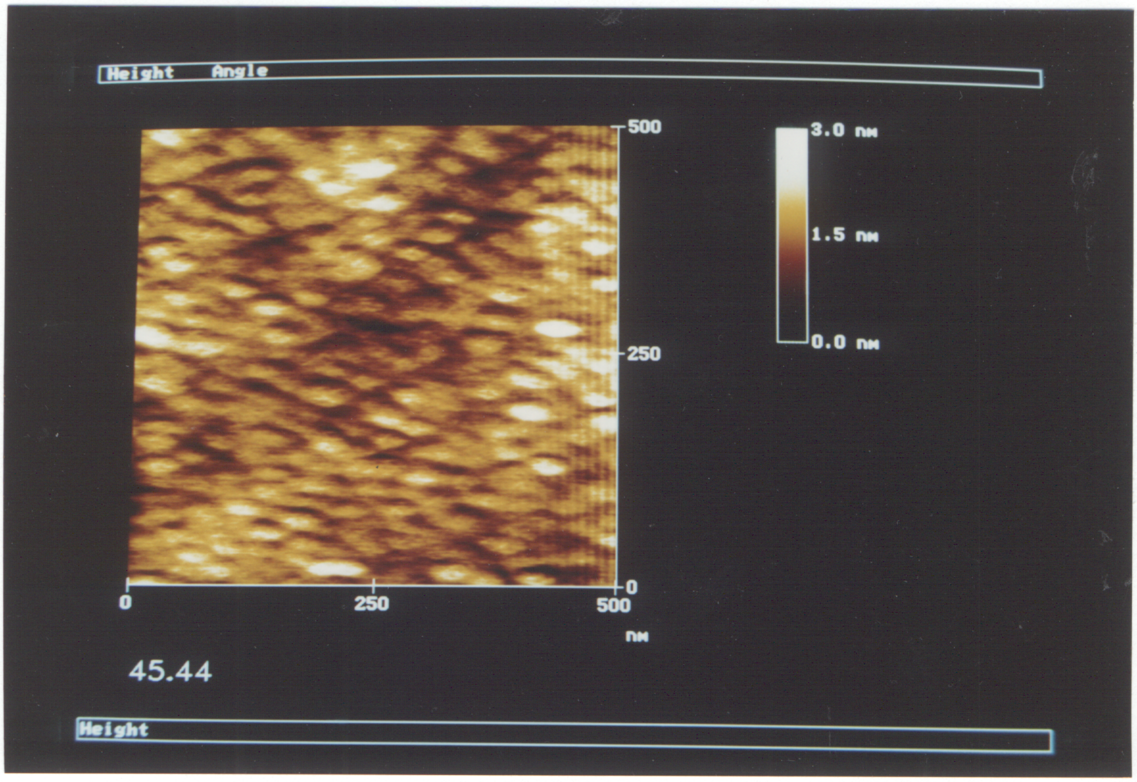
Height Angle
500
250
0
0
250
500
nm
3.0 nm
1.5 nm
0.0 nm
45.44
Height

Figure 2.7b Atomic force microscope image of a silanated surface in air exhibiting an advancing water contact angle of 45°.

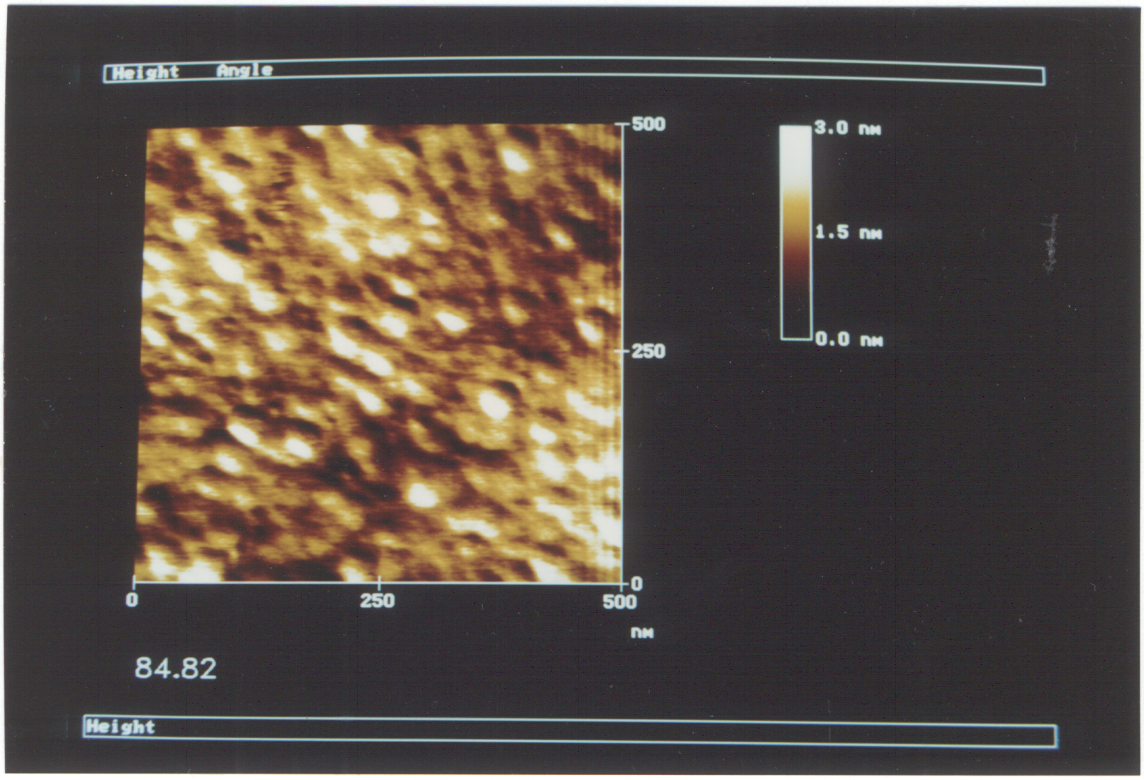

Figure 2.7c Atomic force microscope image of a silanated surface in air exhibiting an advancing water contact angle of 84°.

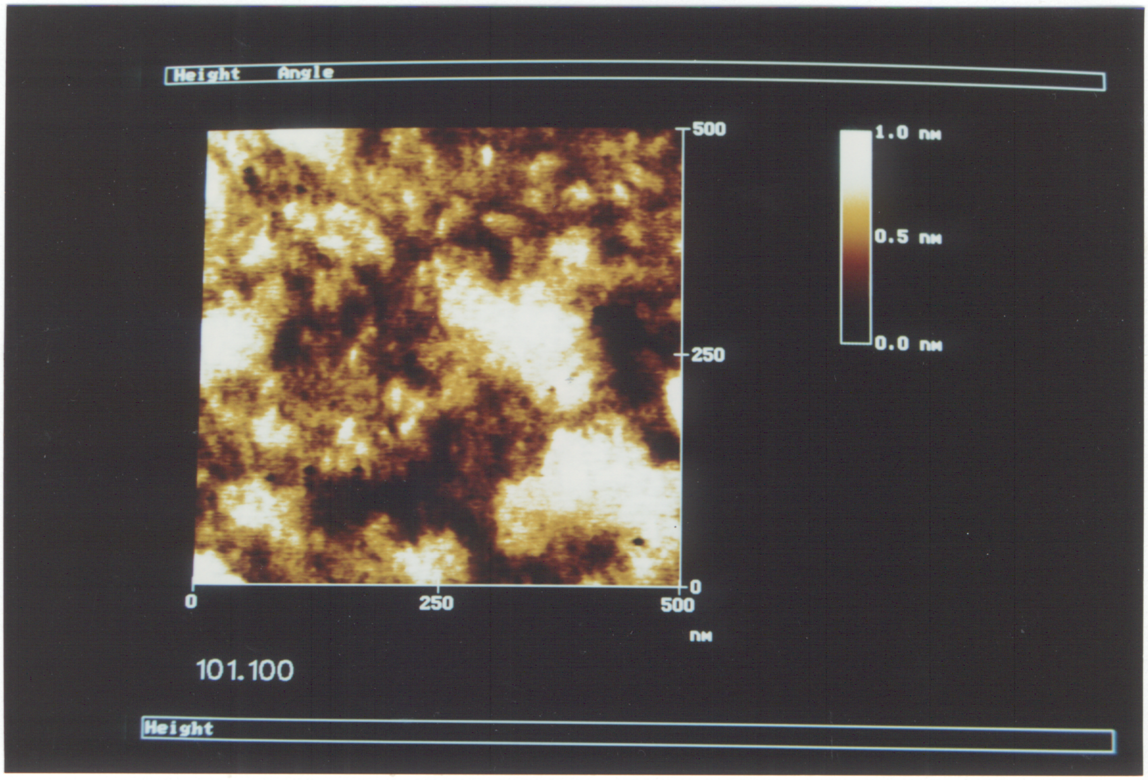
Height Angle
500
250
0
0
250
500
nm
1.0 nm
0.5 nm
0.0 nm
101.100
Height

Figure 2.7d Atomic force microscope image of a silanated surface in air exhibiting an advancing water contact angle of 101°.

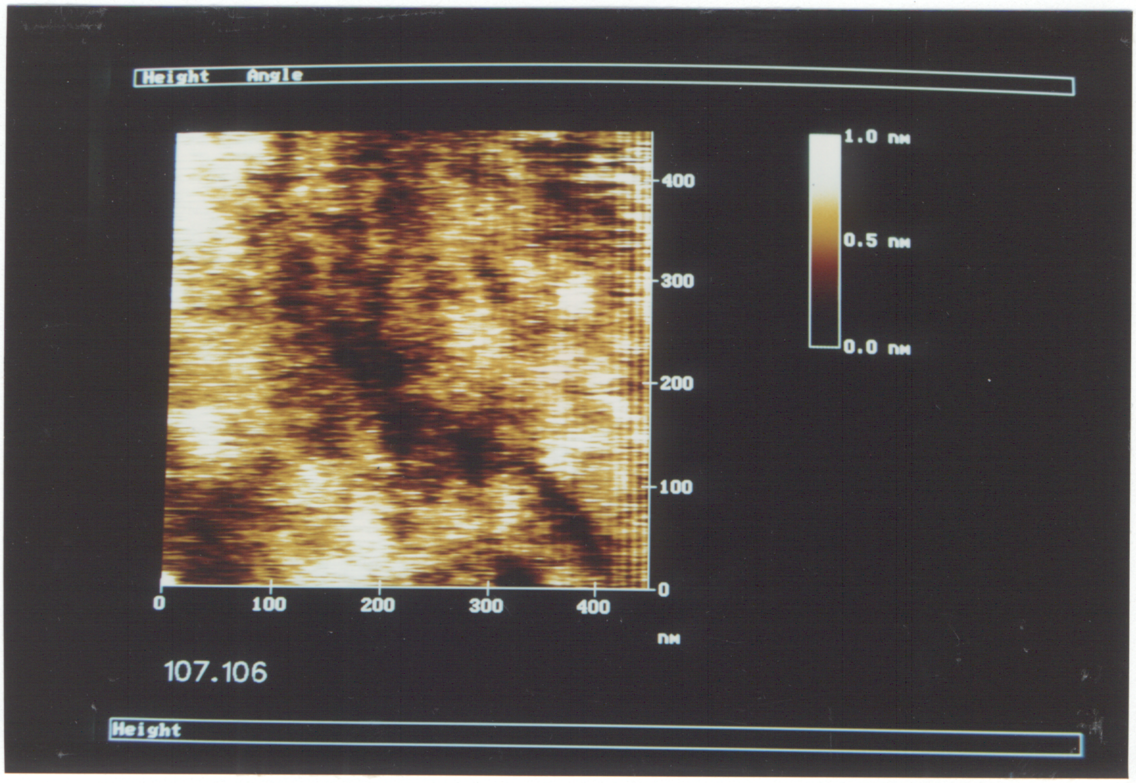
Height Angle
1.0 nm
0.5 nm
0.0 nm
400
300
200
100
0
0
100
200
300
400
nm
107.106
Height

Figure 2.7e Atomic force microscope image of a silanated surface in air exhibiting an advancing water contact angle of 107°.

as determined by AFM are considerably lower than those obtained by FTIR, suggesting that OTS molecules do not form closely-packed monolayers within the patches.

The adsorption density of OTS molecules within a patch (Γ_p) has been estimated from the AFM and FTIR data and presented in Table 1. The value of Γ_p at $\theta = 27°$ is not given because of the uncertainties involved in the FTIR measurements at very low coverages. It is interesting that since the size of the patches remains unchanged, the adsorption density within the patches increases substantially with increasing surface coverage (f_{FTIR}) and contact angle. Although a large contact angle ($\theta = 84°$) has been obtained at a relatively low coverage ($f_{FTIR} = 0.17$), it seems that the area covered by the patches ($f_{AFM} = 0.89$) is more relevant.

The FTIR, AFM, and contact angle studies suggest the following picture of the growth of OTS monolayer films on silica surfaces. At low coverages, OTS molecules form sparsely populated patches, which gives rise to large values of FWHM of the CH_2 stretching bands. As more OTS molecules adsorb, the patches become more numerous without significantly increasing in size. Meanwhile, the adsorption density of the molecules within each patch increases, causing a shift in band frequencies to lower wavenumbers. As the patches cover more of the surface, the contact angle follows Cassie's equation as expected for a macroscopic heterogeneous surface, while the contact angle hysteresis tends to increase only slightly. By the time f_{FTIR} reaches the 0.25-0.3 range, the patches have

TABLE 2.1

Fractional surface coverage values estimated from atomic force microscopy and Fourier transform infrared transmission spectra.

θ_a	f_{AFM}	f_{FTIR}	Γ_p^a
27°	0.07	0.02	-
45°	0.38	0.04	430
84°	0.89	0.17	780
109°	-	1.00	4080[b]

[a] Adsorption density (molecules/patch).
[b] Data for 800 nm^2 area at monolayer coverage.

essentially covered the entire surface, i.e., f_{AFM} becomes unity as indicated by Table 1. It appears that up to this point there exists a good correlation between θ and f_{AFM}. At f_{FTIR} = 0.25 to 0.3, the area per molecule is approximately 0.8 nm^2. Assuming a circular molecular area, this gives a molecular radius (R) of about 0.5 nm. This value is comparable to the value of R ($1.265x17^{.5} = 0.52$ nm) estimated for an 18-carbon chain molecule lying flat in a random walk configuration. Thus, the OTS molecules begin to be crowded by their neighbors. As the coverage increases beyond the 0.25-0.3 range, the FWHM and band frequencies gradually decrease, indicating an increase in chain ordering.

Recently, Schwartz *et al.* (27) have used AFM to examine the growth of an OTS monolayer on mica, and have reported that initially, isolated islands of closely-packed OTS, roughly 88 nm in diameter, are formed at the surface. This differs from the results reported here on silica in that the OTS patches are not densely packed. The size of the OTS islands reported by Schwartz *et al.* is similar to the values obtained in the present study for water-saturated cyclohexane; however, there is no mention of the water content of their solvent (bicyclohexyl).

A Zisman plot using a series of test liquids was constructed and gave a value of 20.2 dyne/cm^2 for the critical surface tension, which is in good agreement with values reported elsewhere for this system (3, 8, 15, 20). A durability study of the silanated silica was also performed by immersing plates in various solvents (carbon tetrachloride, ethanol, cyclohexane, chloroform, 0.1 M NaCl) for 15 days. Variations in the contact angle were within the ±3° of error of the goniometer.

2.3.2 *Kinetics of OTS Film Formation*

Chen and Frank used a transient Langmuir model to obtain kinetic information on the adsorption of fatty acids on glass and carboxylic acids on aluminum. The similarity of their surface coverage vs. time curves to those obtained in the present study naïvely suggests that the present data be treated in a similar manner. The fractional surface coverage, Γ, follows the material balance equation

$$\frac{\partial \Gamma}{\partial t} = \frac{k_a}{N_o} C(1 - \Gamma) - \frac{k_d}{N_o} \Gamma , \qquad [2.4]$$

where k_a and k_d are adsorption and desorption rate constants, C is the solution concentration of OTS, and N_o is the surface adsorbate concentration at full coverage. Integration of Eq. [2.4] leads to

$$\Gamma = \frac{k_a C}{k_a C + k_d} \left\{ 1 - \exp\left[-\frac{k_a}{N_o} \left(C + \frac{k_d}{k_a} \right) t \right] \right\} \qquad [2.5]$$

and can be simplified to

$$\Gamma = \Gamma_{eq} \left[1 - \exp(-kt) \right] , \qquad [2.6]$$

where Γ_{eq} is the maximum surface coverage reached by an adsorption isotherm. Fitting Eq. [2.6] to the results of the FTIR measurements by a least squares method (Figure 2.8a) gives the values of k at each concentration, shown in Figure 2.8b. At low concentrations ($C < 3\text{x}10^{-3}$ M), the data are linear in concentration,

$$k = 1.90\,C - 2.31\text{x}10^{-5}, \qquad [2.7]$$

which, along with the relationship of Γ_{eq} vs. solution concentration (as shown by the plot in Figure 2.8c), enables calculation of the reaction time and solution concentration required to achieve a desired surface coverage. Figure 2.8a should be compared to Figure 2.5a; both sets of curves have the same general shape, illustrating the close relationship between water contact angle and the surface concentration of OTS.

A number of recent studies (2-6, 18) have explored the role of water on the formation of alkylchlorosilane monolayers. Its significance was studied in the present work by using water-saturated cyclohexane in some experiments. Contact angle measurements revealed little difference between the two experiments (Figure 2.9a), although the rate of increase appeared to be faster at short times in water-saturated cyclohexane. The plateau value of the contact angle seemed to be independent of the presence of water, but the addition of water did cause an increase in the hysteresis encountered (Figure 2.9b). The FTIR measurements (Figure 2.9c) show a much greater amount of material adsorbed on the surface in the presence of water. For

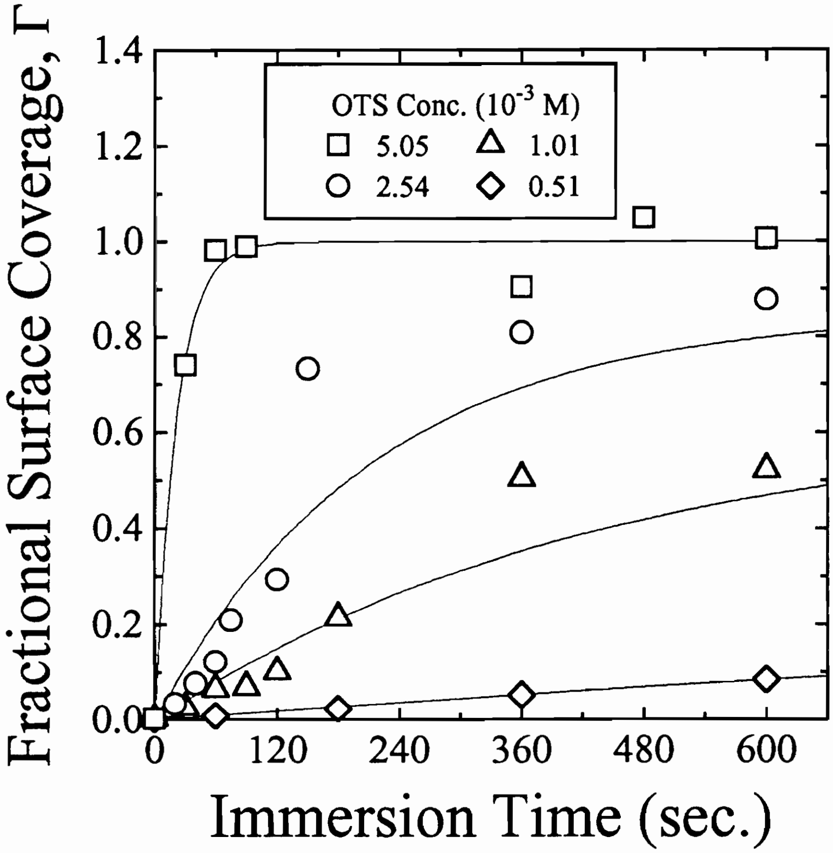

Figure 2.8a Fractional surface coverage (*Γ*) data for silica plates immersed in molar OTS solution concentrations of (□) 5.05×10^{-3}, (○) 2.54×10^{-3}, (Δ) 1.01×10^{-3}, and (◊) 5.05×10^{-4} at various time intervals. Solid lines represent Langmuir-like isotherms as determined by a least squares fit.

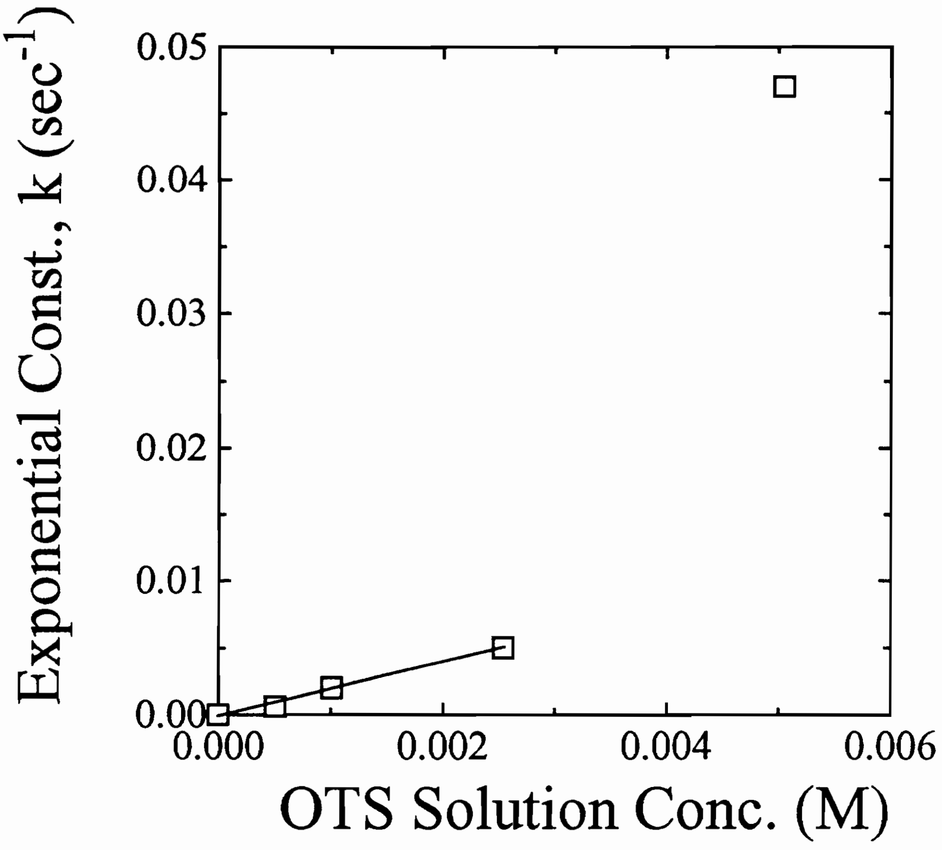

Figure 2.8b Exponential constants (*k*) determined for the isotherms of Figure 2.8a for the given OTS solution concentrations. A linear relationship is found at solution concentrations lower than 3x10^{-3} M.

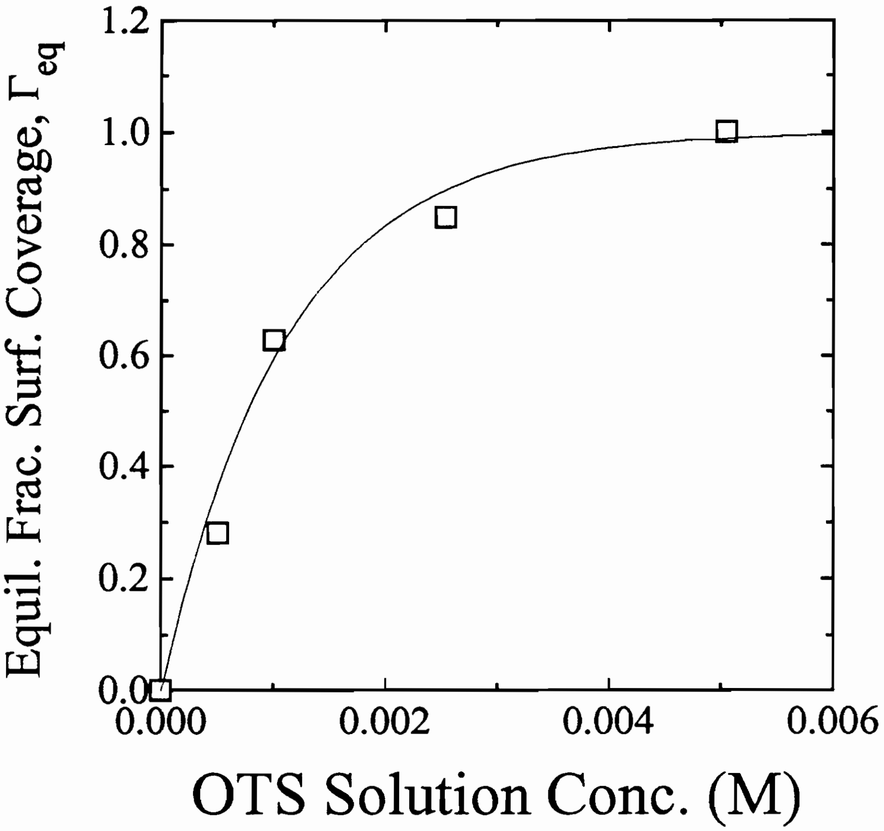

Figure 2.8c Calculated equilibrium fractional surface coverage (Γ_{eq}) values attained by the isotherms shown in Figure 2.8a for the various OTS solution concentrations.

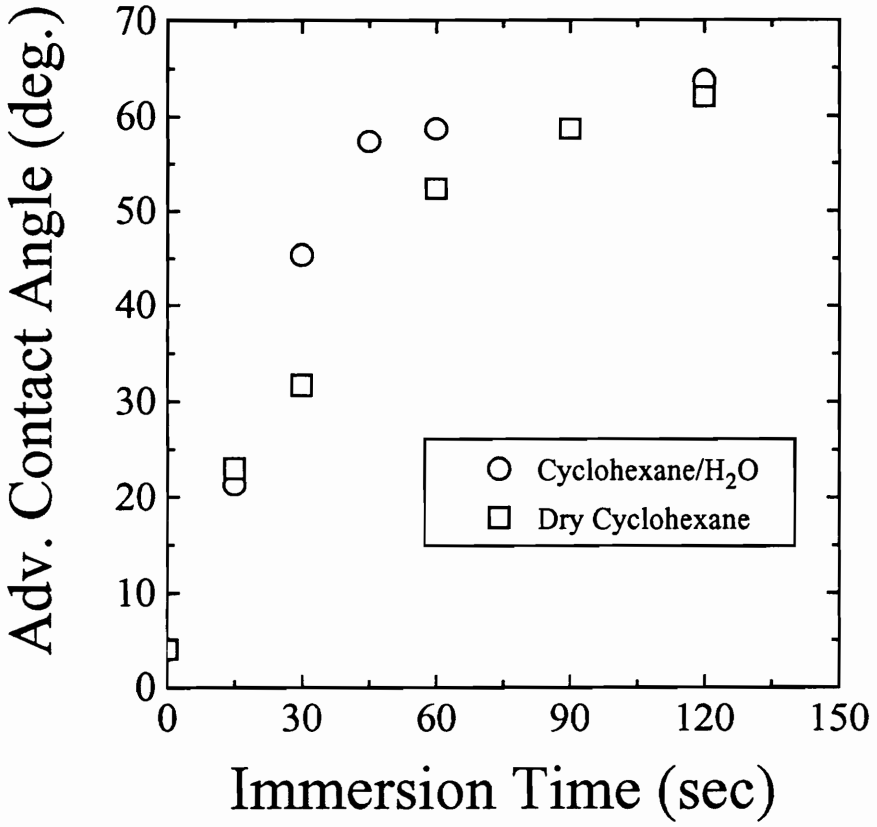

Figure 2.9a Contact angle data for silanation reactions carried out in 1.01×10^{-3} M OTS water-saturated (○) cyclohexane and dried cyclohexane (□) solutions.

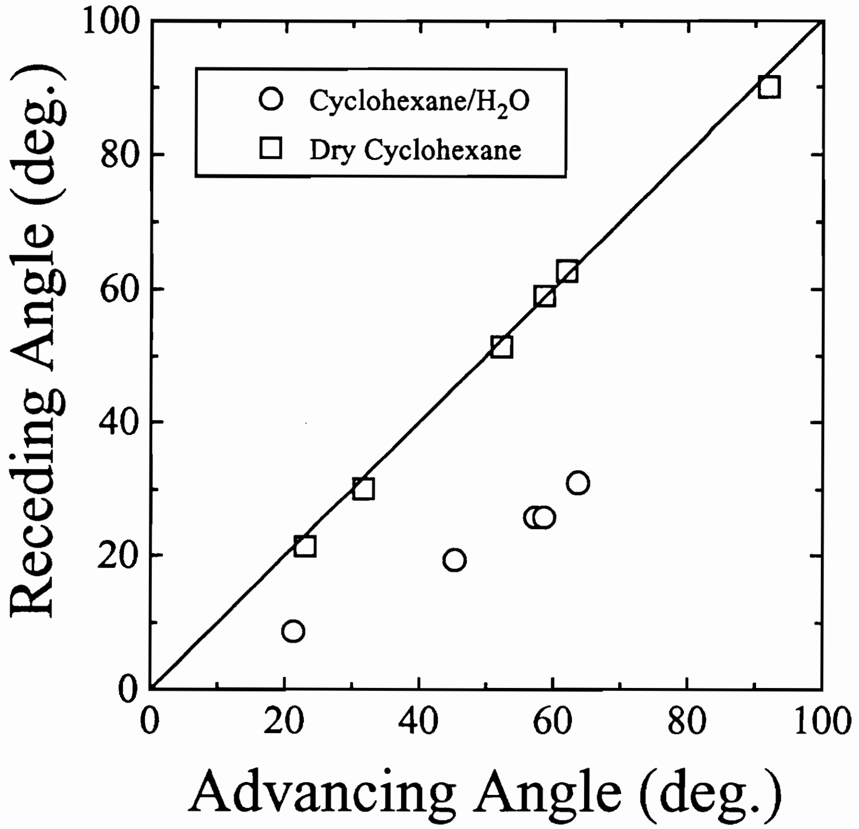

Figure 2.9b Hysteresis plot of advancing and receding contact angle data for silanated samples shown in Figure 2.9a.

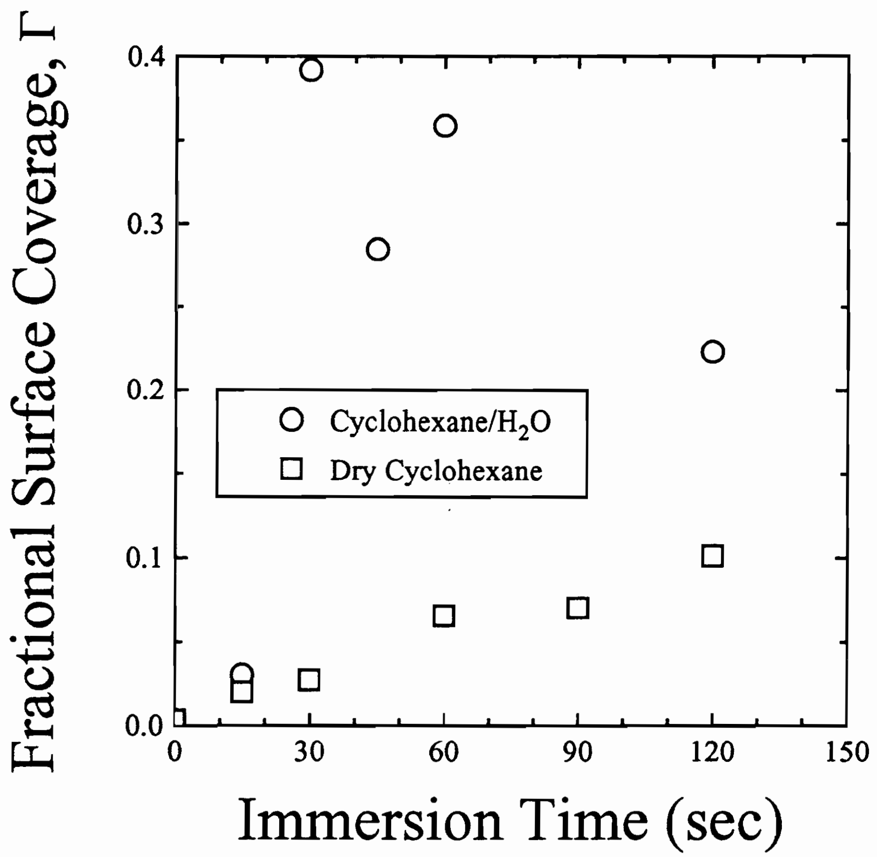

Figure 2.9c Fractional surface coverage (*Γ*) values for the plates in Figure 2.9a plotted against immersion time.

reaction times greater than 15 seconds, the adsorbed amount is several times greater than expected for monolayer coverage and shows a random dependence on reaction time. This difference in behavior is likely a result of the pre-polymerization of OTS in solution.

Figure 2.10 shows an AFM image of a silanated surface reacted with excess water in the OTS solution to exhibit an advancing contact angle of 65° with 10° hysteresis. One can see immediately when comparing to Figure 2.7 that the patches are much larger in size (≈ 110 x 90 nm). Angst and Simmons (6) found that polymerized OTS in solution results in high contact angles on thermally grown SiO_2 films. Adsorption of these larger polymeric OTS clusters results in a heterogeneous, patchy adsorbed structure many layers thick which gives rise to the observed hysteresis. This result is consistent with the large layer thickness and hysteresis reported by Trau *et al.* (18) for OTS adsorption on silica from hexane. The roughness of these surfaces was also noted in the "jaggedness" of the edge of the water drop when making contact angle measurements.

The benefits of ultrasound in reducing surface heterogeneity has been noted by Silberzan *et al.* (3), and, in the present study, it was found that the use of an ultrasonic bath was crucial to obtain reproducible results. When the reaction was not carried out in the ultrasonic bath, the use of water-saturated cyclohexane yielded poorly

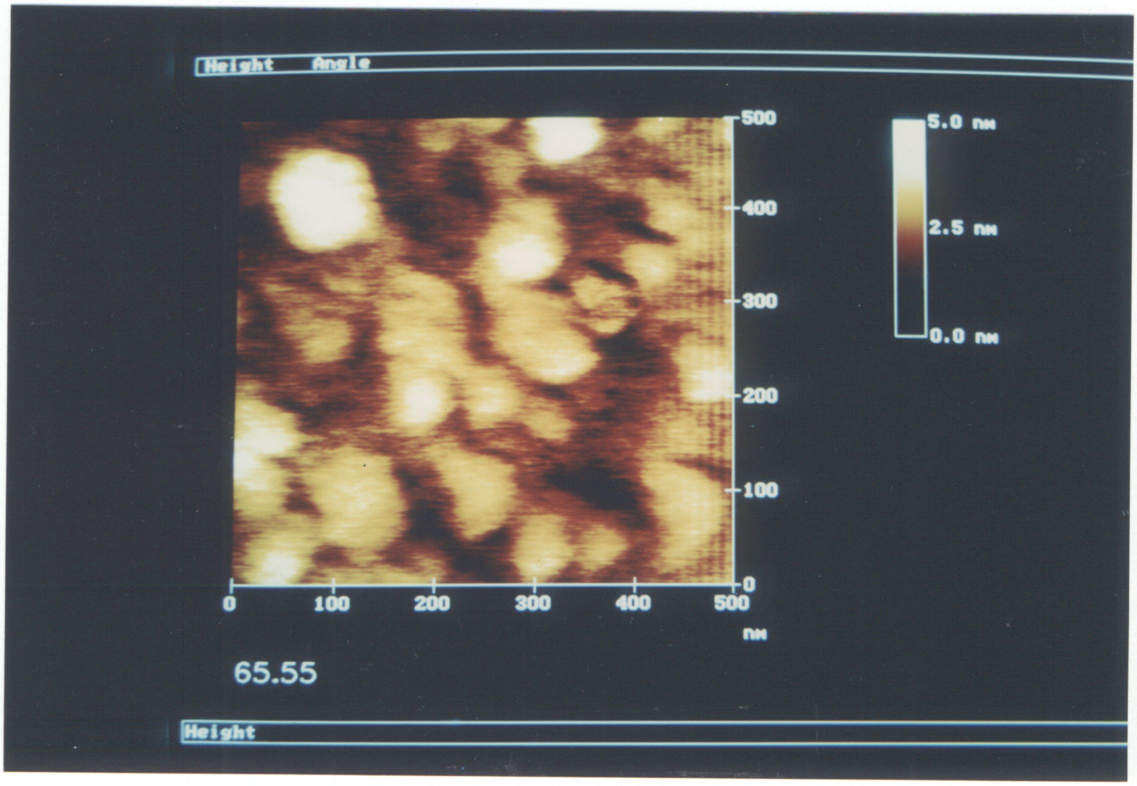
Height Angle
500
400
300
200
100
0
0
100
200
300
400
500
nm
5.0 nm
2.5 nm
0.0 nm
65.55
Height

Figure 2.10 Atomic force microscope image in air of a silanated surface exhibiting an advancing water contact angle of 65° and hysteresis of 10°.

reproducible contact angles, attributed to surface roughness. Some silica plates treated this way produced ultra-high contact angles (up to 160°) and would easily float on water!

Another interesting outcome was the dependence of OTS adsorption on the number of silica plates in solution. It was found that when several plates were reacted at once, the silanation reaction proceeded by an increased rate and to a greater extent than when each plate was reacted separately. It is possible that the larger amount of water introduced into the solution via the hydrated silica plates enhances the silanation reaction; whereas, when only one plate is in solution, the physisorbed water on the silica surface dissolves into the dry cyclohexane solvent before the silanation reaction can occur.

The results of the kinetic experiments, FTIR, contact angle, and AFM studies suggest the following model for the OTS adsorption process, which is illustrated in Figure 2.11. Initially, OTS in solution approaches the water-covered silica surface where it is hydrolyzed at or near the surface as depicted in Figure 2.11a. Sagiv (1) suggested that if the only water present in the system is at the silica surface, then the OTS can only hydrolyze at the surface; however, it is probable that when using an ultra-sonic bath and dried cyclohexane, loosely bound water present on the silica plates will be desorbed into solution, thereby allowing for hydrolysis in the vicinity of the

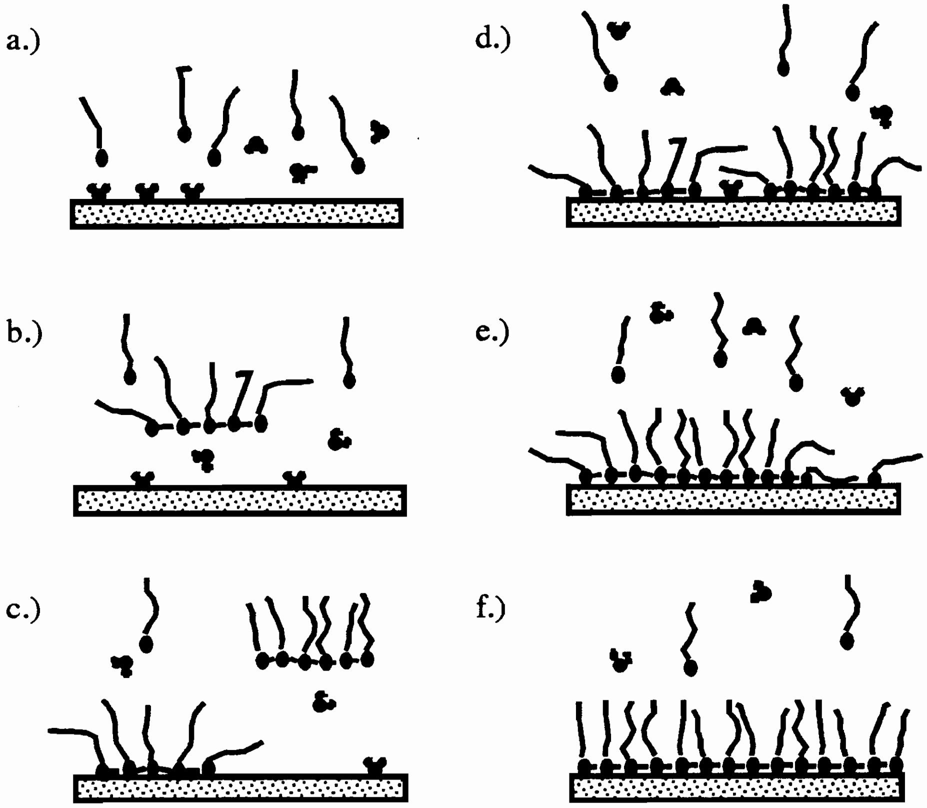

Figure 2.11 A proposed model for the OTS on SiO_2 adsorption process, in which (a) OTS molecules are attracted to the hydrated silica surface and (b) hydrolyze to form clusters. These hydrolyzed molecules or clusters (c) are weakly attracted to the physisorbed water on the silica surface and may eventually form patches on the silica surface. In time, (d) more patches form up to a point when (e) single OTS molecules adsorb (f), increasing the surface density to monolayer coverage.

silica surface. Plueddeman (28) noted that due to increased hydrophobicity, longer chain alkylchlorosilanes hydrolyze more slowly than those with shorter chains; therefore, it may be justified to assume that the hydrolysis of OTS molecules is kinetically favored in the vicinity of the hydrated silica surface where a higher concentration of water molecules exists. The AFM images suggest that small clusters of polymerized OTS form at or near the silica surface (Figure 2.11b), and these clusters then adsorb to form the patches seen in the AFM images (Figure 2.11c). The size of these clusters depends on the water content of the solvent. Silberzan *et al.* (3) suggested that these hydrolyzed OTS molecules or clusters are not bound to the silica surface. As the number of patches increases and completely covers the silica surface (Figure 2.11d), individual OTS molecules adsorb into the patches to increase the adsorption density within the patches (Figure 2.11e). After long immersion times and at the higher OTS concentrations, a highly-ordered and tightly-packed monolayer is formed (Figure 2.11f). The independence of the OTS patch size on the solution OTS concentration and the observed transient Langmuir adsorption kinetics suggest that the formation of the OTS patches is rapid and that the rate constants k_a and k_d describe the adsorption of individual OTS molecules into the patches.

2.4 CONCLUSIONS

It has been shown that durable, homogeneous self-assembled OTS monolayers can be formed on silica at room temperature from relatively low concentration organic solutions. It is also possible to achieve sub-monolayer coatings of varied hydrophobicity; however, these partial monolayers are not molecularly homogeneous. The OTS molecules form small patches on the surface even at low concentrations. Further adsorption increases the packing density within the patches without apparently increasing the size of the patches. The size of the patches and the uniformity of the surface coating are critically dependent upon the amount of water present in the system. No direct evidence has been uncovered as to whether the cross-linked OTS monolayer is chemically bound to the silica surface or only physisorbed on the surface with intervening water molecules; however, the AFM imaging suggests that the binding energy of the OTS patches to the surface is not strong.

2.5 REFERENCES

1. Sagiv, J., *J. Am. Chem. Soc.* **102,** 92 (1980).
2. Tripp, C. P., and Hair, M. L., *Langmuir* **8**, 1120 (1992).
3. Silberzan, P., Léger, L., Ausserré, D., and Benattar, J. J., *Langmuir* **7**, 1647 (1991).
4. Tripp, C.P., and Hair, M. L., *Langmuir* **7**, 923 (1991).
5. Tripp, C.P., and Hair, M. L., *Langmuir* **8**, 1961 (1992).
6. Angst, D. L., and Simmons, G.W., *Langmuir* **7**, 2236 (1991).
7. Tillman, N., Ulman A., and Penner T. L., *Langmuir* **5**, 101 (1989).
8. Tillman, N., Ulman, A., Schildkraut, J. S., and Penner, T. L., *J. Am. Chem. Soc.* **110**, 6136 (1988).
9. Maoz, R., and Sagiv, J., *J. Colloid Interface Sci.* **100**, 465 (1984).
10. Kessel, C., and Granick, S., *Langmuir* **7**, 532 (1991).
11. Guzonas, D. A., Hair, M. L., and Tripp, C. P. *in* "FTIR Spectroscopy in Colloid and Interface Science" (D. R. Scheuing, Ed.), Chapter 14, ACS, Washington D.C., 1990.
12. Hair, M. L., and Hertl, W., *J. Phys. Chem.* **73**, 4269 (1969).
13. Hair M. L. "Infrared Spectroscopy in Surface Chemistry", Chapter 4. Marcel Dekker, New York, 1967.

14. Lamb, R. N., and Furlong, D. N., *Trans. Faraday Soc.* **78**, 61 (1982).

15. DePalma, V., and Tillman, N., *Langmuir* **5**, 868 (1989).

16. Morrall, S. W., and Leyden, D. E. *in* "Silanes, Surfaces, and Interfaces" (D. E. Leyden, Ed.), p. 501. Gordon and Breach, New York, 1985.

17. Zettlemoyer, A. C., and Hsing, H. H. *in* "Colloid and Interface Science, Vol. 1" (M. Kerker, A. C. Zettlemoyer and R. L. Rowell, Eds.), p. 279. Academic Press, New York, 1977.

18. Trau, M., Murray, B. S., Grant, K., and Grieser, F., *J. Colloid Interface Sci.* **148**, 182, (1992).

19. Kern, W., *J. Electrochem. Soc.* **137**, 1887 (1990).

20. Brzoska, J. B., Shahidzadeh, N., and Rondelez, F., *Nature* **360**, 719 (1992).

21. Chen, S. H., and Frank, C. W. *in* "FTIR Spectroscopy in Colloid and Interface Science" (D. E. Scheuing, Ed.), Chapter 9. ACS, Washington D.C., 1990.

22. Casal, H. L., and Mantsch, H. H., *Biochimica et Biophysica Acta.* **779**, 381 (1984).

23. Ulman, A., *in* "FTIR Spectroscopy in Colloid and Interface Science" (D. E. Scheuing, Ed.), Chapter 8. ACS, Washington D.C., 1990.

24. Cassie, A. B. D., *Discuss. Faraday Soc.* **75**, 5041 (1952).

25. Israelachvili, J. N., and Gee M. L., *Langmuir* **5**, 288 (1989).

26. Lea, A. S., Pungor, A., Hlady, V., Andrade, J. D., Herron, J. N., and Voss, E. W., Jr., *Langmuir* **8**, 68 (1992).

27. Schwartz, D. K., Steinberg, S., Israelachvili, J. N., and Zasadzinski, J. A., *Physical Review Letters* **69**, 3354 (1992).

28. Plueddeman, E. P. *in* "Silylated Surfaces" (D. E. Leyden and W. T. Collins, Eds), p. 31. Gordon and Breach, New York, 1978.

CHAPTER 3 HYDROPHOBIC INTERACTIONS BETWEEN DISSIMILAR SURFACES

3.1 INTRODUCTION

Direct force measurements conducted between mica surfaces have revealed new information, especially concerning surface forces not considered in the DLVO theory (1, 2). Bare mica surfaces immersed in aqueous solutions of high electrolyte concentrations exhibited secondary hydration forces (3-6), while those in surfactant solutions exhibited hydrophobic forces (7-11). When force measurements were conducted in water-soluble polymer solutions, steric forces were observed (12-14). Such information is useful for understanding many industrial processes where non-DLVO forces play important roles. A case in point is the flotation process, which is believed to be driven by hydrophobic interactions (15). However, most of the data obtained from direct force measurements are for symmetric interactions, *i.e.*, two macroscopic bodies of the same hydrophobicity interact with each other, while bubbles and particles may have very different hydrophobicities. Therefore, it is difficult to estimate the magnitudes of the hydrophobic forces involved in bubble-particle interactions based on the force data reported in the literature to date.

Surface forces measured experimentally are routinely compared with those predicted from the DLVO theory,

$$F_t = F_d + F_e\,, \qquad [3.1]$$

in which F_t is the total force between two surfaces in close proximity, F_e the ion-electrostatic force between the overlapping electrical double layers, and F_d is the London-van der Waals dispersion force. When hydrophobic forces (F_h) are measured, Eq. [3.1] may be extended to

$$F_t = F_d + F_e + F_h\,. \qquad [3.2]$$

Measured hydrophobic forces are most commonly described by the empirical relationship (7),

$$\frac{F_h}{R} = C_o \exp\left(-\frac{H}{D_o}\right), \qquad [3.3]$$

in which F_h, normalized by the radius R of curvature of the mica surface, is shown to decay exponentially with respect to the closest separation distance H between the two curved surfaces, and C_o and D_o are constants. When stronger hydrophobic forces are measured, it is often necessary to use a double-exponential function,

$$\frac{F_h}{R} = C_1 \exp\left(-\frac{H}{D_1}\right) + C_2 \exp\left(-\frac{H}{D_2}\right), \qquad [3.4]$$

so that long-range hydrophobic forces can be accommodated by the second exponential term. It has been suggested that the pre-exponential parameters C_o and C_1 are related to interfacial tensions at the solid/liquid interface (16), while D_o, D_1 and D_2 are referred to as decay lengths. Hydrophobic forces can also be described by a power law (17),

$$\frac{F_h}{R} = -\frac{K}{H^2}, \qquad [3.5]$$

which is of the same form as the expression most commonly used for dispersion forces. Thus, Eq. [3.5] holds an advantage over Eqs. [3.3] and [3.4] in that force data can be represented by a single parameter, K, which can be directly compared with Hamaker constants. Furthermore, it may be possible that K can be treated in the same mathematical manner as Hamaker constants when deriving a combining rule for asymmetric interactions.

Many of the hydrophobic forces reported in the literature were measured using the Tabor and Winterton-type surface force apparatus (SFA) (18) with curved mica cylinders. When the measurements were conducted with mica surfaces coated with self-assembled monolayers, "short-range" hydrophobic forces with D_o in the range of 1.0 to 2.5 nm were observed (7-11, 19). With insoluble, double-chain surfactants deposited using the Langmuir-Blodgett (LB) technique, the measured forces were of substantially longer-range with D_2 in the range of 10 to 24 nm (20, 21). In the presence of neutral surfactants such as octanol and dodecanol, however, even self-assembled monolayers exhibited long-range hydrophobic forces with D_2 in the range of 4.4 to 9.5 nm (10, 11). It was suggested, therefore, that long-range hydrophobic forces are created when close-packed monolayers of hydrocarbon chains are formed on mica surfaces (22, 23). It was also shown that decay lengths increase sharply when advancing water contact angle (θ_a) is close to or exceeds 90°, suggesting that the long-range hydrophobic force may arise from cavitation (11).

Despite its high accuracy, the SFA can only be used for optically transparent and isotropic materials. These limitations can be overcome by using an atomic force microscope (AFM), which has essentially the same operating principle as that of the SFA. When using a pyramidal tip with a sensitive cantilever spring, the AFM can generate morphological images with atomic resolution (24). By attaching a sphere to the tip, Ducker and Senden (25) were able to measure long-range repulsive ion-electrostatic forces. Using cantilever springs substantially stronger than those used by previous investigators, Rabinovich and Yoon (26, 27) measured hydrophobic forces between glass spheres and silica plates hydrophobized with octadecyltrichlorosilane (OTS). The AFM technique allows the measurement of hydrophobic forces with fewer constraints due to the optical properties of the materials used. Any material with sufficient smoothness and availability in spherical form can be used. Thus, the AFM has been used for surface force measurements with a variety of materials, including polypropylene (28), gold (29, 30), zirconia (14), TiO_2 (31), ZnS (32), and SiO_2 (25-27, 33-35). The AFM has also been used to measure forces between an air bubble and hydrophilic silica (34, 36). One serious limitation associated with the AFM technique is that it cannot give absolute separation distances, which can become a source of error when using surfaces coated with thick adsorption layers. Furthermore, calibration of the cantilever spring is more cumbersome than for the SFA, and the availability of cantilevers with appropriate spring constants is limited. Recently, a new SFA capable of measuring separation distances by means of a piezoelectric material (bimorph) has been developed, so that it can be used to measure surface forces between opaque materials (37-41).

Claesson *et al.* (42) were perhaps the first to conduct asymmetric force measurements using an SFA. The measurement was conducted in water between a bare mica surface and a mica surface coated with dimethyldioctylammonium ($DDOA^+$) ions. These investigators observed attractive forces larger than those between two $DDOA^+$-coated mica surfaces, which was attributed to an electrostatic attraction between oppositely charged surfaces. Tsao *et al.* (43) obtained similar results with the same system, but had a different interpretation. These investigators concluded that the highly charged bare mica surface correlates with the domains of $DDOA^+$ species on the opposing mica surface to give rise to a long-range attraction. Parker and Claesson (41) conducted force measurements between hydrophilic clean glass and hydrophobic silanated glass surfaces (both of which have essentially the same surface potentials), and found no evidence for long-range attractive forces. This finding was corroborated by the results of Rabinovich and Yoon (27), who observed only a slight deviation from DLVO theory when using an AFM with a hydrophilic glass sphere and a silanated silica plate. On the other hand, Ducker *et al.* (34) observed a large unstable non-DLVO attractive force between clean glass and silanated silica.

The purpose of the present investigation was to conduct direct force measurements for asymmetric hydrophobic interactions using an AFM. The force measurements were conducted between a glass sphere with a very high contact angle and silica plates of varying degree of hydrophobicity. Both the glass sphere and silica plates were hydrophobized using OTS. The results were compared with those obtained for symmetric hydrophobic interactions, so that a combining rule for the hydrophobic force constants (*K*) could be developed. The results of the present study would be useful to predict the magnitude of hydrophobic forces between two dissimilar surfaces.

3.2 MATERIALS AND METHODS

3.2.1 *Materials*

Optically smooth Herasil 3 fused silica plates were obtained from Heraeus Amersil, Inc. and cleaned in boiling nitric acid before use. Glass spheres obtained from Duke Scientific were used as received. HPLC grade cyclohexane was obtained from Aldrich Chemical Co. and dried overnight over 3-12 mesh Davidson 3 Å molecular sieves. OTS was also obtained from Aldrich at 95% purity, and used without further purification. Epon R Resin 1004F from Shell Chemicals Co. was used as an adhesive. All experiments were performed using conductivity water produced from a Barnstead Nanopure water purification system.

3.2.2 *Apparatus*

Surface forces between a silanated glass sphere and an OTS-covered flat silica plate were measured using a Digital Instruments Nanoscope III atomic force microscope. The AFM was equipped with a standard liquid cell as depicted in Figure 3.1. A glass sphere ***a*** of 15-25 μm radius was attached to the end of an AFM cantilever ***b*** using an epoxy resin, which has been found not to contaminate the aqueous liquid medium (44). The sphere and cantilever were placed in an AFM liquid cell ***c*** with an O-ring ***d*** between the cell and the silica sample ***e*** to form a water-tight cavity. Conductivity water was injected into the cavity ***f*** through one of the two liquid ports ***g*** by means of a syringe. Monochromatic light emitted from a laser diode ***h*** was reflected

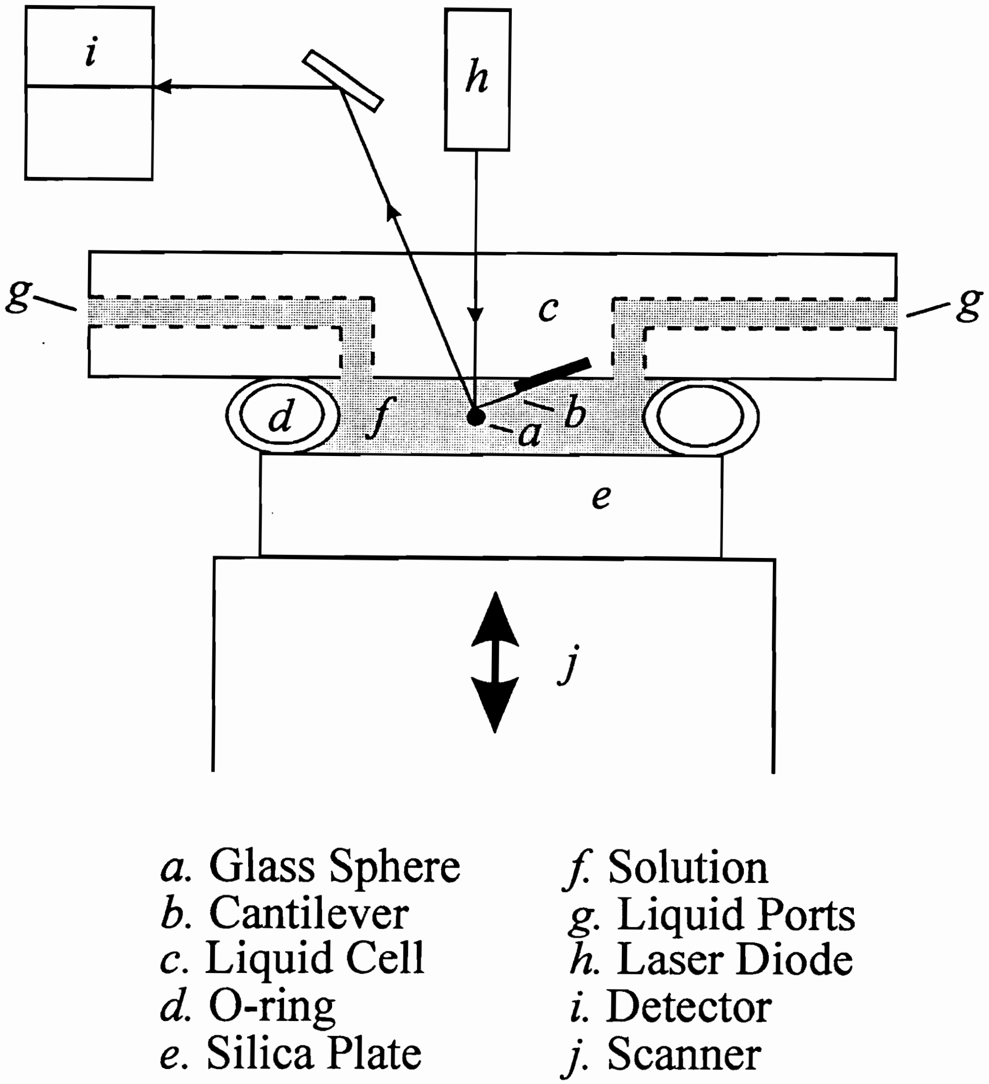
i
h
g
c
g
d
f
b
a
e
j
a. Glass Sphere
b. Cantilever
c. Liquid Cell
d. O-ring
e. Silica Plate
f. Solution
g. Liquid Ports
h. Laser Diode
i. Detector
j. Scanner

Figure 3.1 Schematic representation of the atomic force microscope (AFM) as used for measuring forces in a liquid between a flat silica plate and a glass sphere.

off the cantilever to a split photodetector ***i*** to monitor the position of the sphere. As the piezoelectric scanner ***j*** moved the silica sample toward the probe, the cantilever was deflected from its original position depending on the nature of the surface forces acting between the glass sphere and the silica plate.

The sphere-flat plate geometry used in the present work and shown in Figure 3.1 allows the forces measured to be compared to the free energies of interaction between two flat plates using the Derjaguin approximation (45).

3.2.3 *Cantilever Calibration*

Figure 3.2 depicts the three different types of cantilevers obtained from Digital Instruments, Inc. to cover the range of sensitivities needed for the force measurements. For measuring relatively weak electrostatic repulsive forces, a standard triangular silicon nitride (Si_3N_4) tip was used, while a rectangular tapping etched silicon probe (TESP) cantilever was used to measure strong attractive hydrophobic forces. The force etched silicon probe (FESP), which was longer than the others, was used to measure forces in the intermediate range. Although the manufacturer provided approximate values of spring constants, each cantilever was calibrated in the present work.

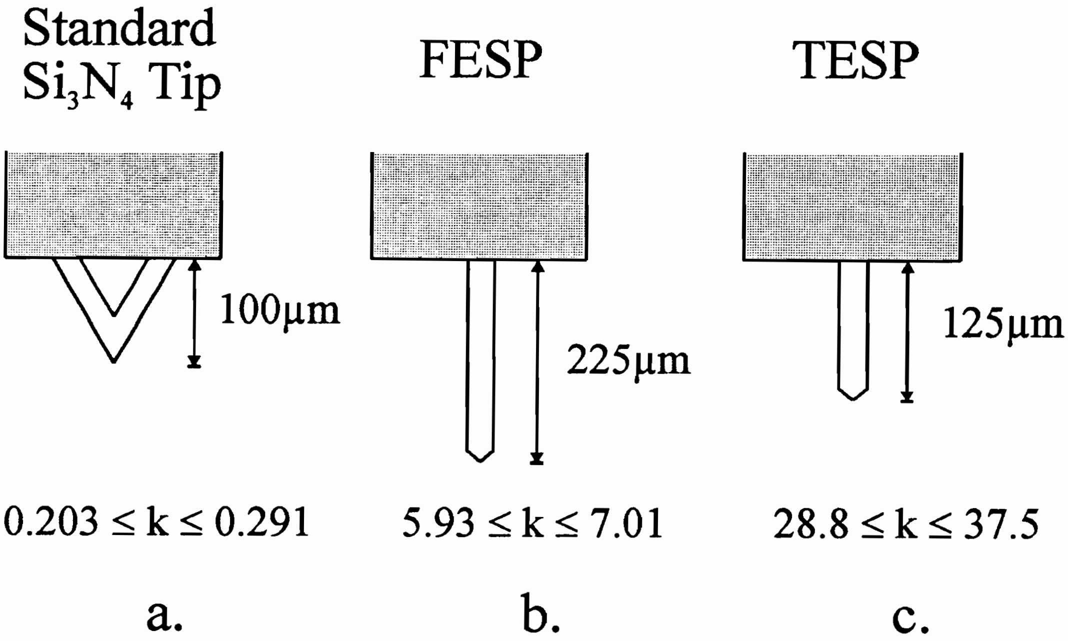
Standard
Si_3N_4 Tip
FESP
TESP
100µm
225µm
125µm
$0.203 \leq k \leq 0.291$
$5.93 \leq k \leq 7.01$
$28.8 \leq k \leq 37.5$
a.
b.
c.

Figure 3.2 Schematic representation of the AFM cantilevers used for force measurements: a) a standard triangular Si_3N_4 cantilever for weak interactions, b) a force etched silicon probe (FESP) for moderate forces, and c) a tapping etched silicon probe (TESP) for strongly hydrophobic forces. A range of spring constants, as determined by the inversion technique, are given for each cantilever.

The cantilever calibration was made using the technique reported by Sender and Ducker (46). In this method, a sphere of known mass is placed at the end of a cantilever spring, and the deflection of the tip is measured as the AFM is inverted. In the present work, tungsten spheres (from GTE Sylvania) were used as the load. From the deflection (x) measured in volts, the spring constant (k) was determined using the following relationship:

$$k = \frac{\frac{4}{3}\pi R^3 \rho g S}{\frac{1}{2}x}, \qquad [3.6]$$

where R is the radius of the tungsten sphere, ρ (= 19.35 g/cm^3) is its density, g is gravitational acceleration, and S is the detector sensitivity in volts/nm. Figure 3.2 shows the range of spring constants determined in the present work for the three different types of cantilevers used. The measured values were found to be up to 50% lower than those given by the manufacturer, particularly for the standard Si_3N_4 tip.

3.2.4 *Silanation*

Fused silica plates were cleaned in a boiling nitric acid solution, and silanated in OTS-in-cyclohexane solutions under a nitrogen atmosphere. The detailed silanation procedure and the characteristics of the silanated silica surfaces are described elsewhere (47). In the present work, a glass sphere was mounted on a cantilever spring by means of an epoxy resin prior to silanation. A fused silica plate was silanated in the same batch of OTS solution, so that the glass spheres and the silica plate would have the same hydrophobicity. The hydrophobicity of the silica plates and glass spheres were controlled by varying the concentration of the OTS in solution and the immersion time.

3.2.5 *Contact Angle Measurements*

Water contact angles were used to assess the hydrophobicity of the silanated silica plates and were measured using a Ramé-Hart Model 100 goniometer. A Hamilton microliter syringe was used to place a 5 μl drop of Nanopure water on a silica surface to measure equilibrium contact angle. The measurements were repeated twice and averaged. It is estimated that an inherent error of ±3° may be associated with the measurement of angles. Contact angles of the hydrophobized glass spheres were considered to be the same as the silica plates silanated in the same batch of OTS solution.

3.3 RESULTS AND DISCUSSION

3.3.1 *Force Measurements for Symmetric Interactions*

Figure 3.3 shows the results of the force measurements conducted between symmetric surfaces, *i.e.*, the silica plates and glass spheres used in the force

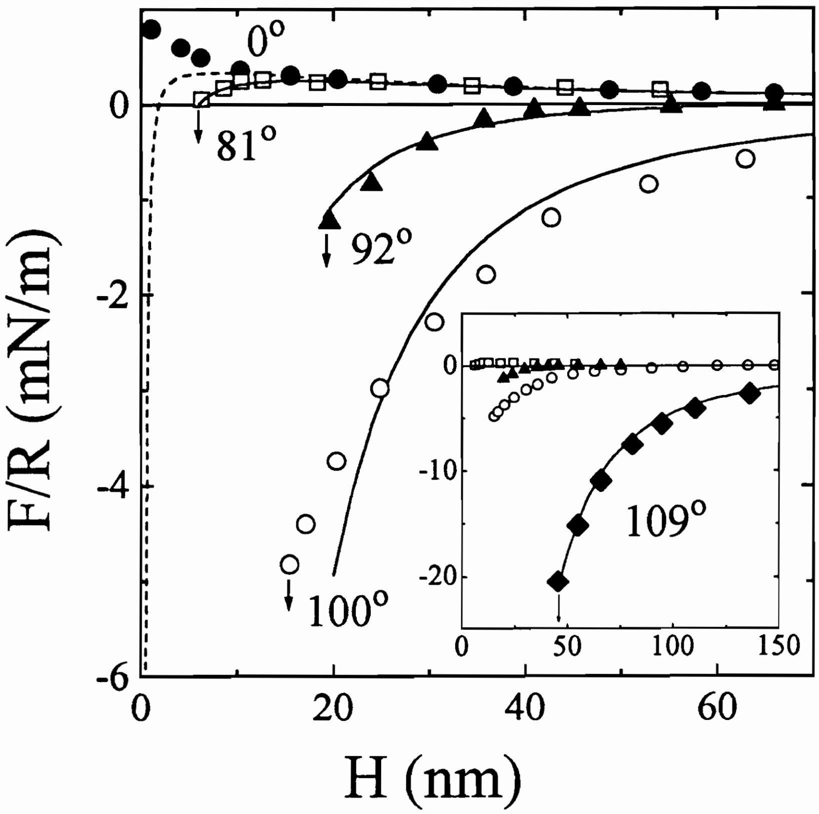

Figure 3.3 Results of the AFM force measurements conducted with glass spheres and silica plates. The force (*F*) was normalized by the radius (*R*) of the glass sphere and plotted versus the closest separation distance (*H*). Each force curve was obtained using a sphere and a plate, silanated with octadecyltrichlorosilane (OTS) under identical conditions so that both were of the same contact angle: ●) 0°, □) 81°, ▲) 92°, ○) 100°, and ◆) 109°. The dashed line represents a DLVO fit of the data with A_{131} = 8×10^{-21} J, ψ_1 = -60 mV, κ^{-1} = 42 nm, while the solid lines represent the extended DLVO theory which includes a power law (Eq [3.5]) to account for the contributions from the hydrophobic force. Hydrophobic force parameters are given in Table 3.1. The arrows show the jump distances.

measurements had been silanated under identical conditions so that both have the same degree of hydrophobicity and, hence, the same contact angle (θ). The measured forces (F), normalized with respect to the radius of the sphere (R) are plotted versus the separation distance (H). At $\theta = 0°$ and $81°$, measured forces are repulsive. As θ is further increased, they become net attractive, their magnitudes increasing with increasing contact angle. Since the attractive forces measured at $\theta = 109°$ are so much larger than those measured at lower contact angles, they are plotted separately at the inset.

The dotted curve in Figure 3.3 represents a DLVO fit of the data using Eq. [3.1]. F_e has been calculated using a constant potential model of Ohshima *et al.* (48). According to Laskowski and Kitchener (49), silanation does not significantly change the ζ-potentials of silica. Therefore, all of the data shown in Figure 3.3 have been fitted with ψ_1 = -60 mV. F_d of Eq. [3.1] was obtained using the well-known relationship

$$F_{\mathrm{d}} = -\frac{RA_{131}}{6H^2}, \qquad [3.7]$$

in which A_{131} (= 8×10^{-21} J) (50) is the Hamaker constant of silica **1** in water **3**.

As Figure 3.3 shows, the DLVO theory does not fit the experimental data obtained in the present work, which is not surprising. According to Derjaguin and

Churaev (51, 52), the DLVO theory is applicable only to lyophobic colloids whose θ is in the range of 20° to 40°, while the θ values for the surfaces used for the force measurements are outside this range. Therefore, the force data obtained at $\theta \geq 81°$ were fitted to the extended DLVO theory (Eq. [3.2]), which incorporates Eq. [3.5] to account for the contributions from attractive hydrophobic forces (F_h). The solid lines represent the extended DLVO curves where ψ_1 = -60 mV, κ^{-1} = 42 nm, and A_{131} = $8\text{x}10^{-21}$ J, and with the K values of Eq. [3.5] as the only adjustable parameters. The fitted parameters of K (actually K_{131} to indicate that this constant is for symmetric interactions in water) are shown in Table 3.1. Also shown in this table for comparison are the K values determined from the jump distances, which are indicated in Figure 3.3 by arrows. For AFM force measurements, jump distances are determined by the changes in the slope of the displacement *vs.* distance diagrams. When the ion-electrostatic force is relatively small, K_{131} can be determined from a jump distance (H_j) by the following relationship (26):

$$K_{131} = \frac{3kH_j^3}{R} - A_{131}, \qquad [3.8]$$

where k is the spring constant. As shown in Table 3.1, the values of K_{131} determined using the equilibrium and jump methods are in reasonable agreement; however, the former method produces more reliable values since there is a degree of uncertainty

TABLE 3.1

Force Parameters Obtained for Symmetric Interactions

θ (°)	H_j (nm)	C_2 (mN/m)	D_2 (nm)	K_{131} (10^{-18} J)		F_{ad}/R (mN/m)
				equil.	jump	
81	6.30	-9.0	2.0	0.07	0.20	4.63
92	19.6	-12	10	3.2	5.82	45.1
100	15.5	-9.0	24	12.5	9.94	38.6
109	45.5	-83	32	270	340	144

associated in determining H_j. Also shown in Table 3.1 are the values of C_2 and D_2 obtained by fitting the data to the extended DLVO theory (Eq. [3.2]) which incorporates the exponential force law (Eq. [3.4]) to represent the contributions from the hydrophobic force. In this fitting exercise, the values of C_1 and D_1 were considered negligibly small as compared to those of C_2 and D_2.

Although some investigators (49, 53) showed that ζ-potentials do not change after silanation with trimethylchlorosilane (TMCS), others (54-56) reported a considerable reduction in the negative ζ-potential particularly when the concentration of TMCS is high. This finding may suggest that the monofunctional TMCS reacts with the silanol groups on the silica surface which serve as charge sites. However, the OTS used in the present work as a silanating agent may react differently from TMCS. According to Tripp and Hair (57), tri-functional alkylchlorosilanes such as OTS do not, to a large extent, form covalent bonds with surface silicon atoms at room temperature. In the presence of sufficient water molecules on the surface, OTS molecules undergo cross-linking polymerization without displacing the surface hydroxyl groups to form covalent bonds with the surface silicon atoms. As a result of the cross-linking polymerization, OTS molecules form clusters on fused silica surfaces even at low surface coverage (47). Such a mechanism may support the assumption made in the present work that OTS-coated silica and glass surfaces have substantially the same double-layer potentials as the fresh unsilanated samples.

The results of the force measurements given in Figure 3.3 and Table 3.1 show that the hydrophobic force increases with increasing contact angle (θ). It is interesting that both D_o and K increase sharply as θ becomes greater than 90°. This finding is consistent with the observation made by Yoon and Ravishankar (11) that long-range hydrophobic forces begin to appear when advancing water contact angle (θ_a) exceeds 90°.

It may be noteworthy that the TESP and FESP cantilevers used in the present work were not sensitive enough to measure attractive forces at $\theta < 81°$. On the other hand, the force curve obtained at $\theta = 109°$ represents one of the strongest hydrophobic forces reported in the literature, and is comparable to that reported by Rabinovich and Yoon (27) for the same system.

Table 3.1 also includes values of adhesion force (F_{ad}), which is defined as the maximum force required to pull two surfaces apart after an initial contact. As shown, F_{ad} increases with increasing θ, which agrees well with the relationship developed by Johnson *et al.* (58) and Derjaguin *et al.* (59):

$$F_{ad}/R = n\pi\,(\gamma_{SV} - \gamma_{LV}\cos\theta)\,, \qquad [3.9]$$

where γ_{SV} and γ_{LV} are the surface free energies at the solid-vapor and liquid-vapor interfaces, respectively, and n = 4 for non-deformable solids, while n = 3 for deformable solids. Theoretically, F_{ad} should fall between the lower limit of n = 3 and the upper limit of n = 4. However, the values of F_{ad} obtained in the present work are below the lower limit, and are up to 50% lower than those reported by Parker and Claesson (41) for similar surfaces. On the other hand, they are in reasonable agreement with the results of Rabinovich and Yoon (27) reported for silica and glass surfaces silanated with OTS. The low adhesion forces may be attributed to the surface roughness of the glass spheres and silica plates used in the present work. Another possible reason may be that the configuration of the AFM allows the two surfaces to be detached prematurely by a shearing force.

As has already been noted, the DLVO theory is applicable to lyophobic colloids with $20° < \theta < 40°$. Likewise, the results obtained in the present work at $\theta = 0°$ cannot be fitted to the DLVO theory (Eq. [3.1]), particularly at $H < 13$ nm (See Figs. 3.3 and 3.4). It has been shown by many investigators that the deviation is due to a hydration force. Therefore, the data obtained at $\theta = 0°$ have been fitted to the extended DLVO theory (Eq. [3.2]) which incorporates Eq. [3.4] to represent contributions from the hydration force. The solid curve in Figure 3.4 represents the extended DLVO fit with $C_1 = 12$ mN/m, $C_2 = 1.1$ mN/m, $D_1 = 0.4$ nm, and $D_2 = 3.0$ nm. These parameters are

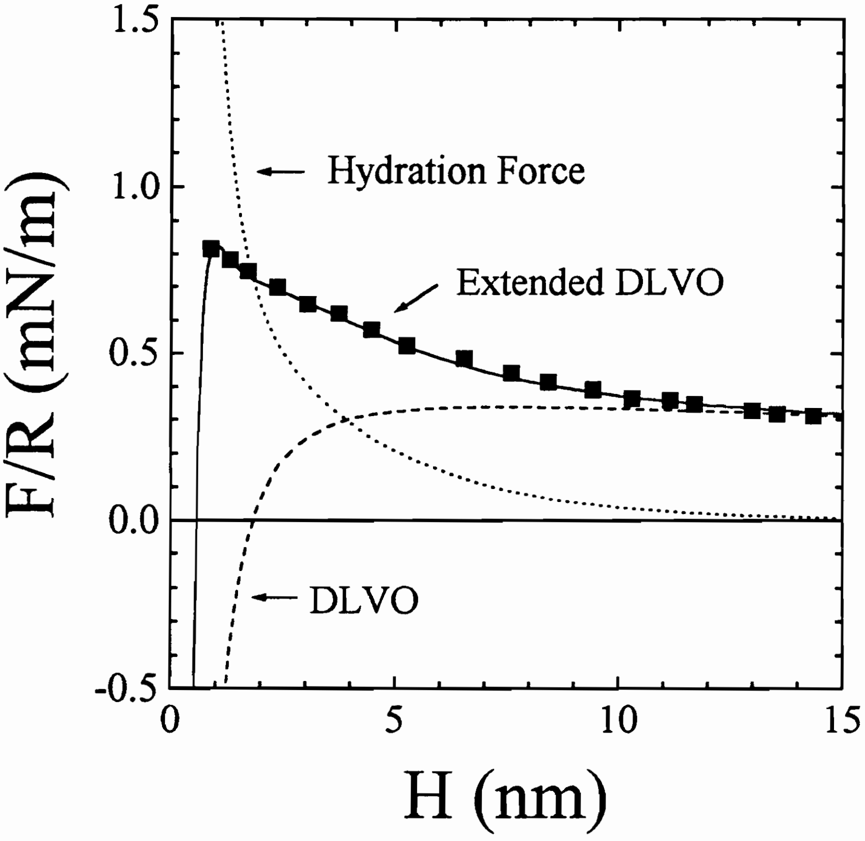

Figure 3.4 F/R vs. H curve obtained with a clean glass sphere and a bare silica plate in water. The dashed line represents a DLVO fit with A_{131} = 8x10^{-21} J, ψ_1 = -60 mV, and κ^{-1} = 42 nm, while the solid line represents the extended DLVO theory which includes the hydration force. The dotted line represents the hydration force (Eq. [3.4]) with C_1 = 12 mN/m, D_1 = 0.4 nm, C_2 = 1.1 mN/m, and D_2 = 3.0 nm.

consistent with those reported for the secondary hydration forces measured with mica in the presence of inorganic electrolytes (3-6) and the primary hydration forces measured with silica (35, 60, 61).

3.3.2 *Force Measurements for Asymmetric Interactions*

Figure 3.5 shows the force curves obtained between glass spheres and silica plates having dissimilar contact angles. The spheres have values of $\theta = 109°$, while those of the silica plates were varied as shown for each force curve. The dashed line represents the classical DLVO theory, while the solid lines represent the extended DLVO theory, which includes an additional term in the form of a power law (Eq. [3.5]) to represent the hydrophobic attraction.

When the force measurements were conducted with a silica plate having $\theta = 0°$, the measured forces were repulsive due to double-layer interactions. At longer separation distances, the data can be fitted to the DLVO theory (constant potential model) with ψ_1 = -60 mV, κ^{-1} = 42 nm, and A_{132} = 8x10^{-21} J. However, the two surfaces jump into contact with each other at a distance greater than that predicted by the DLVO theory. Actual jump distances varied with each measurement, and the value of 16.1 nm reported here was the largest jump observed. Based on this jump distance, the value of K_{132} in Eq. [3.5] was estimated to be approximately 1.1x10^{-20} J, which is

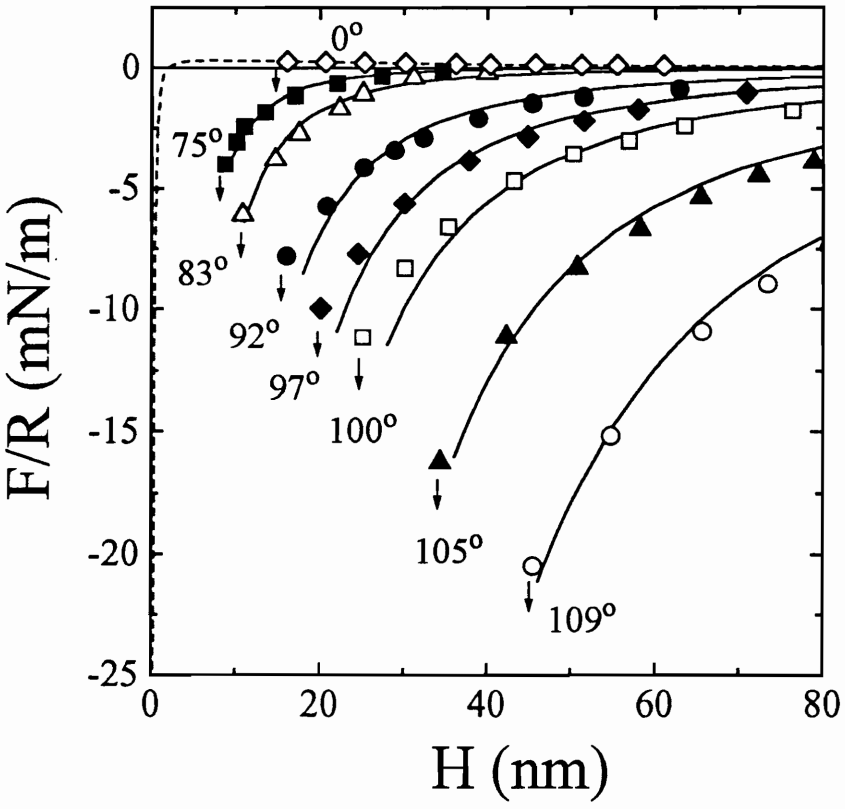

Figure 3.5 *F*/*R* vs. *H* curves obtained between silanated glass sphere with contact angle of 109° and silanated silica plates with the following contact angles: (◊) 0°, (■) 75°, (Δ) 83°, (●) 92°, (◆) 97°, (□) 100°, (▲) 105°, and (○) 109°. The dashed line represents the classical DLVO theory (Eq. [3.1]) with $A_{131} = 8\text{x}10^{-21}$ J, ψ_1 = -60 mV, and κ^{-1} = 42 nm. The solid lines represent the extended DLVO theory incorporating a power law (Eq [3.5]) to account for the contributions from the hydrophobic force. The arrows show the jump distances. Hydrophobic force parameters are given in Table 3.2.

rather close to the Hamaker constant ($8x10^{-21}$ J). For the silica-OTS system, the Hamaker constant is expected to increase by only 10% at monolayer coverage (34); therefore, it may be suggested that there exists a weak hydrophobic force for the interaction between a silica surface with $\theta = 0°$ and a glass sphere with $\theta = 109°$.

Ducker *et al.* (34) and Rabinovich and Yoon (27) also conducted AFM force measurements between untreated glass spheres and OTS-coated silica and observed jump distances significantly larger than predicted by the DLVO theory. On the other hand, the force measurement conducted by Parker and Claesson (41) with a bare silica and a fluorocarbon-coated silica showed a jump distance only slightly larger than that predicted by the DLVO theory. That the latter investigators showed no evidence for hydrophobic force may be attributed to the relatively low contact angle exhibited by the fluorocarbon-coated silica surface. Nevertheless, the apparently weak hydrophobic force observed between a hydrophilic surface and a strongly hydrophobic surface is somewhat surprising, and a further investigation may shed light on the origin of the hydrophobic force.

The forces measured between glass spheres having $\theta = 109°$ and silica plates with $\theta > 75°$ show more definitive evidence for the existence of a hydrophobic force. As shown in Figure 3.5, the measured forces become increasingly attractive as the contact angle of the silica plate increases. The data was fitted to the extended DLVO theory incorporating a hydrophobic force term (Eq. [3.5]), as shown by the solid lines. The values of K_{132} for Eq. [3.5] are given in Table 3.2. Also shown in this table are the values of C_2 and D_2 of Eq. [3.4]. It is interesting that the values of the hydrophobic force parameters obtained between asymmetric surfaces, K_{132}, lie between those for the symmetric interactions, *i.e.*, K_{131} and K_{232}, suggesting that it may be possible to establish a combining rule to predict asymmetric hydrophobic interactions.

3.3.3 *Combining Rules for Hydrophobic Interactions*

Since Eqs. [3.5] and [3.7] are similar in form, it may be reasonable to expect that the force constant (K_{132}) for asymmetric hydrophobic interactions can be estimated from those (K_{131} and K_{232}) for symmetric interactions using the combining rules developed for dispersion interactions. There are two principal combining rules for the dispersion interactions. The first, suggested by Hamaker (62), is based on a microscopic approach which involves a step-by-step summation of the pair molecular potentials to calculate the energy of interaction between bodies **1** and **2** in medium **3**. It has the following form:

$$A_{132} = A_{12} + A_{33} - A_{13} - A_{23}\,, \qquad [3.10]$$

where A_{ij} is the Hamaker constant for the interaction of bodies **i** and **j** *in vacuo*. If body **1** is the same as body **2**, Eq. [3.10] reduces to

TABLE 3.2

Force Parameters Obtained for Asymmetric Interactions

θ (°)	H_j (nm)	C_2 (mN/J)	D_2 (nm)	K_{132} (10^{-18} J) equil.	K_{132} (10^{-18} J) jump	F_{ad}/R (mN/m)
0	16.1	-20	2.0	0.01	-	-
75	8.79	-9.0	9.0	2.20	2.42	36.8
83	10.8	-12	12	4.88	4.55	70.6
92	16.1	-15	20	17.1	13.4	50.2
97	20.1	-25	22	32.5	27.0	58.1
100	25.1	-30	25	55.0	53.0	77.5
105	34.3	-58	28	126	145	124
109	45.5	-83	32	270	340	144

$$A_{131} = A_{11} + A_{33} - 2A_{13}\ . \qquad [3.11]$$

These combining rules are based on the assumption of the additivity of dispersion forces, which is not strictly valid for solids.

A second combing rule is based on the London formula (63),

$$V_{12}(r) = -\frac{\beta_{12}}{r^6}, \qquad [3.12]$$

where V_{12} is the dispersion energy between molecules **1** and **2**, r is the intermolecular distance, and β_{12} is a constant. One can calculate β_{12} using the following expression:

$$\beta_{12} = \frac{3\alpha_{01}\alpha_{02}I_1 I_2}{2(4\pi\varepsilon_0)^2(I_1 + I_2)}, \qquad [3.13]$$

where α_{0i} and I_i are electronic polarizability and first ionization potential, respectively, and ε_0 is the permittivity of vacuum. For the interaction between like molecules, Eq. [3.13] reduces to

$$\beta_{11} = \frac{3\alpha_{01}^2 I_1}{4(4\pi\varepsilon_0)^2}. \qquad [3.14]$$

Likewise, β_{22} becomes

$$\beta_{22} = \frac{3\alpha_{02}^2 I_2}{4(4\pi\varepsilon_0)^2}. \qquad [3.15]$$

From Eqs. [3.13]-[3.15], one obtains the following relationship:

$$\beta_{12} \approx \sqrt{\beta_{11}\beta_{22}}\ , \qquad [3.16]$$

if $I_1 \approx I_2$. By substituting Eq. [3.16] into Eq. [3.12] and integrating, a second combining rule for Hamaker constants is obtained,

$$A_{12} = \sqrt{A_{11} A_{22}}\,, \qquad [3.17]$$

which is applicable *in vacuo*. In a medium **3**, Eq. [3.17] becomes

$$A_{132} = \sqrt{A_{131} A_{232}}\,. \qquad [3.18]$$

From Eqs. [3.11] and [3.18], the following relationship is obtained (64, 65):

$$A_{132} = (\sqrt{A_{11}} - \sqrt{A_{33}})(\sqrt{A_{22}} - \sqrt{A_{33}})\,. \qquad [3.19]$$

Although Eq. [3.19] is also referred to as a combining rule, it is merely a consequence of the two principal combining rules.

The limitations of applying these combining rules have been discussed in detail both theoretically and numerically (66, 67). In general, the limitations arise from the microscopic approach to the dispersion interaction of macroscopic bodies. This approach can give inaccurate Hamaker constants particularly in a medium with a high dielectric constant. Nevertheless, the combining rules have been successfully used to approximate dispersion interactions between dissimilar bodies.

The geometric mean combining rules (Eqs. [3.17]-[3.18]) can also be used for ion-electrostatic interactions, if the potentials are small and of the same sign. Under these conditions, the ion-electrostatic energy between two flat surfaces with constant potentials ψ_1 and ψ_2 can be calculated as follows (68):

$$E_{12} = \frac{\varepsilon\kappa}{2\pi}\psi_1\psi_2\exp(-\kappa H). \qquad [3.20]$$

For symmetric interactions, it follows that

$$E_{11} = \frac{\varepsilon\kappa}{2\pi}\psi_1^2\exp(-\kappa H), \qquad [3.21]$$

and

$$E_{22} = \frac{\varepsilon\kappa}{2\pi}\psi_2^2\exp(-\kappa H). \qquad [3.22]$$

From Eqs. [3.20]-[3.22], the following combining rule for the ion-electrostatic energies is obtained:

$$E_{12} = \sqrt{E_{11}E_{22}}. \qquad [3.23]$$

Thus, the combining rules for both dispersion and ion-electrostatic interactions have been derived from theoretical basis. The geometric mean combining rule has also been used in determining van der Waals interaction constants for real gas mixtures (69, 70), intermolecular distances (71), and components of interfacial energies (72-75).

At present, there are no theoretical equations for hydrophobic forces from which one can derive a combining rule. It is possible, however, to establish an empirical relationship between the hydrophobic force constants obtained in the present work for the symmetric and asymmetric interactions. Figure 3.6 shows experimental K_{132} values compared with those predicted from experimental K_{131} and K_{232} values using three possible combining rules. In this figure, the K_{132} values are plotted versus the contact angles (θ) of the silica plates, which are smaller than that ($\theta = 109°$) of the glass sphere. The first possible combining rule considered was the simple arithmetic mean,

$$K_{132} = \frac{K_{131} + K_{232}}{2}, \qquad [3.24]$$

which gives a value closer to the larger of the two symmetric force constants. When one hydrophobic force constant (*e.g.*, K_{232}) is much larger than the other (K_{131}), K_{132} is dominated by the larger one, *i.e.*, $K_{132} \approx ½ K_{232}$. The second possible combining rule considered was the harmonic mean,

$$K_{132} = \frac{2K_{131}K_{232}}{K_{131} + K_{232}}, \qquad [3.25]$$

which favors the smaller of the two symmetric hydrophobic force constants. The third combining rule tested was a geometric mean,

$$K_{132} = \sqrt{K_{131}K_{232}}, \qquad [3.26]$$

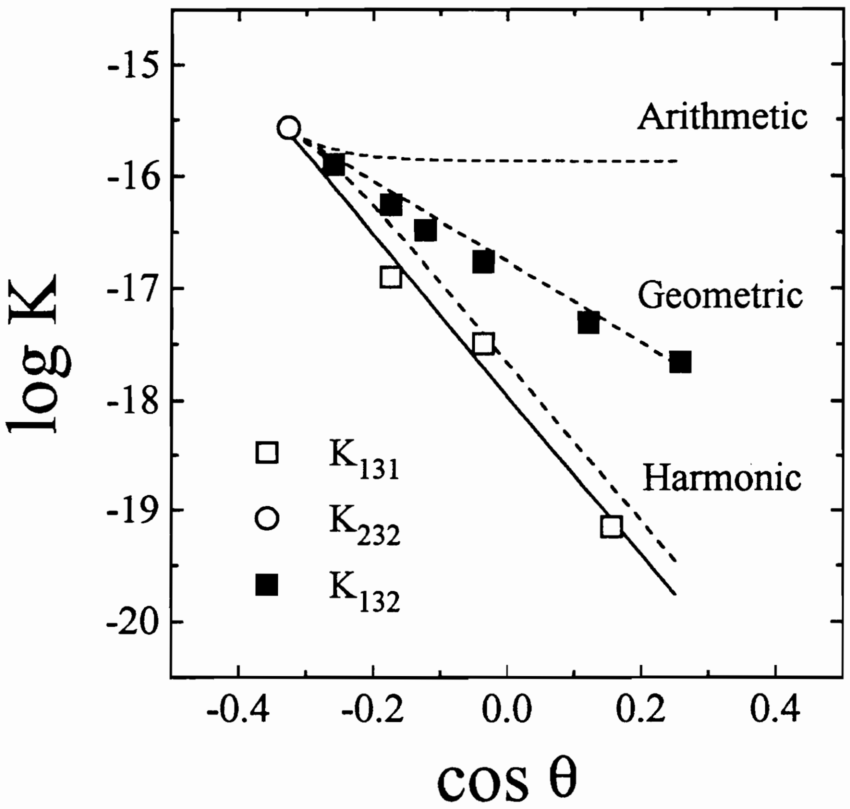

Figure 3.6 Log K vs. cos θ plots for K_{131} (□), K_{232} (○), and K_{132} (■). The solid lines represents the best fit of log K_{131} values. Dashed lines represent the K_{132} values predicted from the values of K_{131} and K_{232} using arithmetic, geometric, and harmonic means.

which has the same form as Eq. [3.18] for Hamaker constants. As shown in Figure 3.6, the geometric mean combining rule provides the best fit to the experimental data obtained in the present work.

Figure 3.6 shows that the logarithms of the symmetric hydrophobic force constants (K_{131} and K_{132}) vary linearly with cos θ, *i.e.*,

$$\log K_{131} = a\cos\theta_1 + b \qquad [3.27]$$

and

$$\log K_{232} = a\cos\theta_2 + b \qquad [3.28]$$

in which a (= -7.0) is the slope and b (= -18.0) is the value of K_{131} (or K_{232}) at cos θ = 0. Taking the logarithm of Eq. [3.26] yields

$$\log K_{132} = ½ (\log K_{131} + \log K_{232}). \qquad [3.29]$$

Substituting Eqs. [3.27] and [3.28] into Eq. [3.29] results in the following relationship:

$$\begin{aligned}\log K_{132} &= a\left(\frac{\cos\theta_1 + \cos\theta_2}{2}\right) + b \\ &= a(\cos\theta)_{\text{avg}} + b.\end{aligned} \qquad [3.30]$$

Thus, if log K_{132} is plotted versus $(\cos\theta)_{\text{avg}}$, experimental K_{132} values should fall on the same line as that for K_{131} and K_{232}, which is found to be the case in Figure 3.7. An important implication of Figure 3.7 is that the hydrophobic force is uniquely determined by contact angles. For symmetric interactions, the hydrophobic force is a function of

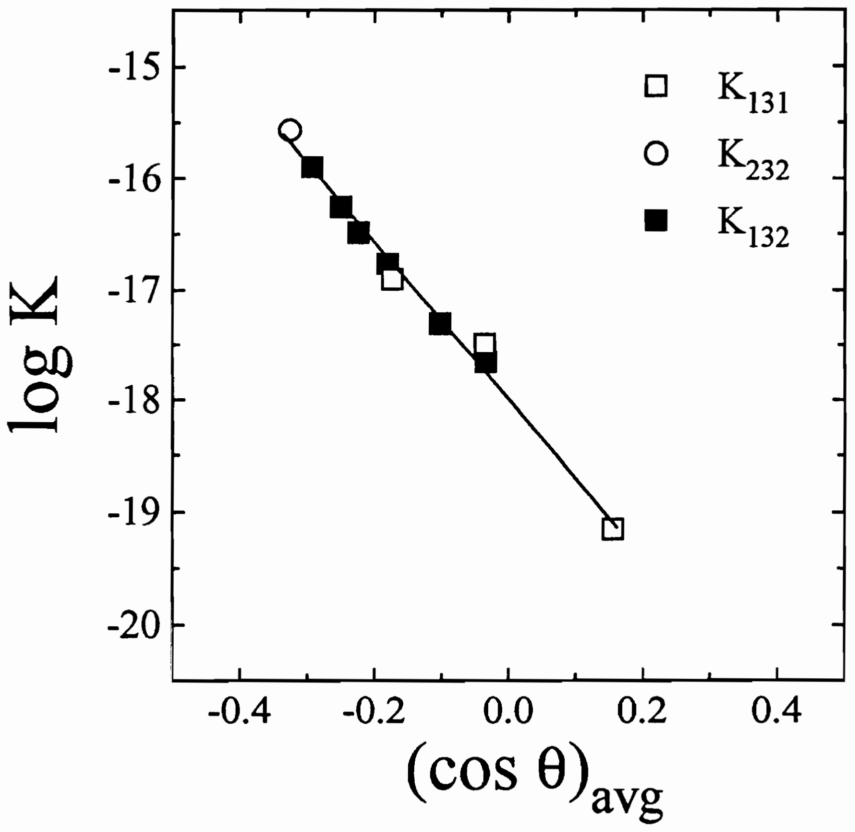

Figure 3.7 Log *K* vs. $(\cos\theta)_{avg}$ plots for the K_{131}, K_{232}, and K_{132} values determined using AFM for silanated glass sphere and silica plates.

the contact angles of the surfaces involved, while for asymmetric interactions it is determined by the average of the cosines of the contact angles involved. A future communication will show that the force data obtained with organosilanes other than OTS fall on the same line shown in Figure 3.7. It is possible, however, that the slope *a* of the curve shown in Figure 3.7 may change as the water contact angle is reduced considerably below 90°. It has been shown by Yoon and Ravishankar (11) that for symmetric interactions only short-range hydrophobic forces are observed at advancing contact angles (θ_a) below 90°.

3.4 CONCLUSIONS

An AFM was used to conduct direct force measurements between a glass sphere and a silica plate. When the measurements were conducted with bare surfaces, the measured forces could be fitted to the DLVO theory at longer separation distances. At separation distances below 13 nm, however, the measured forces were larger than the ion-electrostatic force. This non-DLVO force was attributed to the primary hydration force represented by a double-exponential force law with decay lengths of 0.4 and 3.0 nm. The force measurements were also conducted between the glass sphere and the silica plate hydrophobized with OTS. The results showed large non-DLVO attractive forces, which may be attributed to hydrophobic interaction. The hydrophobic forces were fitted using a power law, which is of the same form as the dispersion force, so that the hydrophobic force constants can be compared with the Hamaker constant. When the force measurements were conducted with the silica plate and the glass sphere hydrophobized under identical conditions, the hydrophobic force constant (K_{131}) for the symmetric interactions increases with the equilibrium water contact angle (θ) measured on the silica plate. The force measurements were also conducted between a glass sphere with $\theta = 109°$ and silica plates of varying contact angles to obtain hydrophobic force constants (K_{132}) for asymmetric interactions. It has been found that the values of K_{132} are close to the geometric means of K_{131} and K_{232}, the latter being the symmetric hydrophobic force constant obtained at $\theta = 109°$. A plot of log K_{131} (and K_{232}) varies linearly with cos θ, while log K_{132} varies linearly with the arithmetic average of cos θ_1 and cos θ_2. These results suggest that hydrophobic forces are uniquely determined by the water contact angles of the surfaces involved.

Chapter 3 Hydrophobic Interactions between Dissimilar Surfaces

3.5 REFERENCES

1. Derjaguin, B. V., and Landau, L. *Acta Physiochim. URSS* **14**, 633 (1941).
2. Verwey, E. J. W., and Overbeek, J. Th. G., "Theory of the Stability of Lyophobic Colloids," Elsevier, Amsterdam, 1948.
3. Israelachvili, J. N., and Adams, G. E., *J. Chem. Soc. Faraday Trans. I* **74**, 975 (1978).
4. Pashley, R. M., *J. Colloid Interface Sci.* **80**, 153 (1981); *J. Colloid Interface Sci.* **83**, 531 (1981); *Adv. Colloid Interface Sci.* **16**, 57 (1982).
5. Pashley, R. M., and Quirk, J. P., *Colloids Surf.* **9**, 1 (1984).
6. Pashley, R. M., and Israelachvili, J. N., *J. Colloid Interface Sci.* **97**, 446 (1984).
7. Israelachvili, J. N., and Pashley, R. M., *J. Colloid Interface Sci.* **98**, 500 (1984).
8. Kékicheff, P., Christenson, H. K., and Ninham, B. W., *Colloids Surf.* **40**, 31 (1989).
9. Herder, P. C., *J. Colloid Interface Sci.* **134**, 346 (1990).
10. Yoon, R.-H., and Ravishankar, S. A., *J. Colloid Interface Sci.* **166**, 215 (1994).
11. Yoon, R.-H., and Ravishankar, S. A., Accepted by *J. Colloid Interface Sci.*
12. Klein, J., and Luckham, P., *Nature* **300**, 429 (1982).
13. Malmsten, M., and Claesson, P. M., *Langmuir* 7, 988 (1991).
14. Biggs, S., *Langmuir* **11**, 156 (1995).

15. Yoon, R.-H., *Aufbereitungs-Technik* **32**, 474 (1991).

16. Claesson, P. M., Blom, C. E., Herder, P. C., and Ninham, B. W., *J. Colloid Interface Sci.* **114**, 234 (1986).

17. Rabinovich, Ya. I., and Derjaguin, B. V., *in* "Proceedings of the 5th Hungarian Conference on Colloid Chemistry", Loránd Eötvös University, Balatonfured, Hungary, 1988.

18. Tabor, D., and Winterton, R. H. S., *Proc. Roy. Soc. London A* **312**, 435 (1969).

19. Pashley, R. M., McGuiggan, P. M., Ninham, B. W., and Evans, D. F., *Science* **229**, 1088 (1985).

20. Claesson, P. M., and Christenson, H. K., *J. Phys. Chem.* **92**, 1650 (1988).

21. Christenson, H. K., Claesson, P. M., Berg, J., and Herder, P. C., *J. Phys. Chem.* **93**, 1472 (1989).

22. Tsao, Y.-H., Yang, S. X., Evans, D. F., and Wennerström, H., *Langmuir* **7**, 3154 (1991).

23. Rabinovich, Ya. I., Guzonas, D. A., and Yoon, R.-H., *J. Colloid Interface Sci.* **155**, 221 (1993).

24. Binnig, G., Quate, C. F., and Gerber, Ch., *Phys. Rev. Lett.* **56**, 930 (1986).

25. Ducker, W. A., and Senden, T. J., *Langmuir* **8**, 1831 (1992).

26. Rabinovich, Ya. I., and Yoon, R.-H., *Langmuir* **10**, 1903 (1994).

Chapter 3 **Hydrophobic Interactions between Dissimilar Surfaces**

27. Rabinovich, Ya. I., and Yoon, R.-H., *Colloids Surf.* **93**, 263 (1994).
28. Meagher, L., and Craig, V. S. J., *Langmuir* **10**, 2736 (1994).
29. Ducker, W. A., Senden, T. J., and Pashley, R. M., *Langmuir* **8**, 1831 (1992).
30. Biggs, S., Mulvaney, P., Zukoski, C. F., and Grieser, F., *J. Am. Chem. Soc.* **116**, 9150 (1994).
31. Larson, I., Drummond, C. J., Chan, D. Y. C., and Grieser, F., *J. Am. Chem. Soc.* **115**, 11885 (1993).
32. Atkins, D. T., and Pashley, R. M., *Langmuir* **9**, 2232 (1993).
33. Ducker, W. A., Senden, T. J., and Pashley, R. M., *Nature* **353**, 239 (1991).
34. Ducker, W. A., Xu, Z., and Israelachvili, J. N., *Langmuir* **10**, 3279 (1994).
35. Meagher, L., *J. Colloid Interface Sci.* **152**, 293 (1992).
36. Butt, H.-J., *J. Colloid Interface Sci.* **166**, 109 (1994).
37. Parker, J. L., Christenson, H. K., and Ninham, B. W. *Rev. Sci. Instrum.*, **60**, 3135 (1989).
38. Parker, J. L. *Langmuir* **8**, 551 (1992).
39. Parker, J. L., and Rutland, M. W. *Langmuir* **9**, 1965 (1993).
40. Parker, J. L., Yaminsky, V., and Claesson, P. M. *J. Phys. Chem.* **97**, 7706 (1993).
41. Parker, J. L., and Claesson, P. M., *Langmuir* **10**, 635 (1994).

42. Claesson, P. M., Herder, P. C., Blom, C. E., and Ninham, B. W., *J. Colloid Interface Sci.* **118**, 68 (1987).

43. Tsao, Y.-H., and Evans, D. F., *Langmuir* **9**, 779 (1993).

44. Pincet, F., Perez, E., and Wolfe, J., *Langmuir* **11,** 373 (1995).

45. Derjaguin, B., *Kolloid Zeitschrift* **69**, 155 (1934).

46. Senden, T. J., and Ducker, W. A., *Langmuir* **10**, 1003 (1994).

47. Flinn, D. H., Guzonas, D. A., and Yoon, R.-H., *Colloids Surf.* **87**, 163 (1994).

48. Ohshima, H., Healy, T. W., and White, L. R., *J. Colloid Interface Sci.* **89**, 484 (1982).

49. Laskowski, J., and Kitchener, J. A., *J. Colloid Interface Sci.* **29**, 670 (1969).

50. Hough, D. B., and White, L. R., *Adv. Colloid Interface Sci.* **14**, 3 (1980).

51. Churaev, N. V., and Derjaguin, B. V., *J. Colloid Interface Sci.* **103**, 542 (1985).

52. Churaev, N. V., *Kolloidn. Zhurnal* **57**, 252 (1995) .

53. Blake, P., and Ralston, J., *Colloids Surf.* **15**, 101 (1985).

54. Sergeeva, I. P., Sobolev, V. D., and Churaev, N. V., *Colloid J. of USSR* **43**, 918 (1981).

55. Yordan, J. L., Ph.D. Thesis, Department of Mining and Minerals Engineering, Virginia Polytechnic Institute and State University, Blacksburg, Virginia, 1986.

56. Xu, Z., and Yoon, R.-H., *J. Colloid Interface Sci.* **134**, 427 (1990).

57. Tripp, C. P., and Hair, M. L., *Langmuir* **11**, 149 (1995).

58. Johnson, K. L., Kendall, K., and Roberts, A. D., *Proc. Roy. Soc. London A* **324**, 301 (1971).

59. Derjaguin, B. V., Muller, V. M., and Toporov, Yu. P., *J. Colloid Interface Sci.* **53**, 314 (1975).

60. Rabinovich, Ya. I., Derjaguin, B. V., and Churaev, N. V., *Adv. Colloid Interface Sci.* **16**, 63 (1982).

61. Grabbe, A., and Horn, R. G., *J. Colloid Interface Sci.* **157**, 375 (1993).

62. Hamaker, H. C., *Physica* **4**, 1058 (1937).

63. London, F., *Trans. Faraday Soc.* **33**, 8 (1937).

64. Israelachvili, J. N., *Proc. Roy. Soc. London A* **331**, 39 (1972);

65. Israelachvili, J. N., "Intermolecular and Surface Forces", Academic Press, London, 1985.

66. Churaev, N. V., *Colloid J. of USSR* **34**, 851 (1972).

67. Owens, N. F., and Richmond, P. J., *Chem. Soc. Faraday Trans. II* **74**, 691 (1978).

68. McCartney, J., and Levin, A, *J. Colloid Interface Sci.* **30**, 345 (1969).

69. Galitzine, B., *Wied. Ann.* **41**, 770 (1890).

70. Berthelot, D., *Compt. rend.* **126**, 1703, 1857 (1898).

71. Good, R. J., and Hope, C. J., *J. Chem. Phys.* **53**, 540 (1970).

72. Girifalco, L. A., and Good, R. J., *J. Phys. Chem.* **61**, 904 (1957).

73. Fowkes, F. M., *Ind. Eng. Chem.* **56**, 40 (1964).

74. Owens, D. K., and Wendt, R. C., *J. Appl. Poly. Sci.* **13**, 1741 (1969).

75. Good, R. J., and Hope, C. J., *J. Colloid Interface Sci.* **35**, 171 (1971).

Chapter 3

Hydrophobic Interactions between Dissimilar Surfaces

CHAPTER 4 DIRECT FORCE MEASUREMENTS FOR THE AMINE-QUARTZ FLOTATION SYSTEM

4.1 INTRODUCTION

One of the most important steps to achieve successful flotation is the attachment of an air bubble to a mineral surface, a process that is facilitated by rendering the mineral surface hydrophobic. Alkylammonium salts are frequently used as collectors to hydrophobize negatively charged oxide minerals such as quartz. Flotability tests of quartz in the presence of alkylammonium salts (1-7) have shown maximum recovery to occur at alkaline pH. Similar results have been reported for hematite (1), magnetite (8), fluorite (9), and various zinc oxide minerals (10).

It has been suggested that the optimum pH for the flotation of quartz using dodecylamine hydrochloride (DAHCl) as a collector occurs in the pH range of 8 to 11, where both dodecylammonium ions (RNH_3^+) and neutral dodecylamine molecules (RNH_2 (aq)) are present. One theory proposes that these species "coadsorb" on the mineral surface and maximize the hydrophobicity. According to Gaudin and Fuerstenau (11), the presence of the RNH_2 species reduces the lateral repulsion between the polar heads of RNH_3^+ ions and, thereby, allows more alkylammonium ions to adsorb (11, 12). At the same time, the coadsorption mechanism increases the density of hydrocarbon chains per unit area of the mineral surface, which may be the main reason for the increased hydrophobicity (13).

Somasundaran and his coworkers offered a different explanation. These investigators proposed that the pH at which maximum flotation is obtained coincides with the pH where concentration of the ionomolecular complex, RNH_2-RNH_3^+, is at its highest (1, 5); therefore, they suggested that the maximum flotation is due to the adsorption of this highly surface-active species on the mineral.

Attempts have recently been made to directly measure forces between an air bubble and a hydrophobic, surfactant-coated solid (14, 15); however, the pliability of the bubble surface made it difficult to determine the separation distances. Nevertheless, the work reported by Butt (14) and Ducker *et al.* (15) indicated the presence of long-range hydrophobic forces, which is consistent with the findings of Craig *et al* (16, 17). From coalescence studies, these investigators showed that air bubbles are hydrophobic. Furthermore, Aksoy (18) measured the equilibrium free film thicknesses of surfactant solutions and estimated the hydrophobicity of air bubbles. He showed that the hydrophobic force constant of a bubble in pure water is comparable to that of a solid surface having a contact angle in excess of 90°. Thus, it may be possible to simulate bubble-particle interactions by conducting direct force measurements between two solid surfaces, provided that one surface is sufficiently hydrophobic to represent an air bubble.

Numerous investigators have conducted direct force measurements between two solid surfaces on which films of amphiphilic surfactants have been formed either from self-assembly (13, 19-23) or Langmuir-Blodgett (LB) deposition (24-26). Force measurements have also been conducted between stable hydrophobic layers formed by chemisorption, such as the reaction of alkylsilanes (27-31). In general, the force, F_t, between bare surfaces can be adequately predicted at long distances using the classical DLVO theory (32, 33),

$$F_t = F_d + F_e\,, \qquad [4.1]$$

in which F_d represents the contribution from the London-van der Waals dispersion forces, and F_e is the force due to the ion-electrostatic interaction of overlapping electrical double layers. At close distances, however, additional repulsive hydration forces have been reported between silica surfaces (34-39) believed to be caused by the surfaces' affinity for water.

Force measurements between surfactant-coated hydrophobic surfaces in water have revealed the presence of an additional non-DLVO attractive force, termed the hydrophobic force. This led to extending the DLVO model,

$$F_t = F_d + F_e + F_h\,, \qquad [4.2]$$

to account for the hydrophobic force, F_h.

The hydrophobic force is often described by an empirical double exponential function,

$$\frac{F_h}{R} = C_1 \exp\left(\frac{-H}{D_1}\right) + C_2 \exp\left(\frac{-H}{D_2}\right), \qquad [4.3]$$

where R is the radius of curvature of the surfaces involved, H is the shortest separation distance between the surfaces, C_1 and C_2 are pre-exponential constants, and D_1 and D_2 are known as decay lengths. The first term in Eq. [4.3] is used to describe short-range ($H < 15$ nm) hydrophobic forces such as those reported between self-assembled surfactant-coated surfaces where $D_1 = 1$ to 2.5 nm (13, 19-22). For stronger hydrophobic forces such as those between LB deposited and alkylsilanated surfaces in water, the second exponential term is included for which typical values of D_2 range from 10 to 32 nm (24, 25, 27, 30).

In lieu of the more cumbersome double exponential expression, it is often more convenient to describe the hydrophobic force using a power law (24, 40),

$$\frac{F_h}{R} = \frac{-K}{H^2}, \qquad [4.4]$$

where the single unknown parameter, K, represents the magnitude of the hydrophobic force.

Recent direct force measurements conducted between mica surfaces in DAHCl solution as a function of pH (41, 42) reported the existence of a hydrophobic force in the pH range of 8 to 10.3. Another investigator (43) has measured forces between two hydrophobized surfaces in DAHCl solutions of varying concentration and found that the presence of dodecylammonium ions significantly reduced the magnitude of the hydrophobic force.

The purpose of the present study was to determine the possibility of obtaining information on bubble-particle interactions by conducting direct force measurements in surfactant solutions between a hydrophobic sphere and a flat silica plate. The force measurements were conducted in DAHCl solutions at different pH values using an AFM. This surfactant was chosen because there exists a wealth of information on the flotation of silica in these solutions that can be compared with the force data obtained in the present work.

4.2 MATERIALS AND METHODS

4.2.1 *Materials*

Optically smooth Herasil 3 fused silica plates were obtained ground and polished from Heraeus Amersil, Inc. and cleaned in boiling nitric acid prior to use. Glass spheres (Duke Scientific) were used as received and adhered to atomic force microscope cantilevers using Epon R Resin 1004F (Shell Chemicals Co.). Hydrophobic surfaces were prepared by adsorbing OTS (95%) from HPLC grade cyclohexane (both from Aldrich Chemical Co.) as described elsewhere (44). Dodecylamine hydrochloride (DAHCl) was obtained from TCI America and recrystallized from ethanol before preparation of a stock solution. Conductivity water obtained using a Barnstead Nanopure water purification system was used in all experiments. NaOH and HCl (both from Fischer Scientific) were used to adjust pH.

4.2.2 *Contact Angle Measurements*

Contact angles were measured using a Ramé-Hart Model 100 goniometer. The captive bubble technique was employed to measure contact angles in the DAHCl solutions. Each solid sample was allowed to equilibrate in a pH-adjusted DAHCl solution for 30 minutes prior to the introduction of an air bubble. The initial contact angle was measured immediately after the air bubble made contact with the solid surface (t < 15 sec.), while the final contact angle was recorded after the bubble had aged for 30 minutes. This process was repeated twice and averaged for each sample.

4.2.3 *Surface Force Measurements*

Direct force measurements were conducted using an atomic force microscope (AFM) equipped with a liquid cell. More specific details for this technique have been discussed in a previous work (27). Most measurements were conducted with a standard Si_3N_4 tip. For measuring large attractive forces, stronger cantilevers such as tapping etched silicon probes (TESP) and force etched silicon probes (FESP) were used. Cantilevers were calibrated using the inversion technique reported by Senden and Ducker (45).

4.3 RESULTS AND DISCUSSION

4.3.1 *Contact Angles*

Smith *et al.* (3, 12) reported that contact angles measured in a dodecylamine salt solution change with time under alkaline conditions. Similar results have been obtained in the present work. As shown in Figure 4.1, contact angle changes on bare silica and OTS-coated silica in a 4×10^{-5} M DAHCl solution at several different pH's. At pH 9.5, the variation in contact angle is nearly undetectable for both types of surface. As pH is increased to 10.3, however, contact angle decreases sharply, dropping nearly 20°, before leveling off to a stable value after approximately two minutes. At pH 11.3, the decrease in contact angle is still more significant, diminishing up to 50° after 10 minutes. Finch and Smith (46, 47) have attributed this dynamic

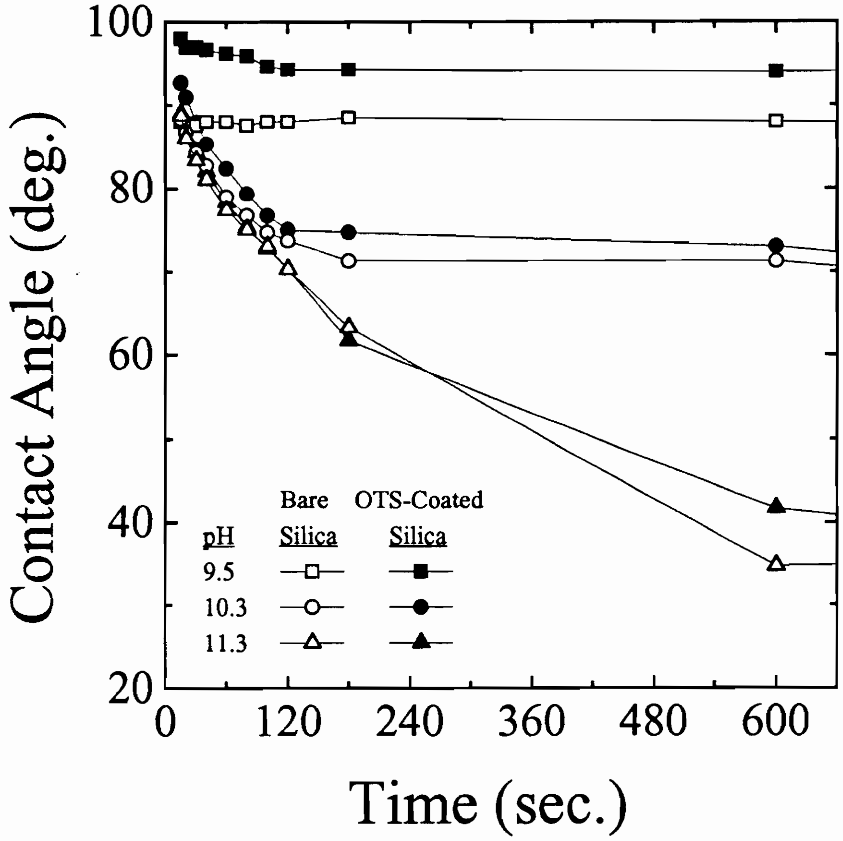

pH	Bare Silica	OTS-Coated Silica
9.5	—□—	—■—
10.3	—○—	—●—
11.3	—△—	—▲—

Figure 4.1. Changes in contact angle with time for bare silica and OTS-coated silica in 4x10^{-5} M DAHCl solutions at different pH.

contact angle to a reduction in surface tension caused by the migration of surfactant to the liquid-vapor interface with time. These authors used the maximum bubble pressure technique to show sharp decreases in surface tension of 4×10^{-5} M dodecylamine salt solutions within the first two minutes at pH values greater than 8.85. Similar to the contact angle results reported here, the effect increased with increasing pH. At pH's below 9, there was no significant change in contact angle with air bubble age.

The dynamic contact angle phenomenon yields two useful values for contact angle. Initial contact angle, θ_i, is taken to be the value of the angle measured within 15 seconds of creating a point of three-phase contact at the sample surface, *i.e.*, the time needed to introduce the air bubble and record the angle. The second value of contact angle is termed the final contact angle, θ_f, which is the angle measured after the air bubble has aged 30 minutes. Both initial and final contact angles are plotted as a function of pH in Figure 4.2a for bare silica and in Figure 4.2b for OTS-coated silica. The data are superimposed over the results of surface tension measurements reported by Castro *et al.* (48) and Aksoy (18). The contact angle data for bare silica in Figure 4.2a agree well with those reported in the literature (2, 3, 12, 49). At low pH, where the alkylammonium ion, RNH_3^+, predominates in solution, adsorption at the solid-liquid (9, 48-51) and liquid-vapor (48, 52) interfaces is relatively low. Above pH 8, however, adsorption at the solid-liquid interface increases sharply, as reflected by the larger

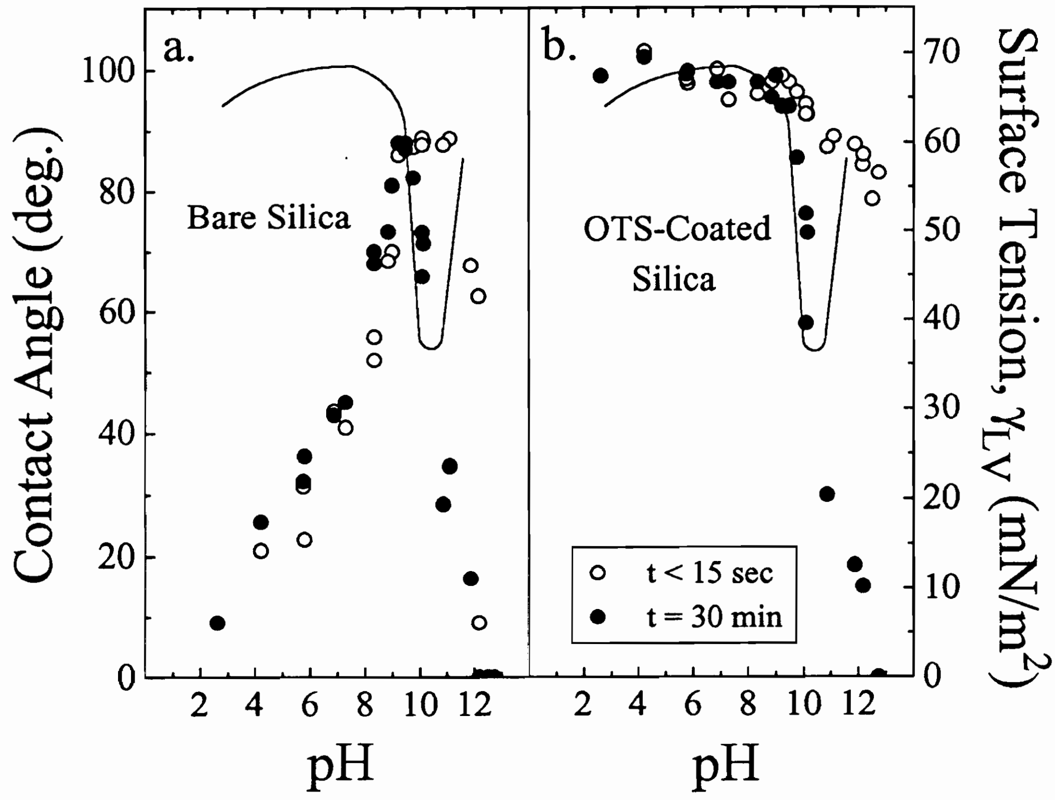

Figure 4.2. Results of contact angle measurements conducted as a function of pH using the captive bubble technique in 4×10^{-5} M DAHCl solutions for a) bare silica surfaces and b) OTS-coated silica surfaces. Open circles represent initial contact angles measured within 15 seconds after introducing the air bubble into the cell, while filled circles are the data obtained after the bubble had aged 30 minutes. Solid lines are surface tension data at the liquid-vapor interface from Refs. 18 and 48.

contact angles, reaching a maximum near pH 9.5. As previously mentioned, neutral amine, RNH_2, plays an important role in the increase in adsorption (4, 11). From pH 9 to near pH 11, initial contact angles for bare silica (Figure 4.2a) remain constant while final contact angles decrease rapidly. This suggests that the diminishing contact angles result from a reduction in surface tension brought on by increased adsorption at the liquid-vapor interface.

For OTS-coated silica surfaces (Figure 4.2b), both initial and final contact angle values decrease only slightly up to pH 9.5, which may be attributed to the possibility that some of the RNH_3^+ ions adsorb on the hydrocarbon surface in an inverse orientation, *i.e.*, with the polar head groups toward the bulk solution. Above pH 9.5, however, initial contact angle values continue to diminish slightly, whereas, final contact angles show a sharp decrease. The influence of surface tension reduction at the liquid-vapor interface is also seen here; however, the lower initial contact angle values suggest more surfactant adsorbs on the solid surface in an inverse orientation, most likely due to the higher surface activity of the ionomolecular complex.

Above pH 10.3, surface tension increases; however, initial and final contact angles for bare silica and final contact angles for OTS-coated silica approach near zero values. Laskowski *et al.* (53, 54) observed that contact angles measured on silanated silica surfaces immersed in pure water progressively decrease with increasing alkalinity and time, presumably due to an increase of OH^- ions at the hydrocarbon surface (55). However, since the solubility limit of DAHCl in water is believed to be $2x10^{-5}$ M (50), it follows that a bulk precipitate is present in solution above pH 10.3 in the form colloidal droplets (48) which may adsorb on the surfaces. Yoon and Ravishankar (42) have reported that such a surface precipitate is hydrophilic.

4.3.2 *Surface Forces*

4.3.2.1 Measurements between Two Bare Silica Surfaces

Figure 4.3 shows the results of direct force measurements conducted between a bare silica plate and a clean glass sphere in $4x10^{-5}$ M DAHCl solution at various pH values. The measured forces, F, are normalized with respect to the radius of the glass sphere, R, and plotted as a function of the shortest separation distance, H. The dashed line represents the force due to the London-van der Waals dispersion interactions, F_d, and was obtained using the expression

$$\frac{F_d}{R} = \frac{-A_{131}}{6H^2}, \qquad [4.5]$$

where A_{131} is the Hamaker constant of identical surfaces 1 interacting through a medium 3. A value of $A_{131} = 8x10^{-21}$ J (56) was used for silica surfaces in water for all calculations of F_d throughout this work.

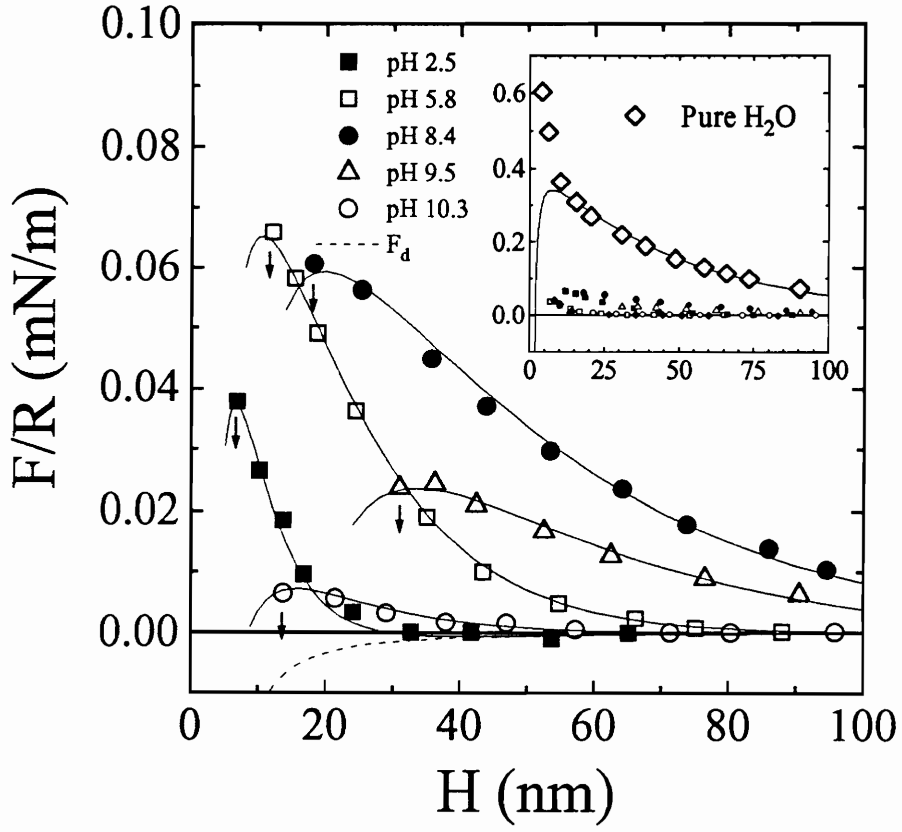

Figure 4.3. Results of AFM force measurements conducted between a clean glass sphere and a bare silica plate in $4x10^{-5}$ M DAHCl solution at different pH values. The measured force (*F*) is normalized by the radius (*R*) of the glass sphere and plotted versus the closest separation distance (*H*). Force data obtained in pure water are shown in the inset. The dashed line represents the London-van der Waals force (F_d) as calculated using Eq. [4.5] with $A_{131} = 8x10^{-21}$ J. The solid lines represent DLVO and extended DLVO fits of the measured forces. Values of the fitting parameters are provided in Table 4.1. The arrows indicate the distances (H_j) at which the surfaces jumped into contact.

The solid lines in Figure 4.3 represent either the classical DLVO theory, Eq. [4.1], or the extended DLVO model, Eq. [4.2], in which F_d is calculated using Eq. [4.5], F_e is determined from the constant potential model of the Poisson-Boltzmann equation (57), and F_h is calculated from Eq. [4.4]. The parameters used in fitting the force data are provided in Table 4.1. The inset in Figure 4.3 shows the results of force measurements conducted between a bare silica plate and a clean glass sphere in pure water at pH 5.8. It is immediately apparent that the forces measured between the same surfaces in a 4×10^{-5} M DAHCl solution are considerably less repulsive than the force measured in pure water. This may be attributed to not only the reduction in the magnitude of the surface charge due to the adsorption of surfactant ions at the sample surfaces, but also the presence of hydrophobic forces.

At pH 2.5, where the silica surfaces are expected to have very little charge (53), the measured force is repulsive at short distances before the surfaces jump into contact. This jump distance, $H_j = 6.8$ nm, is denoted by an arrow in the figure. The force data can be fitted with the classical DLVO theory, Eq. [4.1], where the electrical potentials of both surfaces, ψ_1, are 14 mV and the Debye length, κ^{-1}, is 5.5 nm. Due to the low surface potential of silica at this pH, adsorption of the cationic collector is minimal resulting in the low contact angle observed. It should be noted here that when using the AFM technique to measure forces, it is not possible to determine the sign of the

TABLE 4.1

Force Parameters for Measurements between Bare Silica Surfaces in $4\text{x}10^{-5}$ M DAHCl Solution at Various pH.

pH	θ_i (deg.)	θ_f (deg.)	ψ_1 (mV)	κ^{-1} (nm)	H_j (nm)	K_{131} (10^{-19} J)	F_{ad} (mN/m)
2.5	9	9	14	5.5	6.88	-	0.25
5.8	30	35	-21	14.1	12.1	0.07	0.45
8.4	58	72	-28	31.6	18.2	0.30	0.91
9.5	88	88	-24	30.0	31.0	1.1	3.47
10.3	88	58	-9	13.4	13.7	-	0.37
11.3	89	38	-14	5.5	8.33	-	0.55
12.5	0	0	-	-	-	-	-
H_2O	0	0	-60	42	-	-	-

fitted surface potentials and that the signs provided in this work are based on the streaming potential results of Fuerstenau (2).

At pH 5.8, the measured force is repulsive and longer in range. The data cannot be Fitted to the classical DLVO theory, Eq. [4.1], due to the large jump distance observed (H_j = 12.1 nm). The additional attractive hydrophobic force can be accounted for by fitting the data to the extended DLVO model, Eq. [4.2], where ψ_1 = -21 mV and κ^{-1} = 14.1 nm. Using Eq [4.4] to estimate the hydrophobic force produces a value of 7x10^{-21} J for the hydrophobic force parameter, K_{131}. It is worth mentioning that this value is very close to the Hamaker constant and may be an underestimate since A_{131} may be less than 8x10^{-21} J in the presence of DAHCl.

When pH is increased to 8.4, the force measured between silica surfaces in 4x10^{-5} M DAHCl becomes even more repulsive at long distances. Again, the data can be fitted to the extended DLVO model. The fitted potential (ψ_1 = -28 mV) is most negative at this pH which agrees well with Fuerstenau's results (2); however, the large negative potential is somewhat offset by the presence of an increasingly attractive hydrophobic force, where K_{131} = 3x10^{-20} J. The relatively low contact angle observed on bare silica at this pH indicates that although the surface charge reaches a maximum negative value, there is insufficient neutral DAH available in solution (less than 0.6% of the total amine concentration) to promote monolayer or near monolayer coverage of the surface. Monolayer adsorption, as estimated from de Bruyn's data (50) of $4x10^{-5}$ M dodecylammonium acetate on silica, occurs at $7.1x10^{-10}$ mole/cm^2. Thus, at pH 8.4, surface coverage is estimated to be only 23% of the theoretical monolayer value.

Several studies have shown maximum flotation recovery (2-7, 49), maximum bubble pick up (58, 59), and minimum induction times (7) for silica in DAH solutions occur near pH 9.5. The forces measured at this pH show a slight long-range repulsion. Repulsive forces were also reported by Rutland *et al.* (41) for mica surfaces in $1x10^{-4}$ M DAHCl, which the authors attributed to electrostatic repulsion due to bilayer formation. However, according to Fuerstenau's (2) streaming potential measurements for silica at pH 9.5 in a $4x10^{-5}$ M DAH solution, the potential is slightly less negative than the maximum at pH 8.5, and de Bruyn's data (50) estimate surface coverage to be 85% of theoretical monolayer coverage. When the data is fitted to the extended DLVO theory, where ψ_1 = -24 mV and κ^{-1} = 30.0 nm, a hydrophobic constant of K_{131} = $1.1x10^{-19}$ J must be used to account for the 31.0 nm jump distance. Though at this pH only 7% of the total amine concentration is neutral RNH_2, Yoon and Ravishankar (23, 60) have shown that small amounts of long-chained, neutral surfactant significantly increase the hydrophobic attraction between mica surfaces in DAHCl solution.

At pH 10.3, near the point of charge reversal (2), the measured force is only slightly repulsive and no attractive hydrophobic force is detected. Recently, Yoon and

Ravishankar (60) reported similar observations for force measurements between mica surfaces in DAHCl solution. These authors attributed this sudden absence of the hydrophobic force to the formation of precipitate near the substrate surface at a pH lower than the theoretical pH for bulk precipitate formation as was suggested by Castro *et al.* (48).

As alkalinity increases further, negatively charged colloidal amine precipitate forms in the bulk solution (48). The data for measurements obtained at pH values greater than 10.3 are not shown graphically in the present work, because the AFM technique for directly measuring forces does not allow the determination of the absolute thickness of the surfactant layer, and under highly alkaline conditions, significant precipitate may build up on the surfaces (41, 42). However, forces measured at pH 11.3 are repulsive, increasing sharply at a surface separation of 30 nm before the surfaces jump into contact at a separation distance of 8.3 nm. At pH 12.5, the forces are purely repulsive, exhibiting no jump into contact. Rutland *et al.* (41) reported similar results between mica surfaces at high pH.

Adhesion forces, or the force required to separate the two surfaces after contact, F_{ad}, are also provided in Table 4.1. Values of F_{ad} are much lower than measured with the surface forces apparatus (SFA) when using the AFM technique due to surface roughness of the glass sphere and additional shear forces where the surfaces are in contact. It should be noted, however, that the maximum adhesion force measured occurred at pH 9.5, where the strongest hydrophobic force was detected.

4.3.2.2 Measurements between Two OTS-coated Surfaces

Direct force measurements were also conducted between OTS-coated silica surfaces in the presence of $4\text{x}10^{-5}$ M DAHCl. Force normalized by sphere radius is plotted versus separation distance in Figure 4.4. The dashed line represents the London-van der Waals dispersion force, Eq. [4.5], with $A_{232} = 8\text{x}10^{-21}$ J. Solid lines are the extended DLVO model, Eq. [4.2], using Eq. [4.4] to represent the hydrophobic force. Force parameters for all the surfaces shown in Figure 4.4 are provided in Table 4.2.

The long-range attractive forces measured in pure water at pH 5.8 between a silica plate and a glass sphere both hydrophobized by OTS are shown in the inset of Figure 4.4. When fitted with the extended DLVO model (ψ_1 = -60 mV and κ^{-1} = 42 nm), a value of $K_{232} = 2.7\text{x}10^{-16}$ J is obtained from Eq. [4.4]. This value correlates well with previous values for this system (27, 28). In $4\text{x}10^{-5}$ M DAHCl solution at pH 5.8, however, the attractive forces between OTS-coated surfaces are nearly an order of magnitude lower as indicated by a reduction in jump distance from 45.5 nm to 30.0 nm, denoted by the arrows in Figure 4.5.

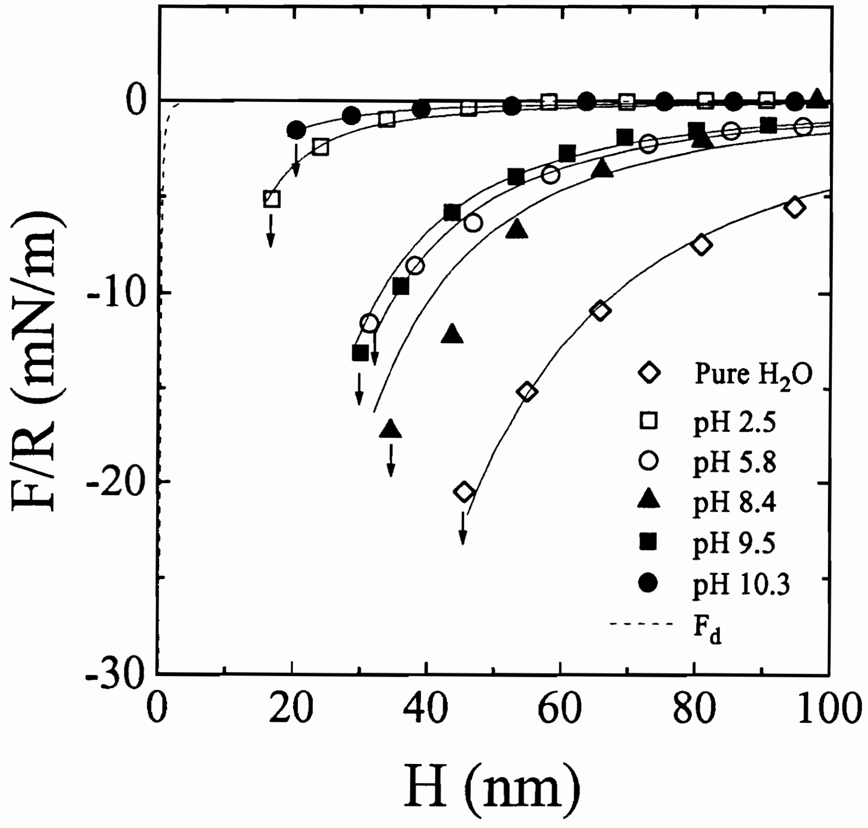

Figure 4.4. *F/R* vs. *H* curves obtained from AFM force measurements conducted between an OTS-coated glass sphere and an OTS-coated silica plate in $4\mathrm{x}10^{-5}$ M DAHCl solutions at several pH values. The force data obtained in pure water are also included. The dashed line represents F_d as calculated using Eq. [4.5] with $A_{232} = 8\mathrm{x}10^{-21}$ J. The solid lines are fits of the force data using the extended DLVO model, Eq. [4.2], in which Eq. [4.4] is used to account for the contributions from the hydrophobic force. Values of the fitting parameters are provided in Table 4.2. The arrows indicate jump distances (H_j).

TABLE 4.2

Force Parameters for Measurements between Hydrophobized Silica Surfaces in 4x10^{-5} M DAHCl Solution at Various pH.

pH	θ_i (deg.)	θ_f (deg.)	ψ_2[a] (mV)	κ^{-1} (nm)	H_j (nm)	K_{232} (10^{-19} J)	F_{ad} (mN/m)
2.5	97	99	6	5.5	16.8	85	41.4
5.8	99	100	-12	14.5	30.0	650	68.7
8.4	98	98	-21	31.6	26.7	1000	79.9
9.5	99	95	-11	30.0	31.3	750	58.3
10.3	93	58	-13	17.3	20.4	40	10.6
11.3	86	25	-22	9.3	6.87	2.0	1.48
12.5	82	0	-	-	-	-	-
H_2O	109	109	-60	42	45.5	2700	144

[a] These potentials were determined from fitting the force data measured between bare silica and OTS-coated glass in 4x10^{-5} M DAHCl solution as shown in Figure 4.5.

Herder (43) showed that attractive forces measured between Langmuir-Blodgett films of dimethyldioctylammonium ions deposited on mica are long-range when measured in pure water, but become short-range in the presence of DAHCl solution, which the author attributes to an apparent shielding of the long-range hydrophobic force by alkylammonium ions. The surfactant concentration used in the present work is well below the critical micelle concentration, 1.2×10^{-2} M, for DAHCl at pH $\approx$ 6 (61); thus, the formation of a well-ordered bilayer with the polar heads of the alkylammonium ions oriented toward the bulk solution is unlikely. It is more probable that the cationic surfactant molecules adsorb in small patches on the OTS-coated surface in an inverse orientation, causing the surface to become more hydrophilic. The even weaker attractive force measured at pH 2.5 supports this hypothesis. The addition of HCl may increase the adsorption of dodecylammonium ions on the OTS surface because the lateral repulsion between the positively charged head groups is reduced by the presence of excess Cl^- counter ions in solution. This same effect also occurs at the liquid-vapor interface, resulting in a reduction of surface tension (62).

The magnitude of the long-range attractive forces remains fairly constant as the DAHCl solution becomes more alkaline, until a pH of 10.3 is reached, where the fitted value of K_{232} is reduced by 95%. The decrease in the hydrophobic force is similar to that already mentioned between bare silica surfaces in DAHCl at pH 10.3, and may likewise be caused by a precipitation of amine on the sample surface. For reasons already mentioned, the force data obtained at pH values above 10.3 are not shown in Figure 4.4; however, the force becomes even less attractive at pH 11.3 as bulk precipitate forms. Finally, at pH 12.5, only a strong repulsive force is measured between the two OTS-coated surfaces.

Adhesion forces between OTS-coated silica surfaces in $4\text{x}10^{-5}$ M DAHCl solution at several pH values are also included in Table 4.2. The adhesion forces measured in DAHCl solutions at pH 5.8 is much lower than that measured in pure water at natural pH, due in part to the reduced surface tension of the DAHCl solution but also caused by the inverse orientation of RNH_3^+ ion on the OTS surface. Values of F_{ad} seem to follow the same trend as those of the hydrophobic force parameter, K_{232}, with changing pH. Adhesion force remains relatively constant from acidic to slightly alkaline pH, showing a dramatic reduction at pH 10.3 and finally no adhesion at pH 12.5.

4.3.2.3 Measurements between One Bare Silica and One OTS-coated Surface

To simulate the asymmetric system of a hydrophobic air bubble interacting with quartz in the presence of a cationic collector, direct force measurements were made between an OTS-coated glass sphere ($\theta = 109°$ in pure water) and a bare silica plate in

4×10^{-5} M DAHCl solution. Force normalized by sphere radius is plotted versus separation distance for measurements conducted at several solution pH's in Figure 4.5. As in Figures 3 and 4, the dashed line represents the London-van der Waals dispersion forces, Eq. [4.5], where $A_{132} = 8\times10^{-21}$ J. Solid lines are fits of the force data by either the classical DLVO theory, Eq. [4.1], or the extended DLVO model, Eq. [4.2], using Eq. [4.4] to account for F_h. Parameters used in the calculations of these fitted curves are presented in Table 4.3. The potentials of the OTS-coated surfaces (ψ_2) were obtained by fitting the force data to either Eq. [4.1] or [4.2] using the potentials obtained between measurements of bare silica (ψ_1) in the same DAHCl solutions as reported in Table 4.1. These values are also reported in Table 4.2. It was not possible to determine the surface potentials directly from the force data in Figure 4.4 due to the magnitude of the hydrophobic attraction observed between two OTS-coated surfaces.

The inset of Figure 4.5 shows the results of forces measured between an OTS-coated glass sphere and a bare silica plate in pure water at pH 5.8. The data can be fitted to the extended DLVO theory with $\psi_1 = \psi_2 = -60$ mV, $\kappa^{-1} = 42$ nm, and $K_{132} = 1\times10^{-20}$ J. The subscripts **1** and **2** denote the bare silica and OTS-coated surfaces, respectively. The weak hydrophobic force detected between these two surfaces is comparable to the dispersion force ($A_{132} = 8\times10^{-21}$ J). When these surfaces approach one another in 4×10^{-5} M DAHCl solution at the same pH, two significant observations

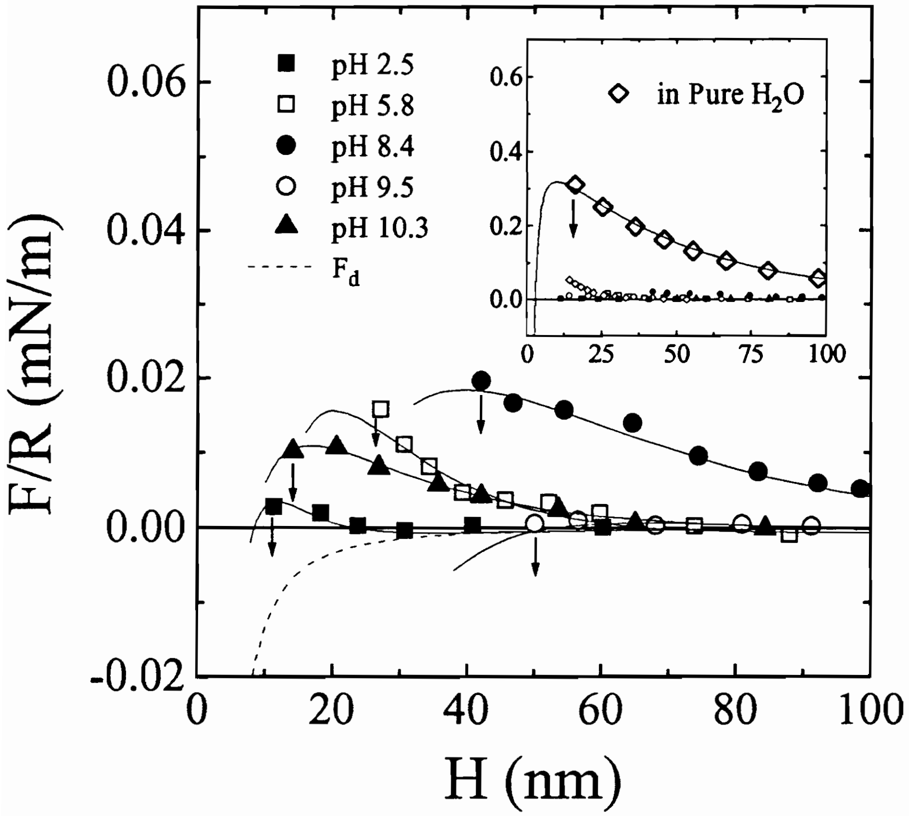

Figure 4.5. *F/R* vs. *H* curves obtained from AFM force measurements conducted between an OTS-coated glass sphere and a bare silica plate in $4\text{x}10^{-5}$ M DAHCl solutions at different pH values. The force data obtained from measurements conducted in pure water are shown in the inset. The dashed line represents F_d as calculated using Eq. [4.5] with A_{132} = $8\text{x}10^{-21}$ J. The solid lines are fits of the force data using the classical DLVO theory (Eq. [4.1]) or the extended DLVO model (Eq. [4.2]) using Eq. [4.4] to account for the hydrophobic force. Values of the fitting parameters are provided in Table 4.3. The arrows indicate jump distances (H_j).

TABLE 4.3
Force Parameters for Measurements between a Bare Silica Surface and a Hydrophobized Silica Surface in $4\mathrm{x}10^{-5}$ M DAHCl Solution at Various pH.

pH	$\theta_{\mathrm{eff,i}}$ (deg.)	$\theta_{\mathrm{eff,f}}$ (deg.)	ψ_1 (mV)	ψ_2 (mV)	κ^{-1} (nm)	H_j (nm)	K_{132} (10^{-19} J)	F_{ad} (mN/m)
2.5	65	65	14	6	6.0	11.3	-	0.40
5.8	68	71	-21	-14	14.5	27.1	0.38	1.92
8.4	80	82	-28	-21	31.6	42.0	1.5	2.65
9.5	93	91	-24	-11	30.0	50.1	1.7	3.05
10.3	90	58	-9	-13	17.3	14.1	-	2.18
11.3	88	30	-14	-22	9.3	14.1	-	1.94
12.5	58	0	-	-	-	-	-	-
H_2O	70	70	-60	-60	42	16.1	0.10	-

can be made. Firstly, the overall force becomes much less repulsive, most likely due to a reduction in magnitude of the negative electrical potentials of both surfaces as well as a four fold increase in the hydrophobic force constant, K_{132}, as shown in Table 4.3. Both of these changes can be explained by the adsorption of the cationic surfactant molecules at the surface.

Secondly, the different fitted potentials obtained for each surface (ψ_1 = -21 mV for bare silica and ψ_2 = -14 mV for OTS-coated glass) indicate that there is a greater adsorption of alkylammonium ions at the OTS-coated surface than at the bare silica surface. This is not surprising if one considers that in addition to the electrostatic attraction between the positively charged surfactant head group and the negatively charged hydrophobized surface, thermodynamics of the system favor the interaction between the amphiphilic surfactant's hydrocarbon tail and the well-ordered OTS hydrocarbon chains.

At pH 8.4, the forces become more repulsive at longer distances due to the increasingly negative surface potential. Increased amine adsorption, however, increases the hydrophobic force, $K_{132} = 1.5\text{x}10^{-19}$ J, causing the surfaces to jump into contact from a larger distance, H_j = 42 nm. An even larger jump distance, H_j = 50.1 nm, is observed at pH 9.5, where the maximum flotation recovery of quartz is reported (1-7). The force data at this pH show no long-range repulsion due, in part, to the less negative potentials of both surfaces as determined by fitting the extended DLVO model but also to a slight increase in the hydrophobic force. At pH 10.3, the forces again become repulsive at separation distances less than 70 nm. The force data fit the classical DLVO model well (ψ_1 = -9 mV, ψ_2 = -13 mV, and κ^{-1} = 17.3 nm), meaning no attractive hydrophobic force was detected.

When forces are measured in the presence of a precipitate at pH 11.3, there is a sharply increasing repulsive force first detectable at a separation distance of 60 nm before the surfaces jump into contact at 9.3 nm. Forces measured at pH 12.5 are only repulsive, and no jump was detected. These force data are not shown in Figure 4.5 as previously explained. It appears that forces measured in DAHCl solution at pH 12.5 are repulsive regardless of the initial hydrophobicity of the surfaces involved. Rutland *et al.* (41) have also reported strong repulsive forces at this pH between mica surfaces in DAHCl. These authors suggested that since the colloidal precipitate droplets are negatively charged above pH 11 (48), it is unlikely that they would adsorb on the negatively charged mica surface; therefore, the repulsive forces result from double layer interactions between the hydrocarbon surfaces. This hypothesis is credible since zeta-potential measurements of paraffin wax have shown the hydrocarbon surface to be negatively charged, possibly from adsorption of hydroxyl ions at the surface (55). As previously mentioned, the technique employed in this work does not allow for the measurement of the thickness of the surfactant layer adsorbed on the silica surface; therefore, it is not clear whether the repulsive forces observed in this work above pH 11 are double layer forces due to a negatively charged hydrocarbon surface or steric forces resulting from amine precipitate deposited on the silica surfaces.

It can now be seen from Tables 1, 2, and 3 that the fitted surface potential pairs determined for each of the force measurements reported are of like sign; thus, the electrostatic double layer force is repulsive in each case. Consequently, the only attractive forces involved in the interactions are the London-van der Waals dispersion forces and the hydrophobic force. The fact that the equations describing these forces, Eqs. [4.5] and [4.4], are of the same form, allows one to compare the Hamaker constant, A_{ikj}, and the hydrophobic force parameter, K_{ikj}, directly. Figure 4.6 shows the sum of both attractive constants plotted on a logarithmic scale as a function of pH. This is a convenient way of plotting the data since, in some cases, the hydrophobic force may be too weak to detect and may be dominated by the London-van der Waals dispersion forces. The dashed line in Figure 4.6 denotes the Hamaker constant (8×10^{-21} J). It is immediately apparent that the hydrophobic forces between two OTS-coated surfaces are several orders of magnitude greater than the forces measured between bare silica surfaces in DAHCl solution. When an OTS-coated surface interacts with a bare silica surface the hydrophobic force is slightly higher than that measured between two

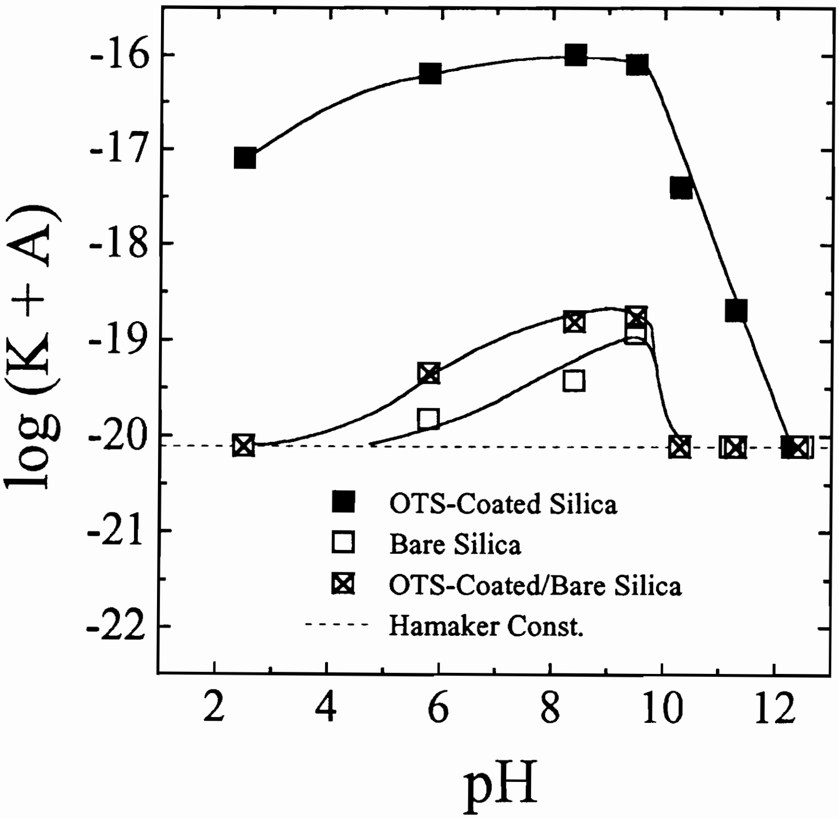

Figure 4.6. Values of the Hamaker constant (*A*) plus the hydrophobic force parameter (*K*) plotted on a logarithmic scale versus pH. The values of *K* were obtained from AFM force measurements between i) bare silica surfaces, ii) OTS-coated surfaces, and iii) a bare silica surface and an OTS-coated surface in 4×10^{-5} M DAHCl solutions at different pH. The dashed line represents $A = 8 \times 10^{-21}$ J for silica in water.

bare silica surfaces. The force constants for all three sets of data reach a maximum near pH 9.5. At pH 10.3, the hydrophobic force measured between two OTS-coated surfaces decreases sharply. Measurements conducted between two bare silica surfaces and those conducted between one OTS-coated and one bare silica surface at this pH provide no evidence for a non-DLVO force. A similar observation has been made between bare mica surfaces in DAHCl solution (42). Under more alkaline conditions, the hydrophobic force between OTS-coated surfaces decreases further until, at pH 12.5, no hydrophobic force can be detected between the surfaces.

When compared to Fuerstenau's (2) flotation recovery data at this concentration, it can be readily seen that the appearance of the hydrophobic force between bare and OTS-coated silica coincides with the onset of flotation. Conversely, the disappearance of the hydrophobic force at pH 10.3 corresponds to diminishing flotation recovery. The correlation of this data adds further support to the argument of the necessity of the hydrophobic force to achieve successful flotation (63).

It is evident from Figure 4.6 (and Tables 1, 2, and 3) that the values of the composite hydrophobic force parameters, K_{132}, determined from measurements between an OTS-coated surface and a bare silica surface are intermittent between values of K_{131} obtained from measurements between two bare silica surfaces and values of K_{232} provided from measurements between two OTS-coated surfaces. A previous study (27) has shown that the hydrophobic force constants obtained between dissimilar surfaces, K_{132}, can be estimated from the geometric mean of the hydrophobic force constants obtained from measurements conducted between like surfaces, K_{131} and K_{232}. A consequence of this is that the logarithms of K_{132}, K_{131}, and K_{232} are linear functions of an effective contact angle, θ_{eff}, which is described by

$$\cos\theta_{\mathrm{eff}} = \frac{\cos\theta_1 + \cos\theta_2}{2}. \qquad [4.6]$$

The hydrophobic force constants obtained from the measurements conducted in the present study are plotted on a logarithmic scale versus the cos θ_{eff} calculated from both initial contact angle, $\theta_{\mathrm{eff,i}}$, and final contact angle, $\theta_{\mathrm{eff,f}}$ in Figure 4.7. Also shown are the values of the hydrophobic force parameters, K_{131} and K_{132}, obtained from measurements conducted in pure water between silica surfaces with various surface coverages of OTS (27) and in various solution concentrations of DAHCl and dodecanol between mica surfaces (60, 64). The dashed line in Figure 4.7 represents the Hamaker constant for silica in water. There are two main features in the figure. Firstly, when values of log K are plotted versus cos $\theta_{\mathrm{eff,f}}$ there appears to be quite a bit of scatter; however, when plotted versus cos $\theta_{\mathrm{eff,i}}$, the hydrophobic force constants obtained at angles greater than 90° agree reasonably well with the literature values. This suggests that the contact angle measured within the first 15 seconds after

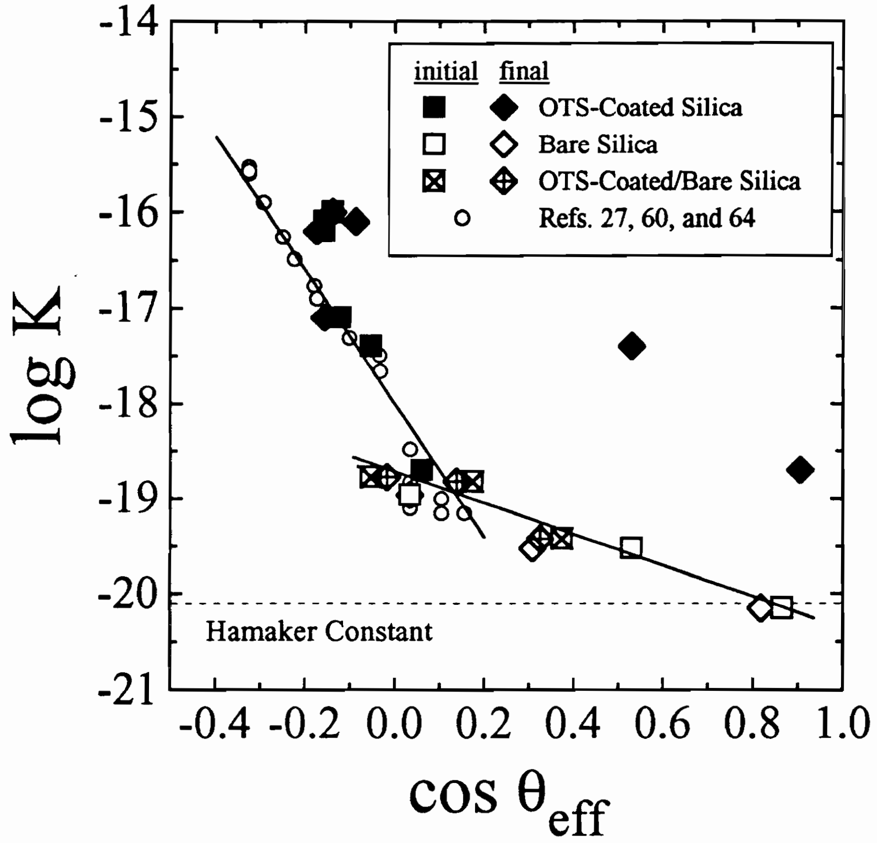

Figure 4.7. Log *K* values obtained in the present study are plotted versus cos θ_{eff} (= ½(cos θ_1 + cos θ_2)). Squares represent K values plotted versus cos θ_{eff} determined from initial contact angles, cos $\theta_{eff,i}$; whereas, diamonds are *K* values plotted against cos θ_{eff} determined from final contact angles, cos $\theta_{eff,f}$. The dashed line represents the value of the Hamaker constant for silica surfaces in water, 8x10^{-21} J.

introducing the air bubble, θ_i, best describes the hydrophobicity of the surfaces when interacting with one another in surfactant solutions.

A second feature of Figure 4.7 is that when initial contact angles are less than 90°, the magnitude of the hydrophobic force parameter is not as sensitive to contact angle as those measured above 90°. This change in slope results in an inflection point near 90°, which correlates very well with the sudden jump in hydrophobic force decay length reported by Yoon and Ravishankar (60). The existence of this inflection point, as well as the importance of θ_i explained above, may provide fodder to proponents of the formation of vapor cavities between non-wetting surfaces being the source of long-range hydrophobic forces (65-67). Another implication of the change in slope is that values of K_{132} cannot be accurately predicted by the geometric mean combining rule (27) when $\theta_{eff} < 90°$. This adds further support to the hypothesis proposed by Yoon and Ravishankar (60) that separate mechanisms are responsible for short-range and long-range hydrophobic forces.

4.3.3 *Relevance to Mineral Flotation*

When comparing the forces observed between a solid surface and a bubble to those observed between two solid surfaces, there are several notable differences that must be taken into consideration. For example, the London-van der Waals dispersion forces, Eq. [4.5], can make very different contributions to the overall force observed depending on the materials involved. The Hamaker constant, A_{132}, used to determine the magnitude of the dispersion forces acting between surfaces **1** and **2** in medium **3** can be estimated from the expression (68)

$$A_{132} = \left(\sqrt{A_{11}} - \sqrt{A_{33}}\right)\left(\sqrt{A_{22}} - \sqrt{A_{33}}\right), \qquad [4.7]$$

where A_{ii} is the Hamaker constant of substance **i** *in vacuo*. For most systems, including a bare silica surface interacting with OTS-coated glass in water, A_{132} is positive, resulting in an attractive force. However, the Hamaker constant for a non-condensed phase such as air is zero; thus, the composite Hamaker constant for bare silica interacting with an air bubble in water is negative, $A_{132} = -1.03\text{x}10^{-20}$ J (56). Using this value in Eq. [4.4] results in a short-range repulsive London-van der Waals force. It is not certain how the adsorption of surfactant at the liquid-vapor interface would affect the Hamaker constant. A surfactant-laden air bubble may behave as a condensed phase and cause F_d to become less repulsive or even attractive at very short distances (69). Nevertheless, in flotation, bubble-particle interactions are believed to occur when the bubble is still "fresh", *i.e.* with little surfactant adsorption.

Just as F_d may be repulsive for the interaction of a bubble and a quartz surface in DAHCl solution, the electrical double layer force, F_e, can also be attractive.

Electrophoretic mobility measurements of air bubbles in DAHCl solutions (70, 71) have shown that at low pH values, where only alkylammonium ions are present, the bubble retains a positive zeta potential. The positive charge is due to the adsorption of RNH_3^+ ions at the liquid-vapor interface. As pH becomes more alkaline, the positive zeta potential decreases and becomes negative near pH 9. Thus, the ion-electrostatic electrical double layer force becomes repulsive under highly alkaline conditions.

A convenient way of comparing the interactions studied in the present work between a bare silica surface and a hydrophobic solid sphere to those between a silica surface and an air bubble is to determine the magnitude of the energy barrier that must be overcome for surface contact. The Derjaguin approximation (72) allows for the conversion of the forces measured between a sphere and flat plate ($F_{\text{sp-fl}}$) in this study to the interaction energy between two flat plates ($E_{\text{fl-fl}}$) using the following relationship:

$$E_{\text{fl-fl}} = \frac{1}{2\pi R} F_{\text{sp-fl}}, \qquad [4.8]$$

in which R is the radius of the sphere. Figure 4.8 shows the activation energy per unit area, E_a, plotted as a function of pH for measurements between two bare silica surfaces and between one OTS-coated surface and a bare silica surface in 4×10^{-5} M DAHCl solution. There was no perceptible energy barrier for interactions between two OTS-coated surfaces in DAHCl solution. Though the top curve in Figure 4.8 may provide

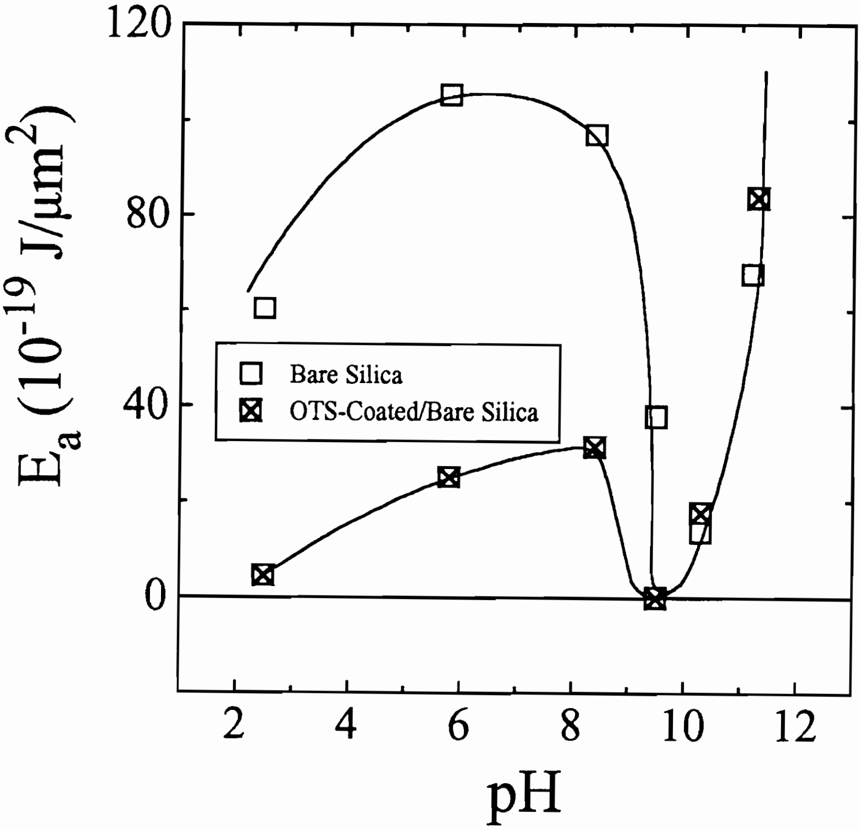

Figure 4.8. The pH dependence of activation energy (E_a) per unit area determined from AFM force measurements conducted in 4×10^{-5} M DAHCl solutions between i) a clean glass sphere and a bare silica plate and ii) an OTS-coated sphere and a bare silica plate.

information for coagulation studies, it is the curve generated from data acquired from asymmetric force measurements between a bare silica surface and a hydrophobized OTS-coated sphere that is of interest to the study of flotation. The presence of a hydrophobic body as one of the surfaces in the interaction reduces the activation energy at all pH values. The energy barrier disappears near pH 9.5, which is in the range of maximum flotation recovery, but increases sharply under more alkaline conditions where bulk precipitate is present.

Energy barriers were also calculated for a bare silica surface interacting with an air bubble in DAHCl solution as a function of pH and are shown in Table 4.4. Values of E_a were determined using the results of electrokinetic measurements of microbubbles in DAHCl solution to represent surfactant-coated "aged" bubbles (71, 73) and measurements of microbubbles generated in pure water to portray surfactant-deficient "fresh" bubbles (71). In the E_a calculations, the Hamaker constant was taken to be $A_{132} = -1.03\times10^{-20}$ J, and the hydrophobic force parameters, K_{132}, were assumed to be the same as those measured between bare silica and OTS-coated silica as reported in Table 4.3. At low pH, near the point of zero charge of silica, the double layer force is negligible and the repulsive London-van der Waals force dominates, resulting in no adhesive contact. As pH increases, the activation energy steadily decreases between the silica surface and the bubble devoid of surfactant because the increasingly repulsive

TABLE 4.4
Calculated Activation Energy Values for a Bare Silica Surface Interacting with a Fresh Air Bubble and an Aged, Surfactant-Coated Air Bubble in DAHCl Solutions at Varying pH.

pH	Contact Angle (deg.)		E_a (10^{-19} J/μm^2)	
	θ_i	θ_f	Fresh	Aged
2.5	9	9	∞	∞
5.8	30	35	157	0
8.4	58	72	124	0
9.5	88	88	92	0
10.3	88	58	46	∞
11.3	89	38	∞	∞

double layer force is offset by the presence of an attractive hydrophobic force. In the case of a surfactant-coated bubble, however, E_a decreases sharply to zero due to an attractive double layer force, indicating successful particle-bubble attachment from pH 5.8 to 9.5. A sudden increase in activation energy is again detected for both cases as amine precipitate is present in bulk solution after pH 10.3. Using the data of Yoon and Mao (74) for a single silanated glass sphere with $\theta = 52°$ interacting with an air bubble, an E_a value of $2.4\text{x}10^{-17}$ J/μm^2 is calculated, which is reasonably close to the value of $1.24\text{x}10^{-17}$ J/μm^2 reported in Table 4.4 for a comparable contact angle.

The values of interaction energy reported in Table 4.4 for a surfactant-coated air bubble predict successful particle-bubble attachment for pH values between 5.8 and 9.5; whereas, interactions involving a "fresh" air bubble exhibit a decreasing energy barrier with a minimum near pH 10.3. A comparison to flotation recovery data at this concentration (2), where recovery exceeds 70% only between pH 9 and pH 11, indicates that the true values of interaction energy may lie somewhere between these limiting values but closer to those of the surfactant-deficient air bubble. The amount of surfactant molecules adsorbed on the bubble surface under real flotation conditions is not only dependent on the few seconds that a bubble ages before interacting with a mineral particle (47), but also on the mobility of the bubble. It is believed that as a bubble rises, surfactant is swept towards the bottom of the bubble, thereby reducing the surfactant adsorption density and increasing the surface tension at the top portion of the bubble, where the initial bubble-particle interaction is likely to occur (75).

One can conclude then that to properly simulate particle-bubble attachment in the flotation process with respect to direct force measurements, it would be necessary to devise a technique that allows ample time for the solid surface to equilibrate with the surfactant, while introducing the air phase immediately prior to conducting a measurement. In the absence of such a technique, direct force measurements using a hydrophobic solid in the place of an air bubble may provide vital information on the effect of changing conditions (e.g. pH, inorganic salt concentration, depressants, activators, etc.) on bubble-particle attachment.

4.4 CONCLUSIONS

An AFM was used to conduct a series of force measurements between a clean glass sphere and a bare silica plate, between an OTS-coated sphere and an OTS-coated silica plate, and between two OTS-coated surfaces in 4×10^{-5} M DAHCl solution as a function of pH. When the measurements were conducted between bare surfaces, an additional non-DLVO attractive force, believed to be the hydrophobic force, was detected in the pH range of 5.8 to 9.5. Measurements between an OTS-coated sphere and a bare silica surface exhibited an even larger hydrophobic force in this pH range which coincides with the pH range for successful flotation of quartz using dodecylamine as a collector.

Contact angles measured for both bare silica and OTS-coated silica surfaces under alkaline conditions decreased with time; however, it was found that values measured within the first 15 seconds of three-phase contact more accurately described the hydrophobicity of the sample with respect to force measurements. Relating this concept to the quartz-amine flotation system, activation energies were determined for the limiting cases of both a surfactant-deficient "fresh" air bubble and a surfactant-laden "aged" air bubble interacting with a silica surface in DAHCl solution.

4.5 REFERENCES

1. Ananthpadmanabhan, K., Somasundaran, P., and Healy, T. W., *Trans. Amer. Inst. Min. Metall. Pet. Eng.* **266**, 2003 (1979).
2. Fuerstenau, D. W., *Trans. AIME* **208**, 1365 (1957).
3. Smith, R. W., and Lai, R. W. M., *Trans. AIME* **235**, 413 (1966).
4. Somasundaran, P., *Int. J. of Miner. Process.* **3**, 35 (1976).
5. Somasundaran, P., and Ananthpadmanabhan, K. P. *in* "Solution Chemistry of Surfactants, Vol. 2" (K. L. Mittal, Ed.), p.777. Plenum, New York, 1979.
6. Novich, B. E., and Ring, T. A., *Langmuir* **1**, 701 (1985).
7. Yoon, R.-H., and Yordan, J. L., *J. Colloid and Interface Sci.* **141**, 374 (1991).
8. Iwasaki, I., Cooke, S. R. B., and Kim, Y. S., *Trans. AIME* **223**, 113 (1962).
9. Pugh, R. J., *Colloids Surf.* **18**, 19 (1986).
10. Bustamante, H., and Shergold, H. L., *Trans. Inst. Min. Metall. Sec. C* **92**, C201 (1983).
11. Gaudin, A. M., and Fuerstenau, D. W., *Trans. AIME* **202**, 958 (1955).
12. Smith, R. W., *Trans. AIME* **226**, 427 (1963).
13. Yoon, R.-H., and Ravishankar, S. A., *J. Colloid and Interface Sci.* **166**, 215 (1994).
14. Butt, H.-J., *J. Colloid and Interface Sci.* **166**, 109 (1994).

15. Ducker, W. A., Xu, Z., and Israelachvili, J. N., *Langmuir* **10**, 3279 (1994).

16. Craig, V. S. J., Ninham, B. W., and Pashley, R. M., *J. Phys. Chem.* **97**, 10192 (1993).

17. Craig, V. S. J., Ninham, B. W., and Pashley, R. M., *Science* **364**, 317 (1993).

18. Aksoy, B. S., Ph.D. Dissertation, Mining and Minerals Engineering, Virginia Polytechnic Institute and State University, Blacksburg, Virginia, 1996.

19. Israelachvili, J. N., and Pashley, R. M., *J. Colloid and Interface Sci.* **98**, 500 (1984).

20. Kékicheff, P., Christenson, H. K., and Ninham, B. W., *Colloids Surf.* **40**, 31 (1989).

21. Herder, P. C., *J. Colloid and Interface Sci.* **134**, 346 (1990).

22. Pashley, R. M., McGuiggan, P. M., Ninham, B. W., and Evans, D. F., *Science* **229**, 1088 (1985).

23. Parker, J. L., Yaminsky, V. V., and Claesson, P. M., *J. Phys. Chem.* **97**, 7706 (1993).

24. Claesson, P. M., and Christenson, H. K., *J. Phys. Chem.* **92**, 1650 (1988).

25. Christenson, H. K., Claesson, P. M., Berg, J., and Herder, P. C., *J. Phys. Chem.* **93**, 1472 (1989).

26. Christenson, H. K., and Claesson, P. M., *Science* **239**, 390 (1988).

27. Flinn, D. H., Rabinovich, Ya. I., and Yoon, R.-H., *J. Colloid and Interface Sci.* Submitted.

28. Rabinovich, Ya. I., and Yoon, R.-H., *Colloids Surf.* **93**, 263 (1994).

29. Rabinovich, Ya. I., and Yoon, R.-H., *Langmuir* **10**, 1903 (1994).

30. Rabinovich, Ya. I., and Derjaguin, B. V., *Colloids Surf.* **30**, 243 (1988).

31. Parker, J. L., and Claesson, P. M. *Langmuir* **10**, 635 (1994).

32. Derjaguin, B. V., and Landau, L., *Acta. Physiochim. URSS* **14**, 633 (1941).

33. Verwey, E. J. W., and Overbeek, J. Th. G. "Theory of the Stability of Lyophobic Colloids", Elsevier, Amsterdam, 1948.

34. Meagher, L., *J. Colloid and Interface Sci.* **152**, 293 (1992).

35. Rabinovich, Ya. I., Derjaguin, B. V., and Churaev, N. V., *Adv. Colloid Interface Sci.* **16**, 63 (1982).

36. Grabbe, A., and Horn, R. G., *J. Colloid and Interface Sci.* **157**, 375 (1993).

37. Rabinovich, Ya. I., and Derjaguin, B. V., *Langmuir* **3**, 625 (1987).

38. Horn, R. G., Smith, D. T., and Haller, W., *Chem. Phys. Letters* **162**, 404 (1989).

39. Peschel, G., Belouschek, P., Müller, M. M., Müller, M. R., and König, R., *Colloid Polymer Sci.* **260**, 444 (1982).

40. Rabinovich, Ya. I., and Derjaguin, B. V. *in* "Proceedings of the 5th Hungarian Conference on Colloid Chemistry", Loránd Eötvös University, Balatonfured, Hungary, 1988.
41. Rutland, M., Waltermo, A., and Claesson, P., *Langmuir* **8**, 176 (1992).
42. Yoon, R.-H., and Ravishankar, S. A., *J. Colloid and Interface Sci.* In press.
43. Herder, P. C. *J. Colloid and Interface Sci.*, **134**, 336 (1990).
44. Flinn, D. H., Guzonas, D. A., and Yoon, R.-H., *Colloids and Surf. A* **87**, 163 (1994).
45. Senden, T. J., and Ducker, W. A., *Langmuir* **10**, 1003 (1994).
46. Finch, J. A., and Smith, G. W., *Trans. Inst. Min. Metall. Sec. C* **81**, C213 (1972).
47. Finch, J. A., and Smith, G. W., *J. Colloid and Interface Sci.* **45**, 81 (1973).
48. Castro, S. H., Vurdela, R. M., and Laskowski, J. S., *Colloids Surf.* **21**, 87 (1986).
49. Gaudin, A. M., and Morrow, J. G., *Trans. AIME* **199**, 1196 (1954).
50. de Bruyn, P. L., *Trans. AIME* **202**, 291 (1955).
51. Nishimura, S., Tateyama, H., and Tsunematsu, K., *J. Colloid and Interface Sci.* **159**, 198 (1993).
52. Somasundaran, P., *Trans. AIME* **241**, 105 (1968).

53. Laskowski, J., and Kitchener, J. A., *J. Colloid and Interface Sci.* **29**, 670 (1969).

54. Laskowski, J., and Iskra, J., *Trans. IMM, Sec. C* **79**, C6 (1970).

55. Parreira, H. C., and Schulman, J. H., *Adv. Chem Ser.* **33**, 160 (1961).

56. Hough, D. B., and White, L. R., *Adv. Colloid Interface Sci.* **14**, 3 (1980).

57. Ohshima, H., Healy, T. W., and White, L. R., *J. Colloid and Interface Sci.* **89**, 484 (1982).

58. Buckenham, M. H., and Rogers, J., *Trans. Inst. Min. Metall.* **64**, 11 (1954-55).

59. Finch, J. A., and Smith, G. W., *Canadian Metall. Quart.* **14**, 47 (1975).

60. Yoon, R.-H., and Ravishankar, S. A., *J. Colloid and Interface Sci.* In press.

61. Watson, D., and Manser, R. M., *Trans. Inst. Min. Metall. Sec. C* 77, C57 (1968).

62. Ozeki, S., Tsunoda, M.-A., and Ikeda, S., *J. Colloid and Interface Sci.* **64**, 28 (1978).

63. Yoon, R.-H., *Aufbereit. Tech.* **32**, 474 (1991).

64. Ravishankar, S. A., Ph.D. Dissertation, Materials Engineering Science, Virginia Polytechnic Institute and State University, Blacksburg, Virginia, 1995.

65. Yaminsky, V. V., Yushchenko, V. S., Amelina, E. A., and Shchukin, E. D., *J. Colloid and Interface Sci.* **96**, 301 (1983).

66. Yushchenko, V. S., Yaminsky, V. V., and Shchukin, E. D., *J. Colloid and Interface Sci.* **96**, 307 (1983).

67. Yaminsky, V. V., and Ninham, B. W., *Langmuir* **9**, 3618 (1993).

68. Israelachvili, J. N., "Intermolecular and Surface Forces", Academic Press, London, 1985.

69. Usui, S. and Barouch, E., *J. Colloid and Interface Sci.* **137**, 281 (1990).

70. Yoon, R.-H., and Yordan, J. L., *J. Colloid and Interface Sci.* **113**, 430 (1986).

71. Okada, K., Akagi, Y., Kogure, M., and Yoshioka, N., *Can. J. Chem. Eng.* **68**, 393 (1990).

72. Derjaguin, B., *Kolloid Zeitschrift* **69**, 155 (1934).

73. Yordan, J. L., Ph.D. Dissertation, Mining and Minerals Engineering, Virginia Polytechnic Institute and State University, Blacksburg, Virginia, 1989.

74. Yoon, R.-H., and Mao, L. *J. Colloid and Interface Sci.* Accepted.

75. Schulze, H. J., "Physico-chemical Elementary Processes in Flotation", Elsevier, New York, 1984.

CHAPTER 5 CONCLUSIONS

A summary of the major findings in this work are presented as follows:

1) It was shown that octadecyltrichlorosilane (OTS) can be adsorbed on a silica surface from a cyclohexane solution at room temperature. Well-ordered monolayers can be formed that exhibit a high degree of hydrophobicity (θ = 109°) and durability.

2) Sub-monolayer coverages of silica by OTS were achieved by varying OTS concentration in solution and immersion time of the silica sample. Thus, hydrophobic silica surfaces were produced having contact angles ranging from 0° to 109°.

3) Analysis of atomic force microscopy (AFM) and IR transmission results showed that OTS molecules adsorb on the silica surface in clusters. As the number of clusters increases, contact angle increases sharply. AFM images show the silica surface to be completely covered with OTS clusters near θ = 109°. A further

increase in OTS adsorption increases the packing density of the adsorbate within each cluster until monolayer coverage is reached at $\theta = 109°$.

4) Plots of advancing contact angle, contact angle hysteresis, band frequencies for the CH_2 symmetric and asymmetric stretching modes, and full width at half maximum values for the CH_2 adsorption spectra exhibited inflection points at fractional surface coverages of 0.25 to 0.30. At this coverage, OTS molecules begin to assume a vertical orientation on the silica surface, and give rise to a contact angle of approximately 90°.

5) The amount of water involved in the silanation reaction of OTS on silica was determined to be the critical factor in producing well-ordered, homogeneous monolayers. Experiments conducted with excess water in solution produced sample surfaces having high contact angle hysteresis resulting from large pre-polymerized OTS clusters randomly deposited on the silica surfaces.

6) An atomic force microscope (AFM) was used to measure surface forces between an OTS-coated glass sphere and a fully silanated flat silica plate in water. When both surfaces were silanated to the same extent, the measured

forces could not be fit to the classical DLVO theory due to the presence of an extra long-range attractive force. This non-DLVO force, which becomes stronger and longer in range as surface coverage of OTS was increased, was attributed to the hydrophobic attraction.

7) The AFM force measurements were also conducted with asymmetric systems, *i.e.*, the OTS-coated glass sphere has a contact angle of 109°, while the silica plates have varying contact angles. Values of the hydrophobic force constant, K_{132}, obtained by fitting the asymmetric force data to a power law, were larger than those obtained from symmetric force measurements conducted between surfaces having partial OTS coverage, K_{131}, and smaller than values determined from measurements between two fully hydrophbized surfaces, K_{232}.

8) The logarithms of the hydrophobic force parameters obtained from the asymmetric measurements, K_{132}, can be estimated from those obtained from symmetric force measurements (K_{131} and K_{232}). The relationship is one of a geometric mean, i.e., $K_{132} = \sqrt{K_{131} \cdot K_{232}}$.

9) The logarithms of K_{131} and K_{232} vary linearly with cos θ. The logarithms of K_{132}, on the other hand, vary linearly with the effective contact angle, which is an arithmetic mean of the cosines of the angles of the two interacting surfaces.

10) Contact angles measured on hydrophilic bare silica and hydrophobic OTS-coated silica surfaces in DAHCl solutions were pH-dependent. The highest values of contact angles were observed between pH 8 and pH 10, where coadsorption of alkylammonium ions and neutral amine molecules is believed to take place. This pH range also corresponds to the range of maximum recovery of quartz in DAHCl solutions. In alkaline solutions, contact angles decreased with time, which is believed to result from the dynamic surface tension effect and the formation of bulk amine precipitate.

11) Surface forces measured with an AFM between a glass sphere and a flat silica plate in aqueous solutions DAHCl were less repulsive than forces measured between the same surfaces in pure water. Neutralization of the surface charge by dodecylammonium ions and the presence of hydrophobic forces are believed to be the causes of the reduction in the repulsive forces measured.

12) Force measurements conducted in DAHCl solutions between OTS-coated surfaces exhibited long-range attractive forces, though smaller in magnitude than those measured between OTS coated surfaces in pure water. The effect is more pronounced at low pH where alkylammonium ions may adsorb on the surface with inverse orientation in which their polar head groups are exposed to the aqueous phase. No hydrophobic force is detected above pH 10, which may be attributed to the formation of hydrophilic amine precipitate.

12) Surface forces between a hydrophobic OTS-coated glass sphere and a bare silica plate in DAHCl solution were most attractive near pH 9.5. The appearance of a strong attractive hydrophobic force coincided with the pH range of maximum flotation for the quartz-amine system, indicating that a strong hydrophobic force is necessary for successful particle-bubble attachment.

13) Log K values for measurements between two bare silica surfaces, between two OTS-coated surfaces, and between an OTS-coated surface and a bare silica surface were plotted as a function of contact angle. It was found that K values were best described by contact angle values measured on a given surface within the first 15 seconds of formation of a point of three-phase contact. Values of

K obtained from force measurements between surfaces exhibiting contact angles below 90° were less sensitive to changes in contact angle than those measured when $\theta > 90°$, indicating that short-range and long-range hydrophobic forces may be caused by different mechanisms.

14) Values of the hydrophobic force parameter obtained from force measurements between an OTS-coated sphere and a bare silica surface in DAHCl solution were used to estimate the energy barrier that must be overcome between an air bubble and a silica surface in DAHCl solution as a function of pH. Activation energy values determined from electrokinetic data for air bubbles in pure water and those in DAHCl solution are believed to be upper and lower limits of true bubble-particle interaction values.

CHAPTER 6 RECOMMENDATIONS FOR FUTURE RESEARCH

Based on the research and findings presented in this work, the following are suggested areas of future research:

1) It has been demonstrated that the role of water plays a significant role in the adsorption of octadecyltrichlorosilane (OTS) on silica. It would be of great interest to conduct a series of experiments in which the amount of water present on the silica surface was controlled. This might be done by controlling the relative humidity of the atmosphere in a closed chamber in which the silica was placed. The samples could then be transferred to an anhydrous solvent having a given concentration of OTS. After a fixed reaction time, the silica surfaces could be analyzed using goniometry, FTIR, and scanning probe microscopy to asses the formation of OTS clusters.

2) It was shown in the present work that the magnitude of the hydrophobic force parameter, K, is uniquely determined by the contact angle, θ, of the surfaces involved in the interaction when θ exceeds 90°. Below 90°, the dependence of

contact angle is not as sensitive. indicating that there may be more than one mechanism producing the long- and short-range hydrophobic forces. Because investigators have used many different substrates, surfactants, and methods of adsorption for direct force, the literature is sometimes inconsistent as to the effect of inorganic electrolyte, dissolved gas, temperature, and pH. A series of experiments should be conducted in one apparatus with two types of insoluble hydrophobic surfaces (one in which $\theta < 90°$, and the other with $\theta > 90°$) to systematically explore the influence each of these conditions. The results of these experiments may then shed some light on the origin of the hydrophobic force.

3) Though the hydrophobic force between two solid surfaces was first directly measured over ten years ago, there is still uncertainty about its origin. The current theories include rearrangement of water molecules between hydrophobic surfaces, formation of vapor bridges between the surfaces, and the correlation of surfactant domains on the surfaces. The optical technique of sum-frequency generation (SFG) has recently been used to study the orientation of water molecules at the vapor-water, hydrophilic solid-water, and hydrophobic solid-water interfaces. It has also been used to study the

orientation of anionic surfactant at the water-organic liquid interface. This technique may provide critical information about the mechanisms causing the hydrophobic force if it were used to monitor the orientation of surfactant and water molecules as a function of separation distance between two hydrophobic surfaces.

4) It has been shown that direct force measurements between a hydrophobized sphere and a solid sample surface can provide relevant flotation data concerning bubble-particle interactions. The present work used a cationic surfactant to study the effect of changing pH. The technique should also be validated by using an anionic and nonionic surfactant as well. Zeta-potential measurements of air bubbles in sodium dodecylsulfate and polyoxyethelene dodecylether solutions are available in the literature. Also, the effect of inorganic salt, the addition of a long-chain alcohol, and the effect of temperature could be studied and compared to flotation recovery data. Other experimental possibilities such as measuring the forces between a hydrophobized sphere and a sulfide mineral surface could also be explored. The use of the AFM electrochemical cell would allow force measurements in xanthate solution as a function of potential on the

mineral sample surface. The limitation being the availability of a smooth sulfide mineral surface.

5) Ideally, the most significant flotation data would result from direct force measurements between an air bubble and a solid sample surface. Attempts to use the AFM for such measurements have been complicated by the pliability of the bubble surface. The bubble tends to jump towards the solid, resulting in underestimated force values and false separation distance values. It is also difficult to separate the surfaces once contact has been made. Perhaps some or all of these problems could be alleviated by a few modifications to the AFM technique. The air bubble could be formed through a pinhole in the a solid surface below the cantilever holding a solid particle. The size of the bubble would be controlled with a sensitive manometer or pressure transducer which would also serve as means to monitor the pressure of the bubble. A thin silica fiber terminating just below the bubble surface and leading through the pinhole could provide information on the absolute thickness between the bubble surface and the particle using the extrinsic Fabry-Perot interferometer (EFPI) technique. As the bubble approaches the particle, both the deflection of the

cantilever and the change in pressure due to deformation of the bubble would comprise the overall force curve.

VITA

Darrin Heinz Flinn was born on 18 January 1967 in Silver Spring, Maryland. He received his primary education in Wiesbaden, Germany; Clinton, Maryland; and Hampton, Virginia. He attended Winston Churchill High School in San Antonio, Texas for 3 years; however, he spent his senior year and graduated *cum laude* from Ramstein American High School in Ramstein, Germany in May 1985. He immediately enrolled himself in the Mineral Processing Engineering program at the Montana College of Mineral Science and Technology in Butte, Montana where he received his B.Sc. degree in the Spring of 1989. During his undergraduate career, he spent several Summers working in the precious metals industry for Johannesburg Consolidated Investments, Ltd. in South Africa. In the Fall of 1989, he was awarded a research assistantship and enrolled in the master's program for Mining and Minerals Engineering at Virginia Polytechnic Institute and State University. Two years later, he was promoted to the doctoral program. He is a member of the Society of Mining Engineers, the Minerals, Metals, and Materials Society, and the American Chemical Society. He has accepted an offer as a Senior Research Engineer in the Research and Development department of Phelps Dodge Corporation in Morenci, Arizona.

Darrin H. Flinn